NASA CONTRACTOR REPORT

MINIMUM-IMPULSE TIME-FREE TRANSFER BETWEEN ELLIPTIC ORBITS

by Frank W. Gobetz, Michael Washington, and Theodore N. Edelbaum

Prepared by
UNITED AIRCRAFT CORPORATION
East Hartford, Conn.
for Langley Research Center

NATIONAL AERONAUTICS AND SPACE ADMINISTRATION • WASHINGTON, D. C. • NOVEMBER 1966

NASA CR-636

MINIMUM-IMPULSE TIME-FREE TRANSFER BETWEEN ELLIPTIC ORBITS

By Frank W. Gobetz, Michael Washington, and Theodore N. Edelbaum

Prepared under Contract No. NAS 1-4688 by
UNITED AIRCRAFT CORPORATION
East Hartford, Conn.

for Langley Research Center

NATIONAL AERONAUTICS AND SPACE ADMINISTRATION

For sale by the Clearinghouse for Federal Scientific and Technical Information
Springfield, Virginia 22151 – Price $3.00

Minimum-Impulse Time-Free Transfer Between Elliptic Orbits

ABSTRACT

Minimum-impulse orbit transfer between coplanar ellipses and between neighboring low-eccentricity ellipses was investigated. In the former case, all optimal elliptic transfer arcs were isolated and cataloged, and a graphical method for determining the optimal transfer between arbitrary coplanar ellipses was presented. In the latter case, explicit relations were derived for the optimal transfer between adjacent ellipses whose elements are known.

FOREWORD

This report was prepared by United Aircraft Research Laboratories of United Aircraft Corporation, East Hartford, Connecticut. It presents the final documentation of a research study on minimum impulse requirements for orbital transfer problems done by United Aircraft for the Langley Research Center under Contract NAS 1-4688. This work is an outgrowth of the interest at Langley Research Center in problems of orbital transfer and rendezvous and results from the support of an unsolicited proposal submitted by U.A.C. to Langley. This research study was administered by the National Aeronautics and Space Administration with Mr. R. L. Collins, Jr. acting as technical monitor.

The research presented in this report began in February 1965, was completed in February 1966, and was carried out by the authors at the U.A.C. Research Laboratories in East Hartford, Connecticut.

Minimum-Impulse Time-Free Transfer Between Elliptic Orbits

Contract NAS1-4688
Final Report

TABLE OF CONTENTS

TABLE OF CONTENTS
(Contd.)

Minimum-Impulse Time-Free Transfer Between Elliptic Orbits

Contract NAS1-4688
Final Report

by
Frank W. Gobetz, Michael Washington and Theodore N. Edelbaum

SUMMARY

The method of primer vector maximization has been applied to two classes of time-free, impulsive, orbit transfer problems. The first class concerns coplanar transfers between arbitrary elliptic orbits. For this case, two distinct families of transfer arcs were isolated, one with Lawden's symmetric transfer as a limiting solution, and one limited by the Lawden spiral. A complete catalog of data for all optimal arcs of these families was made in terms of parameters useful in solving specific problems. A sample problem was successfully solved using these data.

In addition to the cataloging of optimal arcs, a geometric interpretation of the coplanar problem is described. By a digital simulation, spool-shaped figures discovered by Contensou were visually displayed and photographed. The results are discussed as they apply to the families of coplanar solutions.

The second problem treated is that of time-free transfer between neighboring orbits of small eccentricity. A complete analytic solution was obtained for this problem. Explicit expressions are given for the optimum location, direction, and magnitude of each impulse. The solutions are found to require either two or three impulses. In the three-impulse cases, the solutions are singular and may be replaced by finite-thrust solutions of arbitrary magnitude with no increase in fuel consumption.

INTRODUCTION

The problem of transferring between elliptic orbits with minimum expenditure of impulse in the restricted two-body problem is one which has been solved only for certain special cases. In general, minimum-impulse solutions to particular orbit transfer problems have been obtained either by numerical search or by approximate analytical methods. These solutions serve limited purposes because they are designed to apply only to particular

terminal orbits or families of orbits, and because they are based on assumptions regarding the number of impulses involved in the transfer. The complexity of minimal-impulse problems has prevented the attainment of more general solutions, but a clear need exists for such solutions.

The purpose of this study was to explore the case of time-free, minimum-impulse transfer, utilizing a method inspired by the contributions of Lawden, Contensou, and Breakwell, and with the hope of tabulating solutions to this problem for use with a wide range of possible elliptic terminal orbits. In view of the large number of parameters involved, the problem has been divided into two categories. The first concerns coplanar, time-free transfers between elliptic orbits. The second involves a linearized, three-dimensional model with neighboring terminal orbits of low eccentricity. Treatment of the general three-dimensional problem, while it is feasible in principle by the method described herein, would require consideration of additional variables, thereby greatly complicating the task of tabulating transfers. Therefore, this most general time-free case was not considered in this study.

Solution of an orbital transfer problem requires the determination of a coasting arc (or arcs) to join the terminal orbits. Since departure and arrival terminals are left unspecified, a multitude of possible arcs must be chosen from in order to select the optimum transfer. The appropriate figure of merit in making this selection is minimum characteristic velocity, i.e., ΔV. It is apparent that a direct method of solution would be to express ΔV as a function of the state variables of the problem, perhaps orbital elements, and to successively differentiate ΔV to optimize these state variables. Unfortunately this method of solution, although feasible, results in a set of simultaneous equations which cannot be solved explicitly and which provide no physical interpretation of the results.

The approach taken herein may be described as the method of primer vector maximization. Specifically, the technique permits isolation of all possible elliptic coasting arcs of optimal transfer trajectories. These arcs are merely segments of elliptic orbits, but not all segments of arbitrary elliptic orbits are candidates for optimal coasting arcs. By exclusion of those arcs which do not fulfill the necessary conditions derived by Lawden in Ref. 1 for optimal coasting ellipses, the remaining arcs may be tabulated. A major objective of this contract was the tabulation of these data for both the nonlinear coplanar problem and a linearized noncoplanar problem.

LIST OF SYMBOLS

a	Semi-major axis
A,B,C,D,E,F	Integration constants
c	Cos τ_1
e	Eccentricity
E	Eccentric anomaly
f	True anomaly
i	Inclination
$I\ (e,\ f)$	Function of e and f
ℓ	Semi-latus rectum
n	Sin ϕ
p	Primer vector
P	Maximum magnitude of p
r	Radius
R,M,N,Q	Constants
s	Sin τ_1
t	Time
T	Tan $(\bar{\omega} - \bar{\Omega})$
u	$\Delta V/V_o$
ΔV	Characteristic velocity
V_o	Velocity in circular reference orbit
w	Component of velocity normal to p
x_1	a/a_o

x_2	e sin ω
x_3	e cos ω
x_5	sin i sin Ω
x_6	sin i cos Ω
x	$\Delta a/\Delta V$
y	$\Delta e/\Delta V$
z	$\Delta \omega/\Delta V$
α'	Nondimensional thrust acceleration
β	ω + f
β*	β at which $w_{T1} = w_I$ or $w_{T2} = w_{II}$
γ	Gravitational constant
δ	u_2/u
θ	Angle between velocity and circumferential direction
λ	Component of primer in radial direction
μ	Component of primer in circumferential direction
ν	Component of primer in normal direction
τ	$\dot{f}_o t$(nondimensional time)
φ	Angle made by primer with perpendicular to radius
ω	Longitude of peri-apsis
$\bar{\omega}$	$\tan^{-1}(\Delta x_2/\Delta x_3)$
$\psi(\tau_1, \tau_2)$	Function of τ_1 and τ_2
Ω	Longitude of ascending node

$\bar{\Omega}$	$\tan^{-1}(\Delta x_6/\Delta x_5)$

Subscripts

1, 2	Junction points
I, II	Terminal orbits
i	1, 2, 3, ...
T	Transfer arc
o	Circular reference orbit
A, B, A'	Families of noncoplanar solutions

BACKGROUND

In general, determination of optimum impulsive transfer trajectories requires answers to four questions. First, how many impulses should be applied to effect the desired transfer? Second, where should these impulses be applied? Third, in what directions should the impulses be applied? And finally, how should the total impulse be distributed if more than one impulse is involved?

The state of current knowledge with regard to the first question has been treated by Edelbaum in a recent paper, Ref. 2. This problem is probably the most difficult of the four. It is apparent that single-impulse transfers are possible only if the terminal orbits intersect; but in most cases which have been investigated numerically, single-impulse transfers have been found to be less economical than multi-impulse transfers. Most frequently, two impulses are considered in planning practical orbit transfers because, on the one hand, terminal orbits do not always intersect and, even when they do, single-impulse transfers may be costly of fuel; and on the other hand, multi-impulse transfers (greater than two) require repeated restarting of propulsion engines which introduces reliability and lifetime problems. These considerations will become less crucial as space flight is made routine, however, and if substantial savings are available through multiple applications of thrust, these savings may eventually be realized.

The question of where to apply the impulses has received somewhat more attention since, once it has been assumed that a certain number of impulses is to be applied in a given problem, the best locations of the impulses can be determined by numerical search. Generally speaking, any point on an ellipse is a possible impulse point, except in a single-impulse transfer when the intersection point of the ellipses must be used. Of the known

minimizing solutions, all but Lawden's symmetric transfer (described below) involve thrust impulses applied at apses of the transfer and terminal ellipses. On the basis of some numerical solutions to two-impulse coplanar transfers in Ref. 3, it was noted that when the terminal orbits intersect, impulse requirements are sensitive to the points of application of the two impulses. For nonintersecting orbits, however, total impulse was found to be relatively insensitive to the location of impulse points.

It has been shown by Moyer, in Ref. 4, that the thrust direction for an optimum single-impulse coplanar transfer always lies between the velocity vector and the local horizontal and tends to be closer to the latter. The impulse may also be exactly opposite, i.e., 180 deg from this direction, but in either case it will result in a relatively small change in direction of the velocity vector.

Magnitudes of the individual impulses in a multiple-impulse transfer vary from case to case, but show one tendency which can be explained. When large energy changes are necessary, the major part of the total impulse is usually applied at the terminal point closest to the center of attraction because energy can be added most efficiently where velocity is greatest, and velocity is greatest near the focus.

Only two minimizing solutions are known for time-free transfer when the orbits are all coplanar ellipses. One of these is the familiar Hohmann-type transfer between co-apsidal ellipses which requires tangential impulses applied at the apses. Figure 1 is a summary of known solutions of this type as described in Ref. 5. The second known solution was obtained by both Plimmer and Lawden, Refs. 5 and 6, and is a transfer between congruent ellipses whose major axes are skewed. This case, referred to herein as a symmetric transfer, involves a coasting orbit whose major axis is the line of symmetry of the transfer. A typical example of a symmetric transfer is presented in Fig. 2 which is taken from Ref. 5.

Some other solutions which are small perturbations of the Hohmann-type transfer have been developed for coplanar coaxial ellipses, Ref. 7, and inclined coaxial ellipses, Ref. 8. In a recent work, Ref. 9, several interesting discoveries were made concerning coplanar transfers. Reference 9 is especially pertinent to the first problem treated in the present study.

METHOD OF ANALYSIS

The problem of determining the optimal, time-free impulsive transfer between two elliptic terminal orbits in an inverse-square field may be treated as a problem in the calculus of variations since it requires the determination of a trajectory $x(t)$ which minimizes a functional, in this case ΔV. Much of

the pioneering work in solving this problem has been done by Lawden, and in Ref. 1 his contributions are summarized in a concise form. Of particular interest for this study has been Lawden's derivation of the primer vector in his general theory of optimal rocket trajectories.

The primer can best be described as a vector formed from components which are Lagrange multipliers introduced in the variational treatment of the problem. The multipliers which constitute the primer are those which are introduced in association with the velocity components of the state vector. Since the multipliers are often referred to as adjoint variables, the primer itself is often referred to as an adjoint vector.

One of Lawden's major contributions, and the foundation upon which the method used in this study was constructed, is the discovery of the primer and its characteristics. The primer always points in the direction of optimum thrust application, and thrusting periods are determined by the value of the primer. That is, when the primer exceeds a certain value, thrust is turned on full, and when it is less than this value, thrust is turned off. If an intermediate thrust arc is part of the trajectory, the primer is constant over this arc.

For the case of impulsive application of thrust treated in the present study, thrust is considered to be infinite in magnitude and to act over an infinitesimally small time duration. Lawden has shown that in this case the following conditions for an optimal trajectory must be satisfied (Ref. 1):

1. The primer and its time derivative must be continuous everywhere,

2. Whenever the rocket motor is operative, the thrust must be aligned with the primer which must have a certain constant magnitude, P,

3. The magnitude, p, of the primer must not exceed P on any coasting arc,

4. The time derivative of p is zero at all junction points not coincident with the terminals.

Because of condition 3, the primer assumes its maximum value, P, at each junction. The magnitude of P is arbitrary and is assumed to be unity in the present study. Therefore, whenever $p = P = 1$, a thrust impulse is applied.

A derivation of the equations for the primer components λ, μ, and ν appears in Chapter 5 of Ref. 1. These components are, respectively, in the radial, circumferential, and normal directions and are depicted in Fig. 3. The circumferential direction is defined to be perpendicular to the radius vector in the plane of and in the same sense as the motion. The normal direction completes the right-handed orthogonal triad. The following are

Lawden's equations describing the components of the primer in terms of orbital eccentricity, e, true anomaly, f, and the integration constants, A, B, C, D, E, and F. These equations constitute the starting point of the present study.

$$\lambda = A\cos f + B\sin f + CI_1(e,f) \tag{1}$$

$$\mu = -A\sin f + B(1 + e\cos f) + \frac{D - A\sin f}{1 + e\cos f} + CI_2(e,f) \tag{2}$$

$$\nu = \frac{E\cos f + F\sin f}{1 + e\cos f} \tag{3}$$

$$p^2 = \lambda^2 + \mu^2 + \nu^2 \tag{4}$$

It is of interest to consider the integration constants. The physical interpretation of these constants is better understood when orbital elements are used as state variables rather than the polar coordinates used by Lawden. It is possible to show that these constants are the Lagrange multipliers associated with orbital element state variables. Since the multipliers can be expressed as the partial derivatives of the payoff with respect to the associated state variables (Ref. 10), the following proportionalities indicate the nature of the integration constants.

$$A \propto \partial\Delta V/\partial\omega \tag{5}$$

$$B \propto \partial\Delta V/\partial a \tag{6}$$

$$C \propto \partial\Delta V/\partial t \tag{7}$$

$$D \propto \partial\Delta V/\partial\ell \tag{8}$$

$$E \propto g_1 \frac{\partial \Delta V}{\partial i} + g_2 \frac{\partial \Delta V}{\partial \Omega} \tag{9}$$

$$F \propto g_3 \frac{\partial \Delta V}{\partial i} + g_4 \frac{\partial \Delta V}{\partial \Omega} \tag{10}$$

where g_1, g_2, g_3, g_4 are functions of Ω, ω, and i. For the special case where the time of the transfer is not prescribed, the constant C is zero, thereby eliminating the integral functions I_1 and I_2 (e, f) from the equations.

Under the assumption of impulsive thrust application, an optimal trajectory can be regarded as a succession of coasting arcs separated by junction points which represent impulses. Included in this series of arcs are the terminal orbits themselves. In effect, with time open, the orbital motion of a body in the initial terminal orbit is part of the transfer, since it will coast in this orbit until it reaches the point where the primer is a maximum. At this point, an impulse is applied, thereby establishing a new orbit which is also entered at a maximum of p. But this new orbit must have the unique feature that the primer goes through another equal maximum at some other point (true anomaly); otherwise subsequent transfer to another orbit would not be optimal. At this second maximum of p, transfer is made to the next arc, which may or may not be the final terminal orbit, depending on the optimum number of impulses required to effect the transfer.

In any case, it is evident that by piecing together transfer arcs, the optimum transfer can be generated in this manner. However, only transfer arcs which are characterized by double maxima of p are candidates for optimum coasting arcs. Therefore, by applying Lawden's conditions on p to all elliptic orbits, those arcs which are candidates for optimal coasting arcs may be determined and cataloged.

COPLANAR TRANSFERS

Analysis

Necessary Conditions

The first task to be undertaken is that of cataloging optimum coasting arcs for coplanar transfers. For this case, the equations for the primer components reduce to

$$\lambda = A \cos f + Be \sin f \tag{11}$$

$$\mu = -A \sin f + B (1 + e \cos f) + \frac{D - A \sin f}{1 + e \cos f} \qquad (12)$$

$$p^2 = \lambda^2 + \mu^2 = 1 \qquad (13)$$

where, in Eq. (13) the maximum value of p is arbitrarily set at unity. Since λ and μ are proportional to the direction cosines of p, a thrust angle, ϕ, may be defined as the angle between the projection of p on the λ, μ plane and the perpendicular to the radius vector in the direction of motion (counterclockwise), as shown in Fig. 3.

If an ellipse contains a coasting arc, it will be possible to find a double maximum of p; i.e., there will be two values of f on the orbit for which p is both a local maximum and equal to unity. As many as three maxima and three minima of p are possible in this coplanar problem, but some primer vector loci will contain fewer than two maxima, and most of those which contain two maxima will have unequal peaks. The result is that the category of optimal arcs is restricted to a particular subset of all possible arcs. It will be noted from the form of Eqs. (11) through (13) that the semimajor axis, a, does not appear. Therefore, optimal arcs may be tabulated according to the eccentricity of ellipses of which they are segments, and the size of the ellipses need not be specified.

It now remains to satisfy

$$\frac{\partial p^2}{\partial f} = 0 \qquad (14)$$

and

$$p^2 = 1 \qquad (15)$$

for two values of f for a given e. This process might be done graphically by selecting f, A, and e, and finding the combinations of B and D which satisfy these conditions. For given f, A, and e, two sets of satisfactory values of B and D are found, so that by varying f these sets will form a locus of possible optimal arcs. Each point on the curve represents a value of f. Therefore, if the curve crosses itself, two values of f exist for which Lawden's conditions are met. In Fig. 4, a typical diagram of the B vs D locus is depicted for e = 0.5, A = 0.3. The upper and lower branches of the curve are seen to be symmetrical, with two crossings shown. These crossings represent two congruent arcs which are reflections about the major axis of an e = 0.5 ellipse as indicated by the true anomaly values noted in Fig. 4.

In principle, all optimum coasting arcs could be determined by this graphical approach. However, problems of sensitivity of the results have made it desirable to choose an alternate method, utilizing a computer to obtain sufficient accuracy. If the conditions of Eqs. (14) and (15) are applied to Eqs. (11) through (13), a system of four equations results. The exact form of these equations is given in Appendix A. In functional form they are:

$$p\,(A, B, D, e, f_1) = 1 \tag{16}$$

$$\frac{\partial p\,(A, B, D, e, f_1)}{\partial f_1} = 0 \tag{17}$$

$$p\,(A, B, D, e, f_2) = 1 \tag{18}$$

$$\frac{\partial p\,(A, B, D, e, f_2)}{\partial f_2} = 0 \tag{19}$$

For fixed e and A, these equations constitute a system of four equations in the four unknowns B, D, f_1, and f_2, where the subscripts 1 and 2 refer to the double maximum of p. In addition, a second derivative test insures that the extrema are maxima and not minima. Using Newton's method, these equations have been programmed for the IBM 7094 computer.

Several problems were encountered in obtaining the solutions. The first problem was to isolate the region of acceptable values of A. In the course of pursuing the graphical approach described above, it was observed that two limiting cases, Lawden's symmetric transfer and the Lawden spiral, constitute upper bounds on A, and that at higher values of A, no crossings occurred. Moreover, the form of the equations requires that solutions for A negative duplicate those determined for A positive. Apparently, A is bounded by these limiting cases, and by thus placing bounds on A, the region to be explored was narrowed and the task of calculating and tabulating solutions considerably reduced.

The second problem was one of convergence of the computation scheme. The derivatives in Eqs. (17) and (19) were driven to zero to five significant figures, and the functions in Eqs. (16) and (18) were driven to unity to the same degree of accuracy. Proceeding from A = 0, convergence was achieved over a range of values of A. Then, before the end of the acceptable range of A values was reached, convergence to the desired accuracy was not achievable by the method being employed. But by an alternate method, employing a numerical search technique, some of the nonconvergent cases were forced to convergence to the desired accuracy. Therefore, it was concluded that the maxima had become

extremely flat in this region, causing the Newton-Raphson iteration to fail. The remaining points in the region of slow convergence were obtained to less than the desired accuracy to avoid an excessive penalty in computing time, but in view of the apparent flatness of the maxima, the penalty in ΔV for slight inaccuracies in these data is inconsequential.

If the equations of Appendix A describing necessary conditions for equal maxima of the primer are expanded, it can be shown that an equation of 6th degree in cos f results. Therefore, as many as three maxima and three minima are theoretically possible. However, the square of the primer has been used rather than the primer itself (as a mathematical convenience) and, consequently, three different roots may not actually be attainable. Furthermore, no evidence of a third root was found in the numerical solutions, thereby indicating that only two equal maxima of p occur in the coplanar case.

Limiting Cases

To determine the acceptable region of values of the constant A, several limiting cases were considered. These are the known optimum coplanar transfer solutions. The first is the Hohmann-type transfer for which f_1 and f_2 must be 0 or π, and A = 0. The latter condition results from the fact that all ellipses in a Hohmann-type transfer are co-apsidal, or alternatively, the longitude of peri-apsis, ω, is constant. By Eq. (5) then, A = 0.

Lawden (Ref. 1) shows that the values of B and D are easily obtained for Hohmann-type transfers. There are basically two families. In the first family, impulses at both junction points act in the same direction, either both supporting or both opposing the motion. For this case, the points of intersection occur when

$$B = \pm \tfrac{1}{2} \tag{20}$$

$$D = \pm \tfrac{1}{2} (1 - e^2) \tag{21}$$

In the second family, one impulse supports the motion and one opposes it.

$$B = \pm 1/2e \tag{22}$$

$$D = \mp(1 - e^2)/2e \tag{23}$$

Another limiting case, the symmetric transfer, has B = D = 0. When necessary conditions are applied with this simplification, an equation for A results.

$$A = \frac{\pm(1 + e\cos f)}{\sqrt{(1 + e\cos f)^2 + (3 + 2e\cos f)\sin^2 f}} \tag{24}$$

For given e, the angle f is determined at once from the condition $\partial p/\partial f = 0$, so that the primer is known.

One other limiting case is Lawden's spiral solution. Although these spirals are really intermediate thrust arcs (which were recently shown to be nonoptimal, Refs. 11 and 12) they may be interpreted as consisting of a series of infinitesimal impulses separated by infinitesimal coasting arcs or by almost a 360-deg coast (Ref. 13). Equations for the constants A, B, and D as well as for true anomaly, f, were obtained from Ref. 13. If ϕ is the angle made by the primer with a perpendicular to the radius vector in the direction of motion, and $n = \sin\phi$, then

$$A = \frac{-3n^3(3 - 4n^2)}{e(3 - 5n^2)} \tag{25}$$

$$B = \frac{3n^2\sqrt{1 - n^2}\ (18 - 91n^2 + 149n^4 - 80n^6)}{e^2(3 - 4n^2)(3 - 5n^2)^2} \tag{26}$$

$$D = \frac{3\sqrt{1 - n^2}}{e^2(3 - 5n^2)(3 - 4n^2)}\left[e^2(3 - 4n^2)^2(1 - 7n^2 + 10n^4)\right. \tag{27}$$

$$\left. + (e^2 - 1)n^2(18 - 91n^2 + 149n^4 - 80n^6)\right]$$

$$\tan f = \frac{-2\sqrt{1 - n^2}\ (1 - 2n^2)(3 - 4n^2)}{n(7 - 21n^2 + 16n^4)} \tag{28}$$

Here, $n = \sin\phi$ must be selected to satisfy

$$e^2 = \frac{9n^4(7 - 21n^2 + 16n^4)^2 + 36n^2(1 - n^2)(1 - 2n^2)^2(3 - 4n^2)^2}{(3 - 5n^2)^4} \tag{29}$$

Catalog of Data

The solutions obtained by the method described above follow a distinct pattern. The most striking result is that all optimum transfer arcs fall into one of two families. The first family begins with a Hohmann-type transfer with both supporting or both opposing impulses, and ends with a Lawden spiral solution. This family is henceforward referred to as spiral-limited. The second family begins with a Hohmann-type transfer with impulses opposing one another, and ends with a symmetric transfer. This family is henceforward referred to as symmetric-limited. Representative solutions from these families are presented in Figs. 5 and 6 for $e = 0.5$.

Spiral-limited solutions possess the property that both impulses either oppose or support the motion. In Fig. 5, straight lines join the impulse points which form extremities of optimum coasting arcs with $e = 0.5$. Either segment of the ellipse, i.e., $\Delta f > \pi$ or $< \pi$, may be used. But first, consider arcs entered nearer the focus. It is apparent that the Hohmann-type transfer, the longest arc, is entered at peri-apsis and departed at apo-apsis; the length of the transfer arc decreases monotonically as the spiral solution is approached. None of these arcs includes an apse. With the direction of motion assumed counterclockwise in Fig. 5 and the thrust directions illustrated in the sketch, all arcs are entered with true anomaly in the first or second quadrant, and end with true anomaly in the second quadrant. The spiral solution itself always lies within the range

$$90^\circ \leq f < 125^\circ$$

If points beyond the spiral solution are entry points into the transfer ellipse (coasting arcs $> \pi$), the thrust directions are reversed. Only half the spiral-limited solutions are shown in Fig. 5. The remainder are described by a reflection of the set shown about the major axis of the ellipse. These transfer arcs are identical to those shown but are described by $f = -f$ and $\phi = -\phi$.

Symmetric-limited solutions show a different character, as illustrated in Fig. 6. Here, impulses are always applied in opposition to one another, and coasting arcs all pass through an apse of the ellipse. The limiting solutions are the symmetric transfer and the Hohmann-type transfer. Thrust directions indicated in the sketch are appropriate for arcs entered near the focus ($\Delta f < \pi$); for $\Delta f > \pi$, thrust directions must be reversed. As in the spiral-limited case, reflections exist for all the coasting arcs shown in Fig. 6. Again, these reflected arcs are described by $f = -f$ and $\phi = -\phi$.

In ascertaining the appropriate thrust directions at each junction point in Figs. 5 and 6, the data of Ref. 4 have been invaluable. The method used

herein predicts only the value of tan ϕ at each point so that thrust directions separated by π are always possible. But in Ref. 4, sufficient conditions are given to exclude one of these directions at each point.

The solutions shown in Figs. 5 and 6 are representative of those obtained in the study. It is evident from these diagrams that, even for e = 0.5, many transfer arcs exist, each characterized by specific terminal points and thrust directions. Cataloging of these solutions has been a major goal of the study. A summary of computer output data describing spiral-limited transfers appears in Figs. 7 through 12 and similar data for symmetric-limited transfers appears in Figs. 13 through 18. In view of the way the solutions were generated, all curves are plotted against A. Subscripts 1 and 2 used with the parameters f and ϕ refer to initial and final impulse locations as indicated in Figs. 5 and 6. It is important to realize that any junction point may be an entry point into or departure point from the transfer ellipse. The subscripts are used only to identify the terminals as being nearer peri-apsis (subscript 1), or nearer apo-apsis (subscript 2).

Summary Curves

In order to use the data summarized in Figs. 7 through 18 in practical orbit transfer problems, it is necessary to substitute parameters of physical significance. However, in order to retain the nondimensional character of the solutions and thereby generalize them to orbits of all sizes, no dimensional parameters should be introduced in the final presentation of the data.

Mindful of the foregoing considerations, the following parameters have been chosen for presentation: the radius ratio, r_2/r_1, where the subscripts correspond to the initial and final junction points (only radius ratios greater than unity are tabulated since it is clear that "reflected" solutions account for all ratios less than one); the central angle of the transfer, $\Delta f = f_{T_2} - f_{T_1}$; eccentricity, e; the thrust angles, ϕ_1 and ϕ_2; and the velocity components, w_1 and w_2, normal to the primer at each junction. The significance of w_1 and w_2 lies in the fact that the component of velocity normal to p remains unchanged across a junction point, since all ΔV is applied in the direction of p. Since $\Delta w \equiv 0$ across every junction, this condition must be tested at each such point and the tabulation of w_1 and w_2 is indispensable. Both w_1 and w_2 are nondimensional velocities, having been normalized with respect to the local circular velocity. For chosen values of A and e, the parameters f_1, f_2, ϕ_1 and ϕ_2 may be read from Figs. 7 through 18. The radius ratio and normal velocity may be calculated from known quantities.

$$\frac{r_2}{r_1} = \frac{1 + e \cos f_1}{1 + e \cos f_2} \tag{30}$$

$$w = \left| \sin \phi \sqrt{1 + e \cos f} - \frac{e \sin f \cos \phi}{\sqrt{1 + e \cos f}} \right| \qquad (31)$$

Since the sign of w is unimportant, absolute value signs are used in Eq. (31) so that w will always be recorded as a positive quantity. The final summary curves are presented in Figs. 19 through 23 for the spiral-limited family and in Figs. 24 through 28 for the symmetric-limited solutions. The first curves in each set display radius ratio and central angle of the transfer with e as the parameter. The succeeding curves relate the remaining variables to e and r_2/r_1.

Using the Summary Curves

The solutions summarized in Figs. 19 through 28 constitute all arcs of elliptic orbits which can be used as transfer arcs in putting together an optimal, coplanar transfer between elliptic orbits. However, the problem usually posed is one of selecting the proper arc or arcs to connect known terminal orbits, and nothing has yet been said to specify what orbits may be entered into or departed from using a particular optimal arc. It is possible to solve the general problem, that is, determination of the arc or arcs which should be used to connect given terminal orbits, by using the summary curves. Before describing the method to be used, however, consider the families of orbits which may be joined to a particular arc at a junction point.

The Family of Terminal Orbits

A terminal orbit need have only a single maximum of p. Therefore, all ellipses are potential terminal orbits, although the family of orbits attainable from a given junction is restricted. To obtain the family of terminal orbits related to a given optimal arc, it is necessary only to treat each junction point as a single-impulse transfer, since the same conditions on the primer must be met. The results of Ref. 4, which treats necessary conditions for single-impulse transfers, are therefore directly applicable here. Lawden (Ref. 1, p. 116) gives expressions sufficient for calculating the primer constants, A, B, and D, in terms of e and f on the terminal orbit. For given ΔV, it is then possible to determine e and f for the terminal orbits in terms of known quantities at the junction, and in such a way that the primer is a maximum at that point. Moyer (Ref. 4) points out that when the impulse exceeds a certain value, the primer no longer has an absolute maximum at the junction point. The impulse must, therefore, vary between bounded values. Each ΔV is then associated with one member of the family of terminal orbits reachable at the given junction.

The upper bound on ΔV is more simply understood by considering some possible primer loci in Fig. 29. The heavy curve displays a double maximum of p and is therefore the locus of a member of the family of optimal transfer arcs. When

an impulse is applied at one of the indicated maxima (point B) the primer locus is deformed; i.e., a new locus is formed which is tangent to the transfer arc locus at the junction point, and which has no higher maxima than that at the tangent point, B. A small ΔV produces a small deformation, such as curve a. Larger ΔV's produce correspondingly larger deformations, e.g., curve b, until, at some value of ΔV, a locus, c, with two equal maxima is produced. It is clear, then, that a still larger ΔV will result in a maximum at C which is higher than that at B. But this case is impossible since the terminal orbit must be entered at an absolute maximum of p. Therefore, as pointed out in Ref. 4, an upper limit on ΔV exists.

Multiple-Impulse Transfers

The summary curves may be used to construct optimum transfers involving more than one coasting arc since the families of optimum arcs include all coasting arcs which may be used to make up an optimum transfer trajectory. For example, a three-impulse transfer would consist of two optimum coasting arcs joined together. At the junction common to both arcs, however, continuity conditions on r, ϕ, and w must be satisfied. That is, the junction requires a unique radius common to the appropriate terminal of each arc, equal values of ϕ to assure continuity of the primer across the junction, and equal values of w, since the normal component of velocity is unchanged by the impulse. If a plot of w vs ϕ is made using the data provided by the summary curves, arcs which may be joined together will be identified by crossings of their curves on the diagram. (The radius constraint is automatically satisfied since w is nondimensionalized by the local circular velocity.)

While the method is feasible in principle, it suffers some serious drawbacks. First, the region of crossings is so extensive, and hence the number of cases to be tested so great, that it is impractical to consider this approach. Secondly, even if the crossings could be analyzed, the resulting transfer arcs would be extremely difficult to catalog, and they would still have to be tested against two-impulse transfers in particular problems to determine which is superior.

Finally, a recent paper by Marchal (Ref. 9), indicates that the region of optimum three-impulse transfers is restricted to a very small class of terminal orbits for which the ratio of the maximum apo-apsis radius to the minimum peri-apsis radius ≥ 21.0. Recently, two further limitations were added, (Ref. 14).

$$0^\circ < |\omega_1 - \omega_2| < 22^\circ$$
$$e_1 + e_2 > 1.7127 \qquad (32)$$

It is clear that both e_1 and e_2 must be large and that the angle between major axes of the terminal orbits is quite restricted.

Fixed Terminal Orbits

The most practical application to which the summary curves can be put is that of determining the optimum transfer by two impulses between prescribed terminal orbits. Fortunately, this problem can be solved, and although the method involved is laborious, it requires only plotting and routine hand calculation to accomplish the desired objective.

The method assumes complete knowledge of the terminal orbits, to be designated by subscripts I for the initial orbit and II for the final orbit. It is assumed that ω_I, the angle between the reference line and peri-apsis of orbit I, is zero as shown in Fig. 30, although this assumption in no way limits the choice of orbits. All angles are measured from a fixed reference line, and the angle β, with appropriate subscript, measures the angular travel from the reference line to a junction point. The subscript T refers to the transfer arc.

The first step is to assume impulse points 1 and 2, that is, to specify β_1 and β_2. This process determines Δf and r_2/r_1.

$$\Delta f = \beta_2 - \beta_1 \tag{33}$$

$$\frac{r_2}{r_1} = \frac{\ell_{II}}{\ell_I} \cdot \frac{1 + e_I \cos \beta_1}{1 + e_{II} \cos (\beta_2 - \omega_{II})} \tag{34}$$

Now, using the summary curves for r_2/r_1 vs Δf, e_T is determined (each family of transfer arcs must be investigated separately). This in turn permits determination of w_{T1}, the velocity normal to the thrust direction on the transfer orbit, and ϕ, the thrust angle at junction 1. The normal velocity on the initial terminal orbit, w_I, may then be calculated.

$$\tan \theta_I = \frac{e_I \sin \beta_1}{1 + e_I \cos \beta_1} \tag{35}$$

$$w_I = \sqrt{2 - r_1/a_I} \sin (\theta_I - \phi_1) \tag{36}$$

The angle θ is measured between the velocity vector and the perpendicular to the radius at the impulse point. (A diagram illustrating the geometry at an impulse point is provided in Fig. 31.) It is noted that Eq. (31) is an alterative

expression for w if appropriate subscripts are used.

Since w_{T1} and w_I will generally be unequal, it is necessary to vary β_2 to find the locations (β_2^*) of the second impulse point for which $w_{T1} = w_I$. By considering many values of β_2, curves of w_{T1} and w_I vs β_2 are generated; crossings of these curves indicate values of β_2^*, i.e., locations of the second impulse point which satisfy the necessary conditions for the assumed β_1. At these points, ϕ_2 and w_{T2} are read from the curves and w_{II} is calculated.

$$\tan \theta_{II} = \frac{e_{II} \sin (\beta_2 - \omega_{II})}{1 + e_{II} \cos (\beta_2 - \omega_{II})} \tag{37}$$

$$w_{II} = \sqrt{2 - r_2/a_{II}} \sin (\theta_{II} - \phi_2) \tag{38}$$

If this calculation is now repeated for a range of values of β_1, curves of w_{T2} and w_{II} vs β_1 are generated; crossings of these curves indicate values of β_1^*, i.e., locations of the first impulse point which satisfy the necessary conditions for the corresponding β_2^*'s. Since it is not known, at the outset, into which family of optimal arcs the final solution will fall, it is necessary to consider both families. In some problems it may be evident that one or the other family cannot contain the solution and this knowledge would result in a considerable saving in labor. However, if a final solution is found in the first family, it is not safe to eliminate the other from consideration, since the solutions obtained can be considered as only local and not global minima.

One simplification which may be made results from a conclusion of Ref. 4, where it was shown that thrust is always applied in a direction which lies between the local velocity vector and the perpendicular to the local radius (or 180 deg from this direction). In view of this result, the assumption can be made that $|\theta| \geq |\phi|$. Furthermore, θ and ϕ will always have the same sign, i.e., both velocity and thrust directions lie on the same side of the local horizontal. Therefore, it is permissible to assume positive signs for both θ and ϕ in performing the calculations, and as a result, w will also be positive.

In using the summary curves for optimal arcs, Figs. 19 through 28, it is important to bear in mind that only radius ratios greater than or equal to unity are plotted. Reflections of these curves occur for $r_2/r_1 > 1$, and such cases must be investigated in solving a problem. Cases not plotted include $\Delta f > \pi$ and $f_{T1} > \pi$. As an aid in relating the data in the summary curves to the pictorial diagrams in Figs. 5 and 6, the following table has been prepared.

TABLE I

Family	r_2/r_1	f_1 Radians	Δf Radians	Impulse Directions
Spiral-limited	> 1	> 0	$< \pi$	S-S
Spiral-limited	> 1	< 0	$> \pi$	S-S
Spiral-limited	< 1	$> \pi$	$< \pi$	O-O
Spiral-limited	< 1	$< \pi$	$> \pi$	O-O
Symmetric-limited	> 1	> 0	$< \pi$	S-O
Symmetric-limited	> 1	< 0	$> \pi$	S-O
Symmetric-limited	< 1	$> \pi$	$> \pi$	S-O
Symmetric-limited	< 1	$< \pi$	$< \pi$	S-O

The last column refers to the thrust directions, S designating an impulse in support of the motion and O an impulse which opposes the motion. It is interesting that all symmetric-limited transfers are of the S-O type, so that if an optimal arc is entered by an opposing impulse it is always of the spiral-limited family.

As a further aid in solving problems by this technique, a flow chart describing the essential features of the method is provided in Appendix B.

Solutions to a number of time-free orbital transfer problems are presented in Ref. 3, using data from Ref. 15. In the latter paper, a steepest-descent program was carried out by a digital computer to obtain the optimum transfer solutions. One of these cases was selected for solution by the graphical approach described above in order to illustrate the method. Terminal orbits of the following characteristics were specified for the sample problem:

$$a_I = 1.01 \qquad a_{II} = 1.43$$

$$e_I = 0.10 \qquad e_{II} = 0.40$$

$$\omega_I = 0^\circ \qquad \omega_{II} = 30^\circ$$

In the course of solving the sample transfer problem, the curves depicted in Figs. 32 through 38 were prepared. Values of β_1 and β_2 between 0 and 2π were chosen, and only enough points were calculated to adequately determine crossings. Since $|\theta| \geq |\phi|$, combinations of β_1 and β_2 which failed to satisfy this inequality were eliminated, thereby resulting in breaks in the curves.

Beginning with Figs. 32 and 34 for the spiral-limited family, it is apparent that several sequences of crossings occur as β_1 is varied between 0 and 2π (the heavy dots for $\beta_1 = 0$ and π are single-point curves which belong to a sequence of crossings). When these are plotted as curves of w_{II} and w_{T2} against β_1, the sequences are seen to describe solutions of the types listed in Table I. However, only one sequence displays a crossing in the w_{II} and w_{T2} vs β_1 plots in Fig. 35; this then is a solution which satisfies all the criteria for a local minimum of ΔV. Similar sets of curves are shown in Figs. 36 to 38 for the symmetric-limited family, and in Fig. 38 a second crossing is indicated. This solution and the spiral-limited solution mentioned previously correspond closely, having almost identical transfer ellipses and impulse magnitudes. However, characteristics of the transfer orbits are such that only the symmetric-limited solution is acceptable. The spiral-limited solution is unacceptable because its transfer orbit has greater angular momentum than either terminal orbit ($\ell_I = 1.00 < \ell_T = 1.265 > \ell_{II} = 1.20$). Since the spiral-limited solution requires both impulses in the same direction, the symmetric-limited solution must be the correct choice.

The final solution involves a supporting impulse to enter the transfer orbit and an opposing impulse to establish the final orbit. The transfer ellipse elements are: $e_T = 0.365$, $\ell_T = 1.265$, $a_T = 1.460$, and $\omega_T = 33$ deg. Entry into the transfer ellipse is at $f_{T1} = 7$ deg and departure is at $f_{T2} = 182$ deg so that $\Delta f = 175$ deg and $r_2/r_1 = 2.145$. In the units of Ref. 3, total characteristic velocity for the transfer is $\Delta V/\sqrt{\gamma/\ell_I} = 0.1510$ of which 0.1310 is applied at the first junction and 0.0200 at the second.

Contensou's Spools

In a paper published several years ago, Ref. 16, Contensou considered optimal impulsive transfer from the point of view of the theory of optimal evolution. Briefly, this theory, which is explained in Ref. 16 and elsewhere, considers a dynamic system defined by a position vector $x_i(t)$ and velocity vector $\dot{x}_i(t)$, and interprets, geometrically, the domain achievable to this system at any time, t, in the accompanying hodograph space. The fundamental condition prescribed by the theory is that the geometric figure which describes the state of the system in the hodograph space be convex to assure an optimum trajectory. If it is not convex, the figure must be imbedded in the smallest possible convex body. The theory itself cannot be adequately explained here, but the result, as it pertains to the present study, is illustrated rather simply.

The dynamic system is represented by the elements of an elliptic orbit, a, ℓ, and ω. The variation-of-parameters equations of celestial mechanics are used to describe the motion of the system. That is, the rates of change of these elements can be written in the form

$$\frac{da}{dt} = \alpha f_1 \ (e, E, \phi) \qquad (39)$$

$$\frac{d\ell}{dt} = \alpha f_2 \ (e, E, \phi) \tag{40}$$

$$\frac{d\omega}{dt} = \alpha f_3 \ (e, E, \phi) \tag{41}$$

where E is eccentric anomaly, α is thrust acceleration, and e and ϕ are as defined previously. These equations are the "velocity" components of a state vector composed of a, e, and ω. If only small changes in the elements are permitted, the derivatives in Eqs. 39 to 41 may be replaced by incremental changes in a, ℓ, ω and t. Since t represents the time during which changes are made, i.e., thrusting time, and since thrusting time is zero in the impulsive case, it is convenient to replace t by V as the independent variable. This is easily done using the relation $\alpha = dV/dt$. In terms of small changes of the elements produced by impulses, ΔV, the equations may now be written as:

$$x = \frac{\Delta a}{\Delta V} (e, E, \phi) \tag{42}$$

$$y = \frac{\Delta \ell}{\Delta V} (e, E, \phi) \tag{43}$$

$$z = \frac{\Delta \omega}{\Delta V} (e, E, \phi) \tag{44}$$

Even though time has been replaced by velocity, the equations still represent the rates of change of the system in the sense that, for small velocity increments ΔV, changes in state, Δa, $\Delta \ell$, and $\Delta \omega$ occur. The x, y, z space, then can be thought of as the hodograph space of the system. Contensou showed that for moderate orbital eccentricities, the figure which results has the shape of a spool, as in Fig. 39A. The spool is hollow with walls of finite thickness, the x-y plane as a plane of symmetry, and the z axis as an axis of symmetry. Both the ends, 1, and the lateral surface, 2, are concave except for two small convex regions, 3, on the ends of the spool.

The origin is the initial state; by a velocity increment, ΔV, a new state is established and the locus of reachable new states, by this ΔV, forms the spool. Because of the definitions of x, y, and z, the velocity change, ΔV, is not a parameter of the diagram and may be thought of as unity. Larger ΔV's result in spools of larger dimensions, but with the same shape, as long as changes in the elements are kept small.

Applying the theory, it is required that the figure be convex. However, the spool is obviously convex only in regions 3. Therefore optimal transfers

to the states within 3 are possible directly from the origin by single impulses of magnitude ΔV. Single-impulse transfers to the regions 1 and 2 are possible but nonoptimizing, because the figure is concave over these portions of the surface. The theory requires that the figure be made convex by imbedding the spool within the smallest convex body, which can be thought of as an elastic membrane stretched over the spool. The membrane joins the convex regions by an envelope of straight line segments such as A-A' and B-B' in Fig. 39A. The points A, A', B, and B' are the contact points of the membrane with the spool, and because each such generating line touches the spool at just two points, two-impulse transfers are optimum over the concave portions of the spool. In effect, by using two impulses instead of one, the set of reachable states with a given ΔV is extended from the spool surface to the membrane; or alternately, a smaller ΔV is required to achieve a given state x, y, z, by constructing a smaller spool such that the membrane and not the spool includes the state point.

Contensou verified the geometrical interpretation by considering a known case, namely the Hohmann-type transfer. It is known that if the orbits are co-axial, a Hohmann transfer is optimum. In the x, y, z domain the co-axial condition implies no change in z, since $\Delta\omega = 0$. Therefore, a diagram in the x-y plane is sufficient to describe such transfers. Such a diagram is illustrated in Fig. 39B. Here it is seen that the entire diagram is concave, and the four contact points, L, M, N, and P, must be used as impulse points. The line LM in Fig. 39B is the locus of $E = \pi$, and NP is the locus of $E = 0$. At L and P, $\phi = 0$, and at M and N, $\phi = \pi$. Thus, for example, to transfer to a state between L and N, these points are the contact points of the spool with the membrane and they determine the optimum values of E and ϕ. A forward impulse is applied at $E = \pi$, followed by a backward impulse at $E = 0$, or vice versa, to effect the transfer.

It is interesting that the families of transfers discovered in the course of the present study occupy unique regions on the spool. The symmetric-limited family occupies the lateral surface of the spool, while spiral-limited transfers exist only on the ends of the spool. These families are separated by the small regions, 3, in Fig. 39A over which single-impulse transfers are optimum.

To determine the use of the spools as a tool in understanding optimum orbit transfers, a program was written for the Research Laboratories' digital simulator. Input to the computer consisted of the variation-of-parameters equations in the form of Eqs. (42) through (44). The output was displayed visually as lines of constant E and/or ϕ in a three-axis representation. Figures 40 and 41 depict the shape of the spools and the character of the generating lines for e = 0.5. Generally, lines of constant E run along the length of the spool, forming closed curves. Lines of constant ϕ also form closed curves, but are more nearly perpendicular to the spool axis.

To study the spools systematically, the same views of the output were photographed for a range of eccentricities. The photographs appear in Figs. 40 through 48 for eccentricities ranging between 0.25 and 0.875, (but not in that order). Unfortunately, eccentricities above 0.875 were precluded by storage limitations of the program, and, while an improved program might have alleviated this limitation, time did not permit such an extension.

Considering first a moderate eccentricity, e = 0.5 in Figs. 42 and 43, the upper photograph shows the spool from the direction of the negative z axis (the x-y-z triad is right-handed). Lines of constant E are used to generate the spool; ϕ varies over each generating line. In the lower view, lines of constant E and ϕ are both used to generate the figure, as seen from the direction of the positive x-axis. Here it is seen that the ends of the spool appear convex. Actually it is the four points, L, M, N, and P, in the x-y plane which cause the ends to look convex from this view. These are, of course, the Hohmann transfer points which separate two distinct regions of single-impulse transfers on each end of the spool.

Another interesting view is one looking into the end of the spool. In Fig. 43, two such views, one using E lines and one using ϕ lines, reveal the hollow nature of the figure. Only the z-axis appears in true length in these views.

When eccentricity is increased, the spool displays a general flattening at the ends and a skewed stretching in the lengthwise direction. Three views for e = 0.75 are shown in Fig. 44, the same two orthogonal views shown for e = 0.5, and the end view. In the lowest picture, the flattening of the spools is evident. The stretching and skewing effects are illustrated by the other shots. Further increases in eccentricity accentuate these effects as shown in Figs. 45 and 46 for e = 0.875.

The limiting case of e = 1.0 results in a doubly infinite extension along the x-axis so that the simulation may not be carried out to very high eccentricities. This limitation is unfortunate since a change in character is to be expected at $e \approx 0.925$, according to Ref. 4, where three-impulse transfers are superior to two impulses for some cases.

For e = 1.0, the variation-of-parameters equations reveal the shape of the spool to be doubly-infinite along the x-axis and to form a surface with four humps, Fig. 47. The contact points of the surface consist of: $x = \pm \infty$, where ϕ is undefined and $E = 0$ and 2π respectively; the extreme points on the y-axis, for which $E = \pi$ and $\phi = 0$ or π; and four "hump" points for which $E = \pi/2$ and $3\pi/2$ and $\phi = 0$ or π. An interpretation of these impulse points for e = 1.0 is shown at the bottom of the diagram. One point is always at the origin, corresponding to $x = \pm \infty$ in the sketch. It is to be expected that the value of ϕ be undefined at the origin, since acceleration here is infinite and velocity (ΔV) may be added in any direction. Actually $\phi = \pi/2$ for the

positive x-axis and $3\pi/2$ for the negative x-axis, and these values may be assumed to hold for the first impulse point. The second impulse point lies between $E = \pi/2$, which is at a distance a from the origin, and $E = \pi$, which is the apo-apsis. The second impulse always features $\phi = 0$ or π. Of the four possible combinations shown, two fall into each of the transfer families determined in the study.

When eccentricity is less than 0.5, the spools undergo a flattening in the opposite direction. In Fig. 48, for $e = 0.25$, this effect is especially evident in the second view, while the first view reveals a flattening of the ends of the spool. As $e \rightarrow 0$, Fig. 49, the spool reduces to a plane such that $x = y$. Furthermore, the spool's ends also become flat with $\phi = 0$ on one end and $\phi = \pi$ on the other, and all constant-ϕ lines are vertical (in the z direction). On the upper and lower boundaries, which are concave, E and ϕ vary, but at the sharp end points, $E = \pi/2$ or $3\pi/2$. Thus, the interpretations shown at the bottom of Fig. 49 are possible with the transfer angle always equal to π. Since the peri-apsis point of the circle is arbitrary, the impulses may be applied at any opposing points on the orbit.

In Ref. 9, solutions have been obtained in expansion form for eccentricities that approach zero and 1.0. These solutions are of interest because, as $e \rightarrow 1.0$, a third family of optimum transfer arcs is introduced. The number and locations of impulses for these limiting cases are presented in Ref. 9. Also, as $e \rightarrow 0$, the spiral-limited solutions appear as arcs of varying lengths, with tangential impulses at each terminal.

LINEARIZED NONCOPLANAR TRANSFERS

Linearization of the Problem

The general noncoplanar transfer problem is difficult to solve, even though Lawden has derived expressions for all three primer components (Eqs. 1 through 3). However, it has been shown in previous analyses, Ref. 17 for example, that if the equations of motion are linearized about a circular orbit, the resulting equations for the primer components are greatly simplified, being independent of eccentricity. Significantly, for the linearized problem, the primer remains unchanged throughout an optimum transfer. That is, it remains the same over impulses and coasting arcs of the trajectory (to first order).

The basic assumption in linearization of the problem is that only small changes are allowed in the orbital elements. This assumption is tantamount to specifying that the terminal orbits, as well as the transfer orbits, must be "neighboring" orbits of small eccentricity. With these assumptions, it was shown in Ref. 17 that the primer equations take the form

$$\lambda = A\cos\tau + B\sin\tau \tag{45}$$

$$\mu = D - 2A\sin\tau + 2B\cos\tau \tag{46}$$

$$\nu = G\cos\tau + H\sin\tau \tag{47}$$

In these equations, the independent variable τ is a nondimensional time parameter which was used in Ref. 17. However, to first order, τ is equivalent to angular travel, and therefore Eqs. (45) through (47) are identical to the equations derived by Lawden in Ref. 1 for the case of $e = 0$.

A simplification introduced by Lawden in Chapter 6 of Ref. 1 is also permissible here. The constants A and B may be replaced by grouping terms in the equations and introducing two new constants, R and τ_o, where the latter is a rotation of the angular reference axis.

$$\lambda = R\sin(\tau + \tau_0) \tag{48}$$

$$\mu = D + 2R\cos(\tau + \tau_0) \tag{49}$$

$$\nu = E\cos(\tau + \tau_0) + F\sin(\tau + \tau_0) \tag{50}$$

But, since the direction of the reference axis is arbitrary, it will be assumed that $\tau_o = 0$. The resulting primer equations for the linearized, noncoplanar problem are

$$\lambda = R\sin\tau \tag{51}$$

$$\mu = D + 2R\cos\tau \tag{52}$$

$$\nu = E\cos\tau + F\sin\tau \tag{53}$$

Analysis

The method of treating transfers in the noncoplanar case is the same in principle as that for coplanar arcs except that the primer equations are much simpler and the maxima may be determined exactly. For given values of the constants, the primer locus lies in a plane. In fact, it is interesting to note that the locus is precisely the intersection of the elliptic cylinder

$$4\lambda^2 + (u - D)^2 = 4 \tag{54}$$

and the plane

$$F\lambda + \frac{E(\mu - D)}{2} - R\nu = 0 \tag{55}$$

Moreover, it is possible to show that double maxima of the primer occur only for certain values of the constants.

The problem is essentially to determine two values of τ, say τ_1 and τ_2, such that the following conditions hold:

$$P_1^2 = P_2^2 \tag{56}$$

$$\frac{\partial p_1}{\partial \tau} = 0 \tag{57}$$

$$\frac{\partial p_2}{\partial \tau} = 0 \tag{58}$$

where $P_1 = P(\tau_1)$, $P_2 = P(\tau_2)$, etc. If two such values exist, then the following equations must also hold:

$$P_1^2 - P_2^2 = 0 \tag{59}$$

$$\frac{\partial p_1}{\partial \tau} - \frac{\partial p_2}{\partial \tau} = 0 \tag{60}$$

$$\frac{\partial p_1}{\partial \tau} + \frac{\partial p_2}{\partial \tau} = 0 \tag{61}$$

When the components of the primer are substituted in the above, a system of equations of the following type results:

$$M\psi_{aa}(\tau_1, \tau_2) + N\psi_{ab}(\tau_1, \tau_2) + Q\psi_{ac}(\tau_1, \tau_2) = 0 \tag{62}$$

$$M\psi_{ba}(\tau_1, \tau_2) + N\psi_{bb}(\tau_1, \tau_2) + Q\psi_{bc}(\tau_1, \tau_2) = 0 \tag{63}$$

$$M\psi_{ca}(\tau_1, \tau_2) + N\psi_{cb}(\tau_1, \tau_2) + Q\psi_{cc}(\tau_1, \tau_2) = 0 \tag{64}$$

where

$$\begin{aligned}
M &= 3R^2 + E^2 - F^2 \\
N &= RD \\
Q &= EF \\
\psi_{aa} &= \sin(\tau_1 + \tau_2)\cos\left(\frac{\tau_1 - \tau_2}{2}\right) \\
\psi_{ab} &= 4\sin\left(\frac{\tau_1 + \tau_2}{2}\right) \\
\psi_{ac} &= -2\cos(\tau_1 + \tau_2)\cos\left(\frac{\tau_1 - \tau_2}{2}\right) \\
\psi_{ba} &= -\psi_{ac} \\
\psi_{bb} &= 4\cos\left(\frac{\tau_1 + \tau_2}{2}\right) \\
\psi_{bc} &= 4\psi_{aa} \\
\psi_{ca} &= \sin(\tau_1 + \tau_2)\cos(\tau_1 - \tau_2) \\
\psi_{cb} &= 4\sin\left(\frac{\tau_1 + \tau_2}{2}\right)\cos\left(\frac{\tau_1 - \tau_2}{2}\right) \\
\psi_{cc} &= -2\cos(\tau_1 + \tau_2)\cos(\tau_1 - \tau_2)
\end{aligned} \tag{65}$$

If Eqs. (62) through (64) are to have a solution for arbitrary values of the constants M, N, and Q, the determinant of coefficients must vanish. That is, omitting the arguments τ_1 and τ_2 to simplify notation,

$$\begin{vmatrix} \psi_{oo} & \psi_{ob} & \psi_{oc} \\ \psi_{bo} & \psi_{bb} & \psi_{bc} \\ \psi_{co} & \psi_{cb} & \psi_{cc} \end{vmatrix} = 0 \tag{66}$$

Expansion of this determinant leads to the very simple result that

$$\cos\left(\frac{\tau_1 - \tau_2}{2}\right) \sin\left(\frac{\tau_1 + \tau_2}{2}\right) = 0 \tag{67}$$

This equation holds for all optimum, linearized, two impulse, noncoplanar transfers. Values of τ_1 and τ_2 which satisfy Eq.(67) constitute the angular positions of the thrusting points of such transfers.

Solutions

Families of Solutions

Examination of Eq. (67) indicates that there are two basic types of possible solutions. These are found by equating to zero each factor of the equation. In addition, there exists a singular solution which results when each of the three coefficients M, N, and Q of Eqs. (62) through (64) vanish. In terms of the constants appearing in Eqs. (51) through (53) the following three families of solutions can be predicted.

(A)
$$\cos\left(\frac{\tau_1 - \tau_2}{2}\right) = 0$$

$$\tau_2 = \tau_1 + \pi$$

$$\tan 2\tau_1 = \left(\frac{2EF}{3R^2 + E^2 - F^2}\right) \tag{68}$$

$$RD = 0$$

(B)

$$\sin\left(\frac{\tau_1 + \tau_2}{2}\right) = 0$$

$$\tau_2 = -\tau_1$$

$$\cos\tau_1 = \frac{-2RD}{3R^2 + E^2 - F^2} \tag{69}$$

$$E = 0$$

$$4R^2D^2 \leq (3R^2 - F^2)^2$$

$$3R^2 < F^2$$

(C)

$$D = 0$$
$$E = 0 \tag{70}$$
$$3R^2 = F^2$$

The inequalities of Eq. (69) insure that $\cos\tau_1 \leq 1$, and that the stationary point is an actual maximum.

It is apparent from Eqs. (68) that all transfers of type (A) have central angles of 180 deg, since τ_1 and τ_2 are longitudes of the impulse points. Noncoplanar transfers of the Hohmann type, as discussed by Long in Ref. 8, must therefore be special cases within (A) since apsidal impulse points are required for the Hohmann-type transfers but are not required in family (A).

Family (B) transfers possess the unique feature that $\tau_2 = -\tau_1$, so that transfers of all central angles are included in this family. The special case $\tau_1 = 90$ deg, $\tau_2 = -90$ deg is one which belongs to both families (A) and (B).

The above equations express the necessary conditions required to determine all the optimal arcs for transfer between neighboring, low-eccentricity orbits. The problem of cataloging these results in some manner so as to be useful in a particular transfer maneuver still remains.

It should be pointed out here that the method followed in cataloging coplanar transfers could have been pursued in the noncoplanar problem too. However, in the former case, an explicit solution of the two point boundary value problem was not possible, whereas the linearized noncoplanar problem can

be solved entirely. The results can be expressed in terms of the characteristics of the terminal orbits, facilitating the calculation of ΔV (and other pertinent parameters) for arbitrary two-impulse transfers. To this end, the Lagrange planetary variables are now introduced as a means of determining instantaneous changes in the orbital elements. These variables are particularly useful because, through their use, singularities are avoided when i and e approach zero. The entire maneuver is now viewed as a perturbation of the elements at time τ_1 caused by an impulse $u_1 = \Delta V_1/V_0$, followed at time τ_2 by another perturbing impulse, $u_2 = \Delta V_2/V_0$. Multiple-impulse transfers can be treated similarly with the total impulse being the sum of the individual u_i's.

The planetary variables as used herein consist of the nondimensionalized semimajor axis, $x_1 = a/a_0$, and the following combinations of the remaining orbital elements:

$$\begin{aligned} x_2 &= e\sin\omega \\ x_3 &= e\cos\omega \\ x_5 &= \sin i \sin\Omega \sim i\sin\Omega \\ x_6 &= \sin i\cos\Omega \sim i\cos\Omega \end{aligned} \tag{71}$$

The equations for small rates of change of these variables were derived previously in Ref. 17 by starting with the equations for variation of the elements, transforming to the planetary variables, and dropping second and higher degree terms in e, i and Δa.

$$\frac{dx_1}{d\tau} = \frac{2a\mu}{p} \tag{72}$$

$$\frac{dx_2}{d\tau} = \frac{a}{p}(2\mu\sin\tau - \lambda\cos\tau) \tag{73}$$

$$\frac{dx_3}{d\tau} = \frac{a}{p}(2\mu\cos\tau + \lambda\sin\tau) \tag{74}$$

$$\frac{dx_5}{d\tau} = \frac{a}{p}\nu\sin\tau \tag{75}$$

$$\frac{dx_6}{d\tau} = \frac{\alpha}{P}\nu\cos\tau \tag{76}$$

where α is the thrust acceleration. While these equations apply for finite thrust periods, a transformation from time to velocity as the independent variable is desirable for the impulsive case. Assuming small changes in the elements, the dx_i may be replaced by Δx_i, and $\alpha d\tau$ by $\Delta V/V_0$.

$$\frac{\Delta x_1}{\Delta V} = \frac{2\mu}{V_0 P} \tag{77}$$

$$\frac{\Delta x_2}{\Delta V} = \frac{1}{V_0 P}\ (2\mu\sin\tau - \lambda\cos\tau) \tag{78}$$

$$\frac{\Delta x_3}{\Delta V} = \frac{1}{V_0 P}\ (2\mu\cos\tau + \lambda\sin\tau) \tag{79}$$

$$\frac{\Delta x_5}{\Delta V} = \frac{\nu}{V_0 P}\sin\tau \tag{80}$$

$$\frac{\Delta x_6}{\Delta V} = \frac{\nu}{V_0 P}\cos\tau \tag{81}$$

For a given transfer, these equations may be integrated or summed to determine the total change in the orbital elements between initial and final terminal orbits.

Before integrating these equations for the families of transfer arcs, Eqs. (68) through (70), it is noted that no solutions exist for F= 0 and arbitrary values of the remaining constants. Accordingly, the primer components may be normalized by this constant F, eliminating F from the remainder of the analysis. The justification for arbitrarily setting F equal to unity is that the magnitude of the primer at the impulse points is arbitrary, as long as the maxima of p are equal. Since F is never zero it is permissible to normalize with respect to it. The following system is thus derived by substituting the primer components and integrating over two impulses:

$$P\cdot\Delta x_1 = 2D(u_1 + u_2) + 4R(u_1\cos\tau_1 + u_2\cos\tau_2) \tag{82}$$

$$P\cdot\Delta x_2 = 2D(u_1\sin\tau_1 + u_2\sin\tau_2) + 3R(u_1\sin\tau_1\cos\tau_1 + u_2\sin\tau_2\cos\tau_2) \qquad (83)$$

$$P\cdot\Delta x_3 = 2D(u_1\cos\tau_1 + u_2\cos\tau_2) + R(u_1(1 + 3\cos^2\tau_1) + u_2(1 + 3\cos^2\tau_2)) \qquad (84)$$

$$P\cdot\Delta x_5 = E(u_1\sin\tau_1\cos\tau_1 + u_2\sin\tau_2\cos\tau_2) + u_1\sin^2\tau_1 + u_2\sin^2\tau_2 \qquad (85)$$

$$P\cdot\Delta x_6 = E(u_1\cos^2\tau_1 + u_2\cos^2\tau_2) + u_1\sin\tau_1\cos\tau_1 + u_2\sin\tau_2\cos\tau_2 \qquad (86)$$

These equations must now be investigated for each of the families predicted in Eqs. (68) through (70). Consider the family of solutions (B) with Eqs. (69) above. It is seen that $\tau_2 = -\tau_1$, $\cos\tau_2 = \cos\tau_1$, and $\sin\tau_2 = -\sin\tau_1$. A few definitions are necessary to facilitate the derivation of the equations.

$$\tan\bar{\varpi} \equiv \frac{\Delta x_2}{\Delta x_3} \qquad \tan\bar{\Omega} \equiv \frac{\Delta x_5}{\Delta x_6} \qquad T \equiv \tan(\bar{\varpi} - \bar{\Omega})$$

$$u = u_1 + u_2 \qquad \delta = \frac{u_2}{u} \qquad 1 - 2\delta = \frac{u_1 - u_2}{u} \qquad (87)$$

Since u represents the total, nondimensional, characteristic velocity of the transfer it is clear that δ is merely the fraction of u expended at the second impulse point. The variables $\bar{\varpi}$ and $\bar{\Omega}$ are explained in Fig. 50. In the upper diagram the variables x_2 and x_3 are seen to represent components of an "eccentricity vector" defined by magnitude e and argument ω. Thus, if subscripts 1 and 2 denote terminal orbits, the vectors $\bar{e}_1$, and $\bar{e}_2$ are described by e_1, e_2, ω_1 and ω_2. The vector change in eccentricity which results from a transfer from orbit 1 to orbit 2 is defined by Δe and $\bar{\varpi}$ as shown in the sketch. It is clear that tan ϖ is the ratio of Δx_2 to Δx_3.

The angle $\bar{\Omega}$ in the lower diagram of Fig. 50 has a similar interpretation. In this case the magnitude of a vector is i and its argument is Ω. Therefore $\bar{\Omega}$ may be thought of as the argument of the vector change in inclination.

Substituting Eqs. (69) as well as the absolute value, P, of the primer in Eqs. (82) through (86) yields

$$\frac{\Delta x_1}{u} = \frac{2c\sqrt{1+R^2}}{\sqrt{(1-3R^2)c^2+4R^2}} \tag{88}$$

$$\frac{\Delta x_2}{u} = \frac{2(1-2\delta)cs}{\sqrt{1+R^2}\sqrt{(1-3R^2)c^2+4R^2}} \tag{89}$$

$$\frac{\Delta x_3}{u} = \frac{2(c^2+R^2)}{\sqrt{1+R^2}\sqrt{(1-3R^2)c^2+4R^2}} \tag{90}$$

$$\frac{\Delta x_5}{u} = \frac{2Rs^2}{\sqrt{1+R^2}\sqrt{(1-3R^2)c^2+4R^2}} \tag{91}$$

$$\frac{\Delta x_6}{u} = \frac{2R(1-2\delta)}{\sqrt{1+R^2}\sqrt{(1-3R^2)c^2+4R^2}} \tag{92}$$

In these equations $c = \cos \tau_1$, $s = \sin \tau_1$, and the constant D has been replaced by its equivalent from Eq. (69), $(1-3R^2)c/2R$. (Note that due to the normalization of the equations, the constant F no longer appears.) It then follows by Eqs. (87) that

$$T = \frac{(1-2\delta)^2c^2s - (c^2+R^2)s}{(1-2\delta)(1+R^2)c} \tag{93}$$

or

$$(1-2\delta) = \frac{T(1+R^2) - \sqrt{T^2(1+R^2)^2 + 4s^2(c^2+R^2)}}{2sc} \tag{94}$$

Noting from Eqs. (71) and (83) through (86) that

$$\frac{\Delta e}{u} = \frac{\Delta x_2}{u} \sin \bar{\omega} + \frac{\Delta x_3}{u} \cos \bar{\omega} \tag{95}$$

and

$$\frac{\Delta i}{u} = \frac{\Delta x_5}{u} \sin \bar{\Omega} + \frac{\Delta x_6}{u} \cos \bar{\Omega} \tag{96}$$

the following equations for small changes in the three orbital elements a/a_o, e, and i may be derived:

$$\frac{\Delta \frac{a}{a_o}}{u} = \frac{2c\sqrt{1+R^2}}{\sqrt{(1-3R^2)c^2 + 4R^2}} \tag{97}$$

$$\frac{\Delta e}{u} = \sqrt{\frac{2}{(1-3R^2)c^2 + 4R^2}} \left[T^2(1+R^2) + 2(c^2+R^2) - T\sqrt{T^2(1+R^2)^2 + 4s^2(c^2+R^2)} \right]^{\frac{1}{2}} \tag{98}$$

$$\frac{\Delta i}{u} = R\sqrt{\frac{2}{(1-3R^2)c^2 + 4R^2}} \left[T^2(1+R^2) + 2s^2 - T\sqrt{T^2(1+R^2)^2 + 4s^2(c^2+R^2)} \right]^{\frac{1}{2}} \tag{99}$$

These equations hold only for family B. However, similar equations may be derived in the same manner for the solutions (A) with Eq. (68). When D = 0,

$$\frac{\Delta \frac{a}{a_o}}{u} = \frac{(1-2\delta)}{\sqrt{1+T^2}} \left(\frac{\Delta e}{u}\right) \tag{100}$$

$$\frac{\Delta e}{u} = 2\sqrt{\frac{(1+4ET)(1+T^2)}{(1+ET)(1+16T^2)}} \tag{101}$$

$$\frac{\Delta i}{u} = \sqrt{\frac{3T(4T-E)}{(1+ET)(1+16T^2)}} \tag{102}$$

A special case (A') for solutions of type (A) exists for which $R = T = 0$ and $D \neq 0$. The following are the equations for the changes in the orbital elements for family A'.

$$\frac{\Delta \frac{a}{a_o}}{u} = \frac{2D}{\sqrt{1 + E^2 + D^2}} \tag{103}$$

$$\frac{\Delta e}{u} = \frac{2D(1 - 2\delta)}{\sqrt{1 + E^2 + D^2}} \tag{104}$$

$$\frac{\Delta i}{u} = \frac{\sqrt{1 + E^2}}{\sqrt{1 + E^2 + D^2}} \tag{105}$$

Representation of Solutions

Because of the large number of parameters required to describe a noncoplanar transfer, it is difficult to represent the optimum solutions in a straight forward manner. For example, while Figs. 5 and 6 clearly describe the behavior of the primer over coplanar transfer ellipses, a similar diagram in the noncoplanar case requires an out-of-plane thrust component. Therefore the behavior of the primer cannot be adequately represented in two dimensions.

Even though the number of physically significant parameters is numerous however, there is a concise way of representing the noncoplanar transfers if new parameters are introduced. These are the quantities $\bar{\Omega}$, $\bar{\omega}$ and T defined in Fig. 50 and by Eqs. (87) above. As has been explained in the preceding discussion the parameters $\bar{\omega}$ and $\bar{\Omega}$ represent the arguments of changes in vector eccentricity and inclination. They therefore have indirect physical significance in that the parameters can be measured in a vector diagram of the type shown in Fig. 50, but they do not appear directly in a diagram of the transfer trajectory itself.

In Figs. 51 through 53 noncoplanar transfers have been summarized for all possible changes in the elements of the elliptic terminal orbits, $\Delta(a/a_o)/u$, $\Delta e/u$ and $\Delta i/u$. The angle $\bar{\omega} - \bar{\Omega} = \tan^{-1} T$ has been held fixed in each diagram. If this angle is 20 deg, for example, and the elemental changes Δa, Δe and Δi are given, then the nondimensional characteristic velocity, u, of the transfer can be determined from Fig. 52. Of course $\bar{\omega} - \bar{\Omega}$ must be calculated from e_1, e_2, i_1, i_2, ω_1, ω_2, Ω_1 and Ω_2 in a particular case, and interpolation between

diagrams would ordinarily be required to determine u. Therefore it is apparent that these diagrams are insufficient to summarize all noncoplanar transfers but are intended only to illustrate the behavior of the solutions, particularly with regard to the domain of solution space occupied by the three families determined in the analysis. The different families of solutions are indicated by shaded areas in these diagrams. It is noted that as $\bar{\omega} - \bar{\Omega}$ increases, the singular region grows, while at $\bar{\omega} - \bar{\Omega} = 0$ the singular region shrinks to a point in the upper right-hand corner of the diagram.

While the practical use of the diagrams is limited, it should be pointed out that the above sets of equations lead to an explicit determination of the optimal transfer between terminal orbits whose elements are known, for it is possible to eliminate the constants in these equations until all the important parameters depend only on the changes in the orbital elements. The algebraic derivation of these relations is simple and straightforward, but lengthy. Therefore the derivation is not included here. However, the complete set of equations governing an optimal transfer, as well as the procedure for calculating these transfers for fixed terminal orbits, may be found in Appendix C. Only the expressions for the total impulse for each case are listed below. Here, u_B refers to the solution defined by Eqs. (97) through (99), u_A to Eqs. (100) through (102), and $u_{A'}$ to Eqs. (103) through (105).

$$u_B^2 = \frac{1}{4}\left[2(\Delta i)^2 + 2(\Delta e)^2 - (\Delta \frac{a}{a_o})^2\right] + \frac{\sqrt{(1+T^2)\left[\left[(\Delta e)^2 + (\Delta\frac{a}{a_o})^2 + (\Delta i)^2\right]^2 - 4(\Delta e)^2(\Delta\frac{a}{a_o})^2\right] - 4(\Delta e)^2(\Delta i)^2}}{2\sqrt{1+T^2}} \tag{106}$$

$$u_A^2 = \frac{(\Delta e)^2(1+4T^2) + 4(1+T^2)(\Delta i)^2}{4(1+T^2)} \qquad T^2 \le \left(\frac{\Delta e}{\Delta a}\right)^2 - 1 \tag{107}$$

$$u_{A'}^2 = 4(\Delta i)^2 + (\Delta\frac{a}{a_o})^2 \qquad (\Delta e)^2 \le (\Delta a)^2 \tag{108}$$

The above discussion outlines the method of determining the optimum among all two-impulse solutions. However, such solutions are determinate only when all the quantities involved (as they appear in Appendix C) are meaningful and all inequality constraints are satisfied. If, for a particular case, these

conditions are not met, then the solution must be of a singular nature. These singular solutions result when the primer vector is everywhere constant, i.e., when $E = D = 0$ and $R^2 = 1/3$. The desired changes in the elements correspond to a point in the singular region on diagrams of the type indicated in Figs. 51 through 53.

The singular solutions correspond to three-or-more-impulse maneuvers. The boundary conditions cannot be satisfied using only two impulses. It is necessary to integrate the equations of state assuming three or more impulses placed so as to satisfy the given boundary conditions. Indications are that three impulses will generally suffice.

Sample Calculation

To illustrate the use of the equations in Appendix C for calculating noncoplanar transfers, a sample case has been computed. It consists of a transfer between low altitude Earth orbits of small eccentricity and inclination. If a reference orbit altitude of 150 n mi is chosen and the terminal orbits are of such size that $\Delta a/a_0 = 0.001$, then $a_2 = 3591.795$ n m and $a_1 = 3588.205$ n m, where Earth's radius is 3440 n m. The eccentricities of the orbits are assumed to be $e_1 = e_2 = 0.001$. For convenience the inclination of the first orbit is assumed to be zero, and Ω_1 is chosen as identical with Ω_2. The remaining orbit elements which must be chosen are i_2, ω_2, and ω_1. The value of Ω_2 is not arbitrary but depends upon the type of transfer and the initial direction of the radial reference axis. The inclination i_2 is set at 0.01 radians, or a little more than half a degree. The other parameters are arbitrarily chosen as $\omega_2 = 90$ deg and $\omega_1 = 1$ deg.

The first step in the computation was to determine the family into which the transfer falls. Accordingly, the inequalities of Equations (C-5) through (C-11) of appendix C were tested and required that this particular transfer belong to family (A).

Equations (C-12) of Appendix C are now employed successively to calculate the characteristics of the transfer. Thus

$$
\begin{aligned}
D &= 0 \\
\tau_1 &= -0.444 \text{ deg} \\
\tau_2 &= 179.556 \text{ deg} \\
u^2 &= 0.0001005 \\
E &= -128.4615021 \\
R &= 4.5019246 \\
\delta &= 0.1433198 \\
\Omega_2 &= -0.444 \text{ deg}
\end{aligned}
$$

The components of the incremental ΔV at each impulse point can be calculated by properly scaling the primer components λ, μ, ν. For example, at the first impulse point Eqs. (51) through (53) give

$$\lambda_1 = -0.0349152$$
$$\mu_1 = 9.0035783$$
$$\nu_1 = -128.4653950$$

If these are scaled so that their modulus is u, then the ΔV components at the first impulse point can be calculated. Thus

$$\frac{\Delta V_\lambda}{V_o} = -0.0000023$$

$$\frac{\Delta V_\mu}{V_o} = 0.0006004$$

$$\frac{\Delta V_\nu}{V_o} = -0.0085674$$

The velocity components on the initial terminal orbit are easily calculated from standard equations so that addition of the above ΔV components yields the velocity components on the transfer ellipse at this point. This in turn permits calculation of the elements of the transfer ellipse.

$$\frac{a_T}{a_o} = 1.0068241$$

$$e_T = 0.0780024$$

$$\frac{\ell_T}{a_o} = 1.0006981$$

$$i_T = 0.5111 \text{ deg}$$

The angular positions of the impulse points are provided by τ_1 and τ_2. In the initial terminal orbit the impulse occurs at $f_1 = \tau_1 - \Omega_1 - \omega_1$. The final terminal orbit is entered at $f_2 = \tau_2 - \Omega_2 - \omega_2$. Therefore, $f_1 = -\omega_1 = -1.0$ deg and $f_2 = 90.0$ deg. Radii of the impulse points are then easily determined by

$$\frac{r}{\ell} = \frac{1}{1 + e \cos f} \tag{109}$$

Thus

$$\frac{r_1}{a_o} = 0.9985006$$

$$\frac{r_2}{a_o} = 1.0004990$$

True anomalies of the impulse points in the transfer ellipse can now be calculated from

$$\cos f = \frac{1}{e}\left[\frac{\ell}{r} - 1\right] \tag{110}$$

Thus

$$f_{T1} = 88.383 \text{ deg}$$

$$f_{T2} = 269.854 \text{ deg}$$

and finally

$$\Delta f_T = 181.471 \text{ deg}$$

The last figure gives an estimate of the error involved in the calculation since type (A) transfers have central angles of 180 deg. The angular error is then 1.471 deg in a transfer arc of 180 deg, for an error of 0.817 per cent in Δf_T.

In using the noncoplanar solution equations it must be understood that it is the parameters Δa, e, and i which have been assumed small. Errors are introduced when any of these parameters are not sufficiently small that their second degree terms may be neglected, although there is no simple way of knowing in advance that this is true in a given case. Still, it is apparent that if values of 0.1 are chosen in these parameters, the square of each parameter is smaller than the parameter itself only by a factor of ten. When the values are chosen to be 0.001, their squares are smaller by three orders of magnitude. In the latter case it is to be expected that the linear solution will be quite accurate, but in the former case large errors may be introduced.

Previous experience with linear solutions of this type indicates that for marginal cases, some of the linear solution equations will closely represent the

exact solution, even while others fail badly. For example, in Ref. 18, a linear solution for low thrust rendevous and transfer was applied to Earth-Mars and Earth-Venus trajectories with some success even though the linearizing assumptions were not expected to hold. In that instance it was found that the prediction of thrust direction was good in cases where fuel consumption was badly in error. Furthermore it was found that though the magnitudes of the errors were large in some cases, the general character of the solutions (i.e., variation with launch date) closely resembled the exact solution.

In view of the significance of near-Earth rendezvous and transfer at the present time, the linearized noncoplanar solution might be applied to predict optimum maneuvers in cases where only small changes are required. Recent experiments in the Gemini program have involved orbit changes which fall within the linearizing assumptions. Therefore it is to be expected that the present linear solution could provide at least a first approximation to fuel consumption, thrusting points, and thrusting directions in such transfers.

CONCLUDING REMARKS

Solution of orbital transfer problems by the method of primer vector maximization has been shown to be feasible for time-free transfers between coplanar ellipses and between neighboring noncoplanar orbits of low eccentricity. The method may also hold promise for transfers in fixed time if the complication introduced by an additional parameter is not severe.

Lawden's symmetric transfer and his spiral solution have been shown to be limiting cases of the two families of coplanar transfer arcs determined in the study. Hohmann-type transfers are also limiting cases in both of these families. By using the catalog of optimal arcs presented herein it is possible to solve problems where the two terminal orbits are specified. Although the method of solution is lengthy, it can be accomplished by plotting and desk calculation alone.

When the coplanar problem is interpreted geometrically using the theory of optimal evolution, as described by Contensou, the families of optimal arcs determined in the study can be observed. The families occupy distinct regions on a spool-shaped figure in a hodograph space, and are separated by regions over which single-impulse transfers are optimal.

In the case of noncoplanar transfers between neighboring orbits of low eccentricity, explicit solutions have been obtained in equation form. These equations allow direct calculation of impulse requirements for one- and two-impulse transfers if knowledge of the terminal orbits is complete. Moreover, the regions of solution space in which three or more impulses may be optimal are indicated.

Because the noncoplanar solutions have been obtained in closed form, the solution equations may be applied directly to practical problems. An immediate application is the rendezvous of bodies in near circular, neighboring, earth orbits when transfer time is left open. Current rendezvous experiments in the Gemini program involve orbits which fall into this class. Estimates of fuel consumption for arbitrary noncoplanar transfers may be obtained by substitution of the orbital elements of the ellipses into the equations derived in this report.

APPENDIX A

Necessary Conditions for Optimum Coplanar Coasting Arcs

Two conditions must be satisfied at each junction. These are indicated functionally by Eqs. (16) through (19) in the text. The exact form of these equations is:

$$p^2 = A^2 + 2B(D - 2A\sin f) + B^2(1 + e^2 + 2e\cos f) + \frac{D^2 - 2AD\sin f(2 + e\cos f) + A^2\sin^2 f(3 + 2e\cos f)}{(1 + e\cos f)^2} \quad \text{(A-1)}$$

$$\frac{\partial p^2}{\partial f} = -2eB^2\sin f - 4AB\cos f + (1 + e\cos f)^{-3}\left\{2eD^2\sin f - 2AD(3e + 2\cos f + e^2\cos f) + 2A^2\sin f(5e + 3\cos f + 2e^2\cos f - 3e\sin^2 f - e^2\sin^2 f\cos f)\right\} \quad \text{(A-2)}$$

With appropriate subscripts, 1 or 2, on p and f these equations can be applied to both junctions.

APPENDIX B

Flow Chart for Solution of Fixed Terminal Orbit Problems

Given: e_I, e_{II}, ℓ_I, ℓ_{II}, ω_{II}, ($\omega_I \equiv 0$)

(a) assume β_1, β_2

(b) compute Δf, r_2/r_1 from Eqs. (33) and (34)

(c) from Figs. 19, 24 determine e_T

from Figs. 20, 25 determine ϕ_1

from Figs. 21, 26 determine w_{T1}

(d) compute θ_I and w_I from Eqs. (35) and (36)

(e) if $w_{T1} \neq w_I$ return to (b) and repeat for new β_2

(f) continue until $w_{T1} = w_I$ at $\beta_2 = \beta_2^*$; find all such β_2^*s

(g) pick a β_2^*; read ϕ_2 and w_{T2} from Figs. 22, 23, 27, 28

(h) compute θ_{II} and w_{II} from Eqs. (37) and (38)

(i) if $w_{T2} \neq w_{II}$ return to (g); repeat for all β_2^*s

(j) continue until $w_{T2} = w_{II}$; all such points are candidates for the optimum two impulse solution; by comparing ΔV's the best solution can be determined

APPENDIX C

Calculation of Noncoplanar Transfers

If the elements of the terminal orbits satisfy e_1, $e_2 \ll 1$, $(a_2 - a_1)/a_0 \ll 1$ and i_1, $i_2 \ll 1$, then the linearizing assumptions are satisfied and the noncoplanar analysis applies. It is assumed that the elements of the terminal orbits are entirely specified. That is, a_1, a_2, e_1, e_2, ω_1, ω_2, i_1, i_2, Ω_1 and Ω_2 are known. A good choice for the circular reference orbit is one for which $a_0 = (a_1 + a_2)/2$, since this minimizes the radial excursion from the origin of the reference axes which lies on the reference orbit.

It is convenient to choose the initial orbit plane as the plane of the reference orbit so that $i_1 \equiv 0$. Since Ω_1 is arbitrary, the choice $\Omega_1 = \Omega_2$ determines the initial direction of the radial reference axis. Then all relevant quantities, including the incremental changes in a, e, and i and the parameter $T \equiv \tan(\bar{\omega}-\bar{\Omega})$, depend only on the geometry of the orbits.

$$\Delta\left(\frac{a}{a_0}\right) = \frac{a_2}{a_0} - \frac{a_1}{a_0} \tag{C-1}$$

$$\Delta e = \sqrt{e_1^2 - 2e_1 e_2 \cos(\omega_1 - \omega_2) + e_2^2} \tag{C-2}$$

$$\Delta i = i_2 \tag{C-3}$$

$$T = \frac{\pm e_1 \sin\omega_1}{\Delta i - e_1 \cos\omega_1} \tag{C-4}$$

The latter three equations follow from trigonometric properties of the diagrams in Fig. 50, where all angles are measured from the same reference line.

The particular family into which a given transfer falls is then determined by the following sets of inequalities:

Family (A)

$$1 + T^2 \leq \left(\frac{\Delta e}{\Delta a/a_0}\right)^2 \tag{C-5}$$

$$(\Delta i)^2 \geq 12T^2/(1+16T^2) \tag{C-6}$$

Family (A')

$$T = 0 \quad \text{and} \quad (\Delta e)^2 \leq (\Delta a/a_o)^2 \tag{C-7}$$

Family (B)

$$T \neq 0 \quad \text{and} \quad 1 + T^2 > \left(\frac{\Delta e}{\Delta a/a_o}\right)^2 \tag{C-8}$$

$$R^2 \leq 1/3 \tag{C-9}$$

Singular

$$1 + T^2 \leq (\Delta e)^2/(\Delta a/a_o)^2 \quad \text{and} \quad (\Delta i)^2 < 12T^2/(1+16T^2) \tag{C-10}$$

$$\text{or} \quad 1 + T^2 > (\Delta e)^2/(\Delta a/a_o)^2 \quad \text{and} \quad R^2 > 1/3 \tag{C-11}$$

In the case of singular solutions, two-impulse transfers do occur and the total impulse for the maneuver can be calculated. However, it is difficult to determine the locations and sizes of these impulses along the transfer ellipse. It is notable that little or no improvement in the total impulse results from resorting to higher numbers of impulses. For the other families of transfers, all important parameters can be calculated.

Family (A)

$$D = 0$$

$$\tan \tau_1 = -4T$$

$$\tau_2 = \tau_1 + \pi$$

$$u^2 = \frac{(\Delta e)^2(1+4T^2) + 4(\Delta i)^2(1+T^2)}{4(1+T^2)}$$

$$E = \frac{12u^2T^2 - (\Delta i)^2(1+16T^2)}{T[3u^2 + (\Delta i)^2(1+16T^2)]} \qquad \text{(C-12)}$$

$$R^2 = \frac{(4T-E)(1+4ET)}{12T}$$

$$(1-2\delta) = \sqrt{1+T^2}\left(\frac{\Delta\frac{a}{a_0}}{\Delta e}\right)$$

$$\Omega_2 = \tau_1$$

Family (A')

$$R = T = 0$$

τ_1 is orbitrary

$$\tau_2 = \tau_1 + \pi$$

$$E = \frac{1}{\tan\tau_1}$$

$$u^2 = \frac{4(\Delta i)^2 + (\Delta\frac{a}{a_0})^2}{4} \qquad \text{(C-13)}$$

$$D = \Delta\frac{a}{a_0}\sqrt{\frac{1+E^2}{4u^2 - (\Delta\frac{a}{a_0})^2}}$$

$$(1-2\delta) = \frac{\Delta e}{\Delta\frac{a}{a_0}}$$

$$\Omega_2 = \tau_1$$

Family (B)

$$u^2 = \frac{1}{4}\left[2(\Delta i)^2 + 2(\Delta e)^2 - \left(\Delta\frac{a}{a_0}\right)^2\right] + \frac{\sqrt{(1+T^2)\left[\left[(\Delta e)^2 + \left(\Delta\frac{a}{a_0}\right)^2 + (\Delta i)^2\right]^2 - 4(\Delta e)^2\left(\Delta\frac{a}{a_0}\right)^2\right] - 4(\Delta e)^2(\Delta i)^2}}{2\sqrt{1+T^2}}$$

$$R^2 = \frac{4u^2 - \left(\Delta\frac{a}{a_0}\right)^2 - 4(\Delta i)^2}{4u^2 - 4(\Delta e)^2 + 3\left(\Delta\frac{a}{a_0}\right)^2}$$

$$\cos^2\tau_1 = \frac{4R^2\left(\Delta\frac{a}{a_0}\right)^2}{4(1+R^2)u^2 - (1-3R^2)\left(\Delta\frac{a}{a_0}\right)^2} \qquad (C\text{-}14)$$

$$\tau_2 = -\tau_1$$

$$D = \frac{(1-3R^2)\cos\tau_1}{2R}$$

$$(1-2\delta) = \frac{T(1+R^2) \pm \sqrt{T^2(1+R^2)^2 + 4\sin^2\tau_1(R^2+\cos^2\tau_1)}}{2\sin\tau_1\cos\tau_1} \qquad \begin{cases} + \text{ for } T < 0 \\ - \text{ for } T > 0 \end{cases}$$

$$\tan\Omega_2 = \tan\tau_1/(1-2\delta)$$

The remaining equations hold for all three families

$$u_2 = \delta u \qquad (C\text{-}15)$$

$$u_1 = u - u_2 \qquad (C\text{-}16)$$

$$\lambda = R\sin\tau \qquad (C\text{-}17)$$

$$\mu = D + 2R\cos\tau \qquad (C\text{-}18)$$

$$\nu = E\cos\tau + \sin\tau \qquad \text{(C-19)}$$

$$p = \sqrt{\lambda^2 + \mu^2 + \nu^2} \qquad \text{(C-20)}$$

REFERENCES

1. Lawden, D. F.: Optimal Trajectories for Space Navigation. Butterworth's, London, 1963.

2. Edelbaum, T. N.: How Many Impulses? AIAA Paper No. 66-7, Third Aerospace Sciences Meeting, New York, January 1966.

3. Bender, D. F.: Optimum Coplanar Two Impulse Transfers Between Elliptic Orbits. Aerospace Engineering, Vol. 21, No. 10, October 1962.

4. Moyer, H. G.: Necessary Conditions for Optimal Single Impulse Transfer. Grumman Research Department Report RE-234J, November 1965. (Also AIAA Paper No. 66-93, January 1966.)

5. Plimmer, R. N. A.: Fuel Requirements for Inter-Orbital Transfer of a Rocket. RAE TN No. G.W. 539, March 1960. Also IAF Proceeding.

6. Lawden, D. F.: Impulsive Transfer Between Elliptical Orbits. Chapter 11 - Optimization Techniques, G. Leitmann, Ed., Academic Press, New York, 1962.

7. Smith, G. C.: The Calculation of Minimal Orbits. Astronautica Acta 5, p. 253-265, 1959.

8. Long, R. S.: Transfer Between Noncoplanar Elliptical Orbits. Astronautica Acta 6, p. 167, 1960.

9. Marchal, C.: Transferts Optimaux Entre Orbites Elliptiques - Duree Indifferente (Optimal Transfer Between Elliptical Orbits - Time Free). Presented at the XVIth International Astronautical Congress, Athens, 1965.

10. Breakwell, J. V.: The Optimization of Trajectories. SIAM Journal, No. 7, p. 215-247, 1959.

11. Robbins, H. M.: Optimality of Intermediate-Thrust Arcs of Rocket Trajectories. AIAA Journal, Vol. 3, p. 1094-1098, June 1965.

12. Kopp, R. E. and H. G. Moyer: Necessary Conditions for Singular Extremals. AIAA Journal, Vol. 3, p. 1439-1444, August 1965.

13. Breakwell, J. V.: Minimum Impulse Transfer. AIAA Paper No. 63-416, AIAA Astrodynamics Conference, New Haven, Connecticut, August 1963.

14. Marchal, C. and H. G. Moyer: Private Correspondence.

REFERENCES (Contd.)

15. Kerfoot and Des Jardins: Coplanar Two-Impulse Orbital Transfers. ARS Paper No. 2063-61, 1961.

16. Contensou, P.: Etude theorique des trajectoires optimales dans on champ de gravitation. Application au cas d'un centre d'attraction unique. (Theoretical Study of Optimal Trajectories in a Gravitational Field. Application in the Case of a Single Center of Attraction). Astronautica Acta, Vol. VIII/FASC. 2-3, 1962. Also Grumman Research Translation TR-22 by P. Kenneth, August 1962.

17. Gobetz, F. W.: Optimal Variable-Thrust Rendezvous of a Power-Limited Rocket Between Neighboring Low-Eccentricity Orbits (Final Report). Contract NAS8-11099, October 1964. Also United Aircraft Research Laboratories Report C-910098-12.

18. Gobetz, Frank W.: A Linear Theory of Optimum Low-Thrust Rendezvous Trajectories. Journal of the Astronautical Sciences, Vol. XII, No. 3, pp. 69 - 76. Fall 1965.

FIG. 1

SUMMARY OF KNOWN HOHMANN-TYPE TRANSFERS BETWEEN ISOECCENTRIC, COAXIAL ELLIPSES

AXES ALIGNED

NON-INTERSECTING

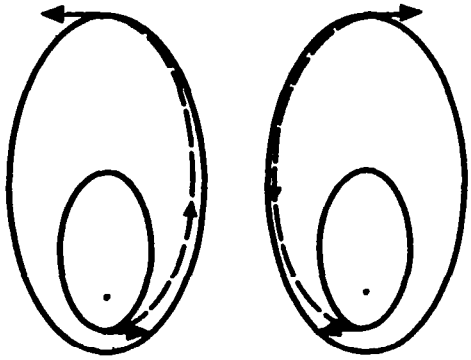

$\frac{a_2}{a_1} > 1$ $\frac{a_2}{a_1} < 1$

INTERSECTING

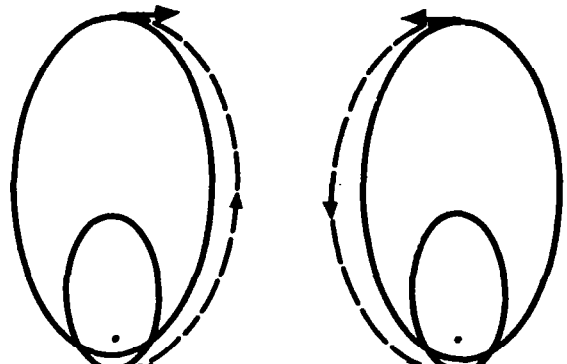

$\frac{a_2}{a_1} > 1$ $\frac{a_2}{a_1} < 1$

AXES OPPOSED

NON-INTERSECTING

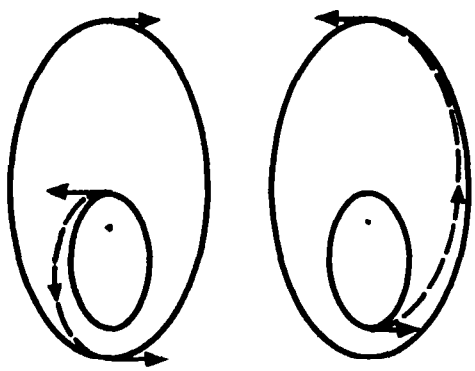

$\frac{a_1}{a_2} < \frac{1-e}{1+e}$ $\frac{1-e}{1+e} < \frac{a_1}{a_2} < 1$

INTERSECTING

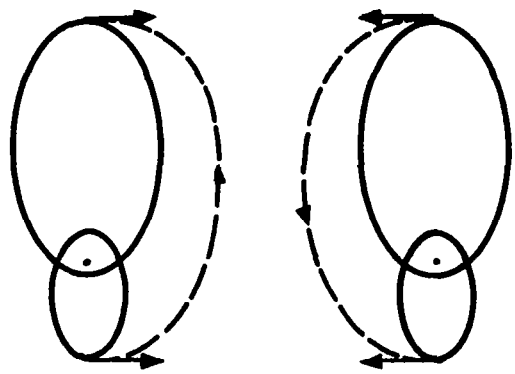

$\frac{1-e}{1+e} < \frac{a_1}{a_2} < 1$ $\frac{a_1}{a_2} < \frac{1-e}{1+e}$

FIG. 2

SYMMETRIC TRANSFER

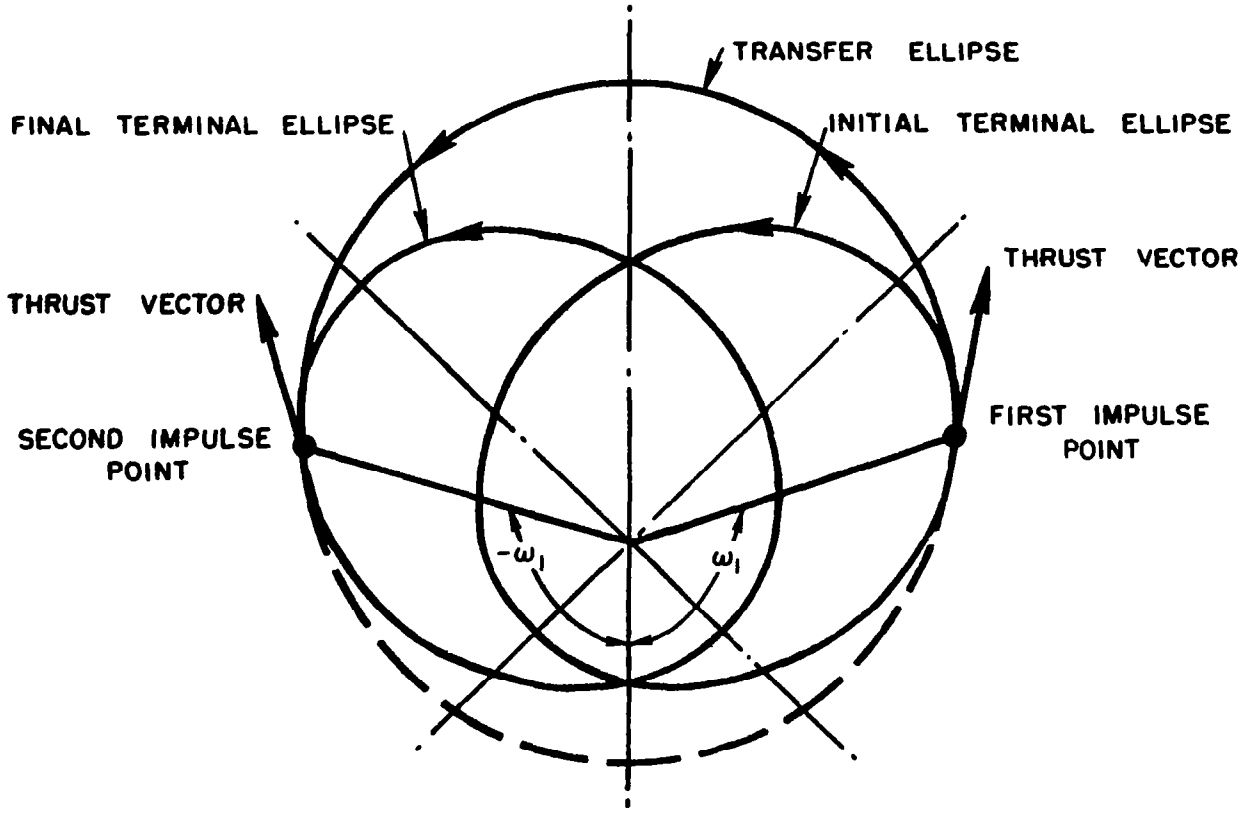

FIG. 3

COORDINATE SYSTEM

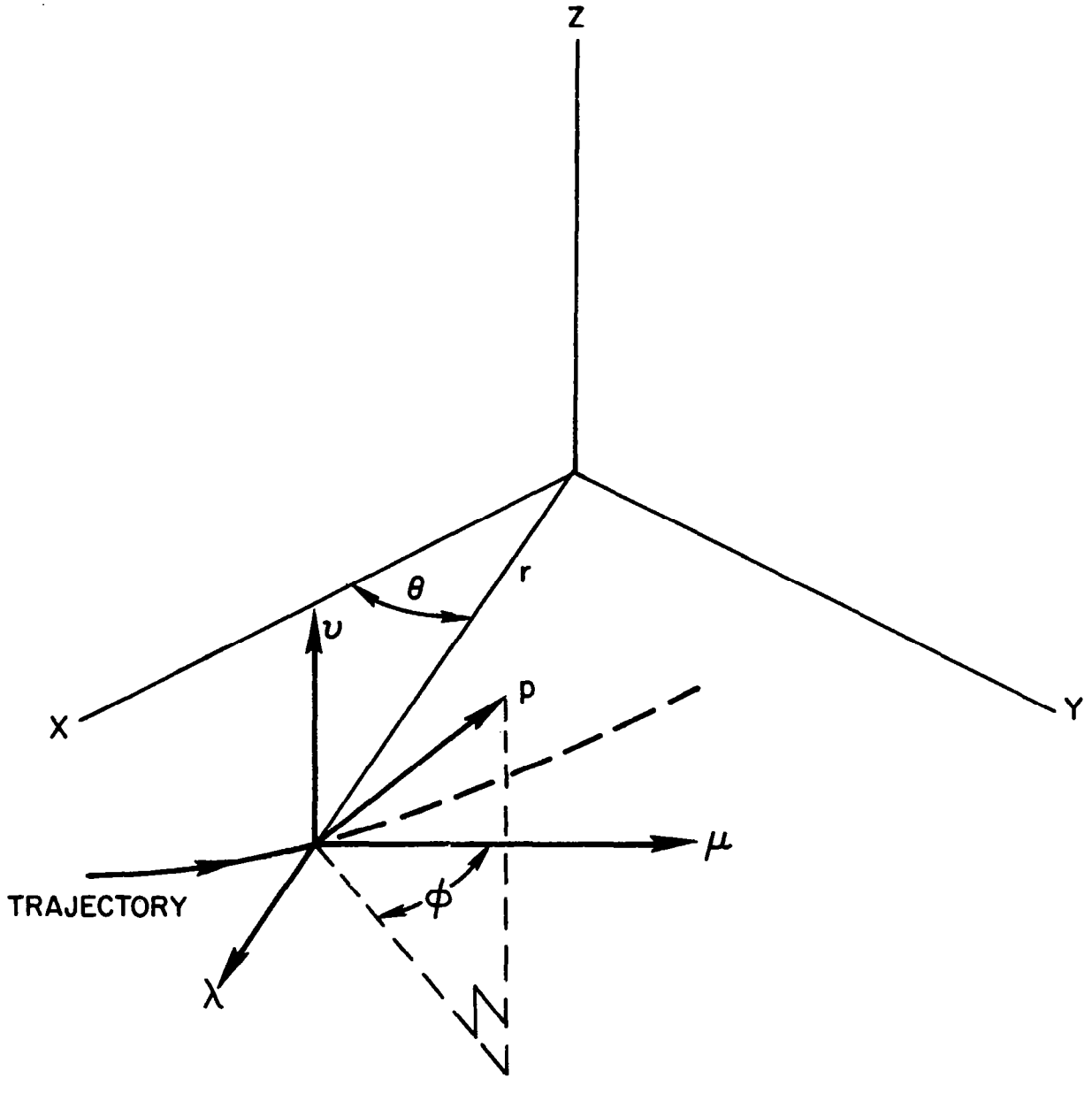

FIG. 4

LOCUS OF PRIMER VECTOR CONSTANTS

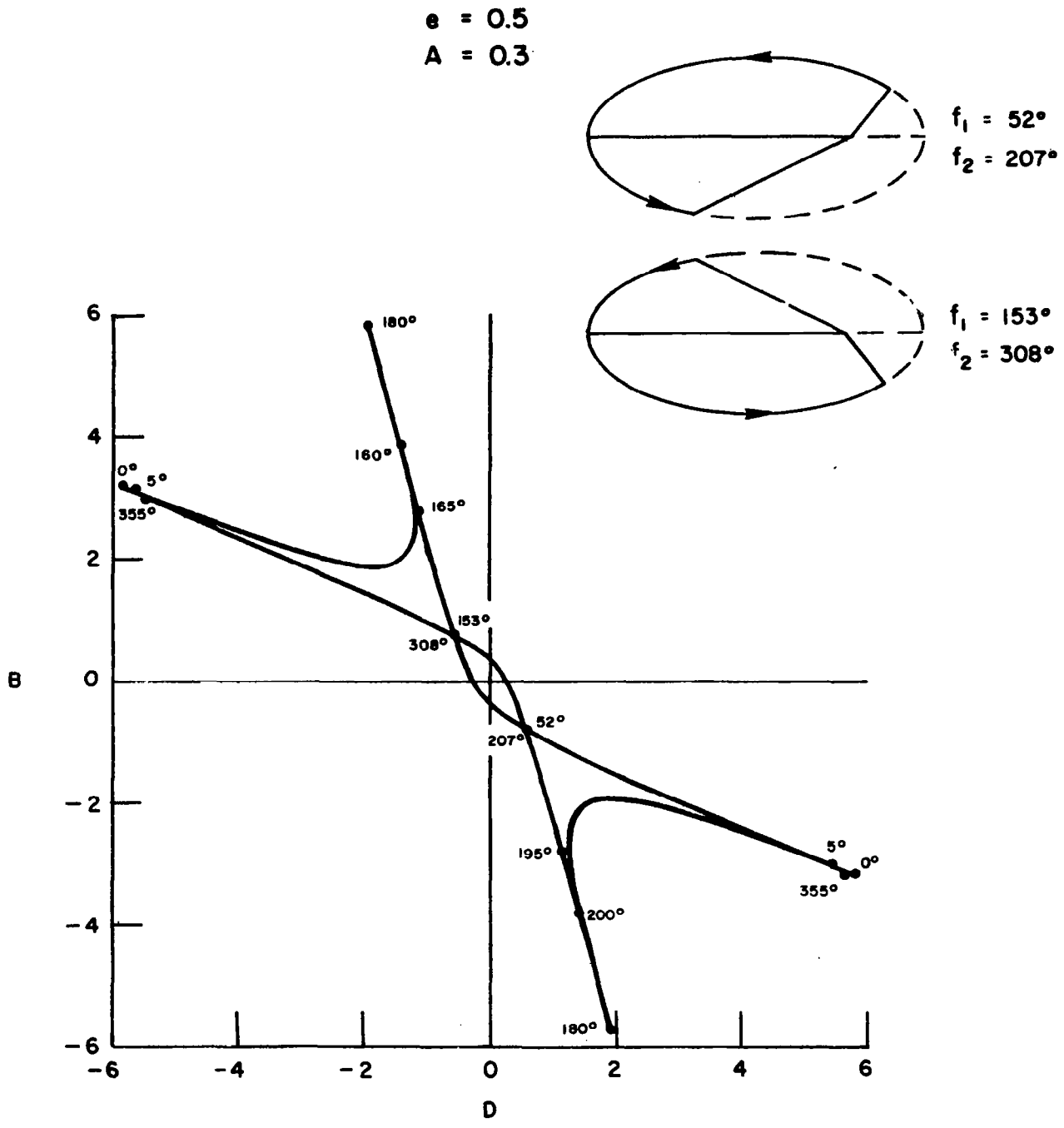

FIG. 5

SPIRAL - LIMITED TRANSFERS

$e = 0.5$

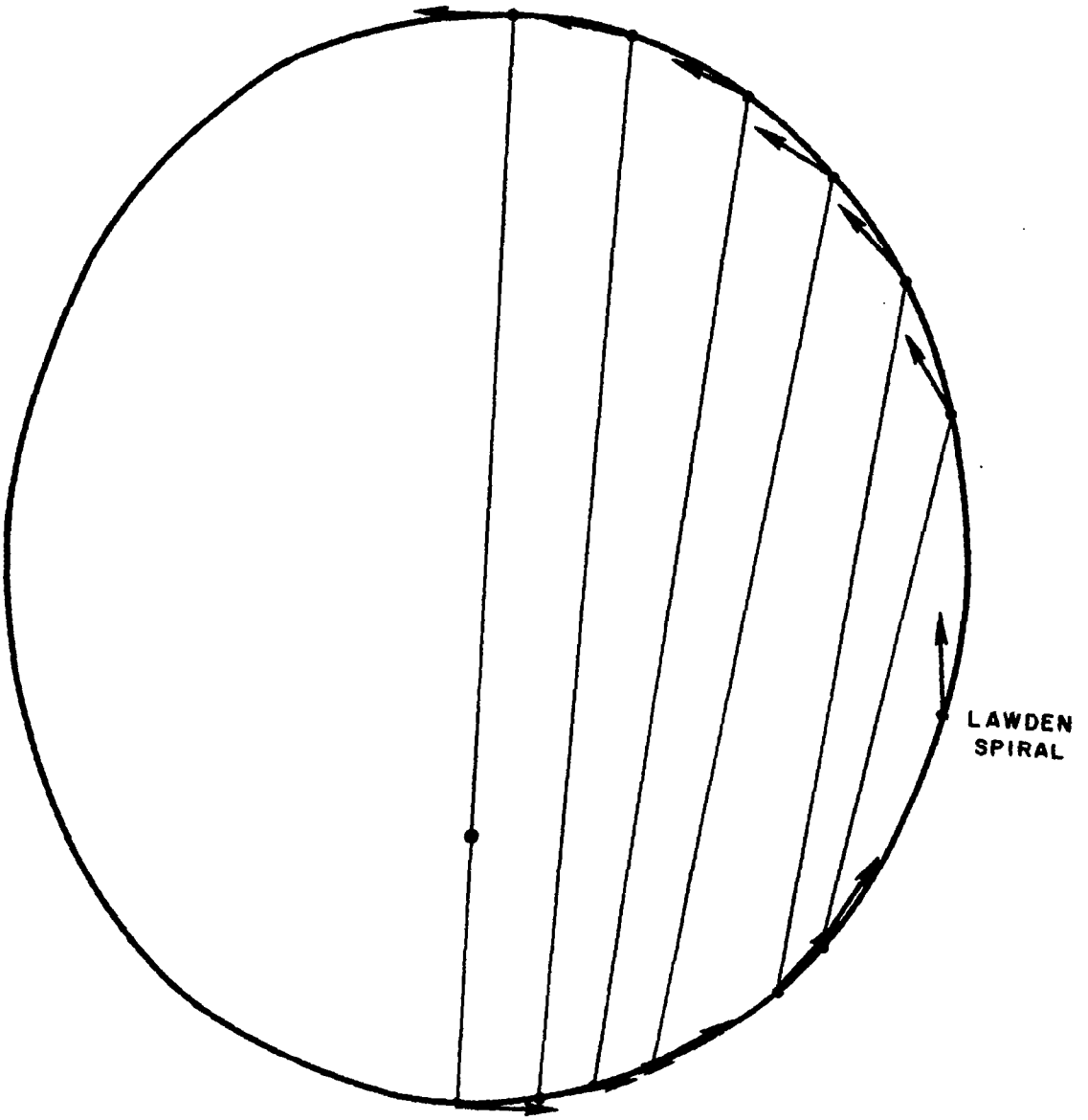

FIG. 6

SYMMETRIC - LIMITED TRANSFERS

$\epsilon = 0.5$

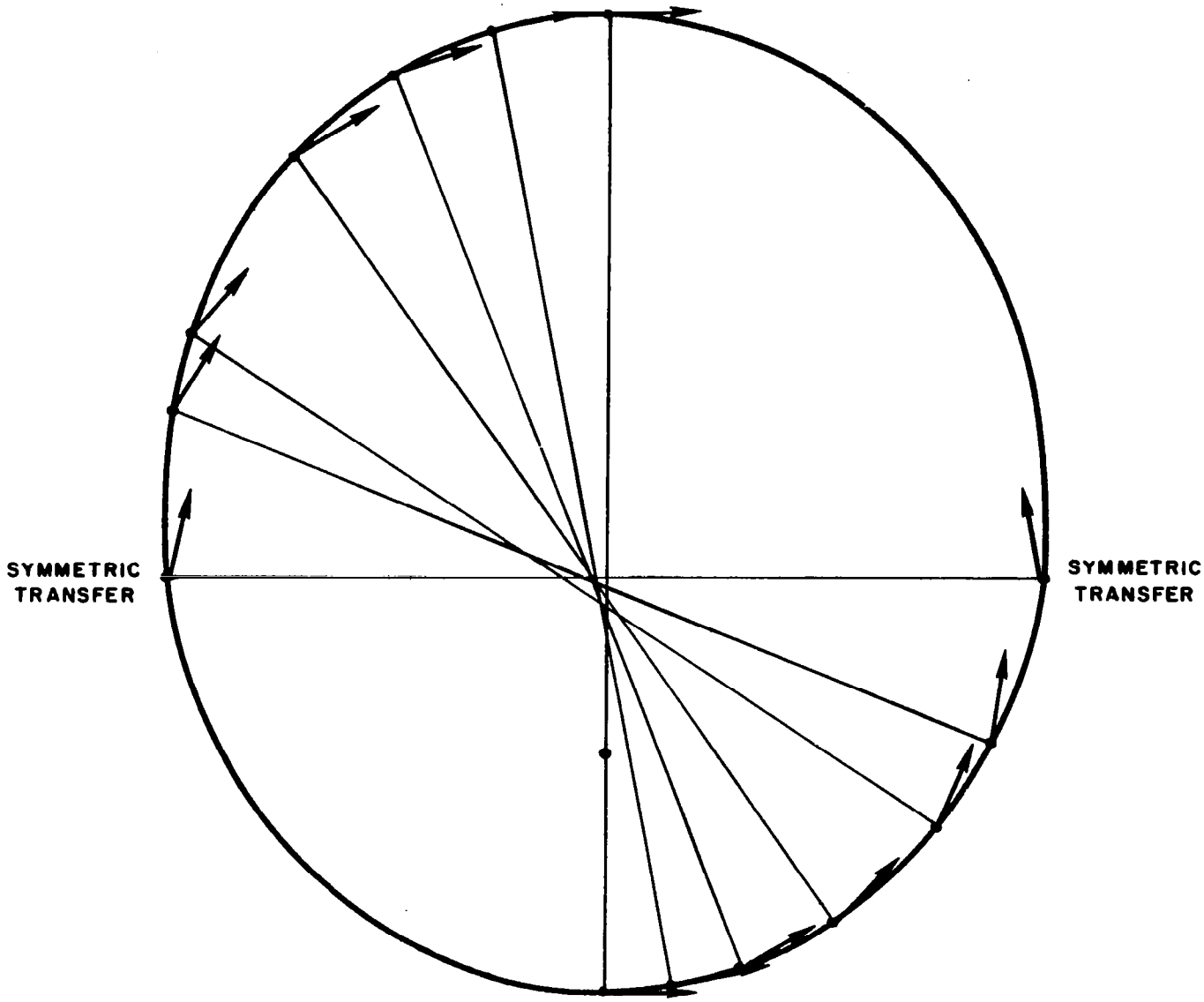

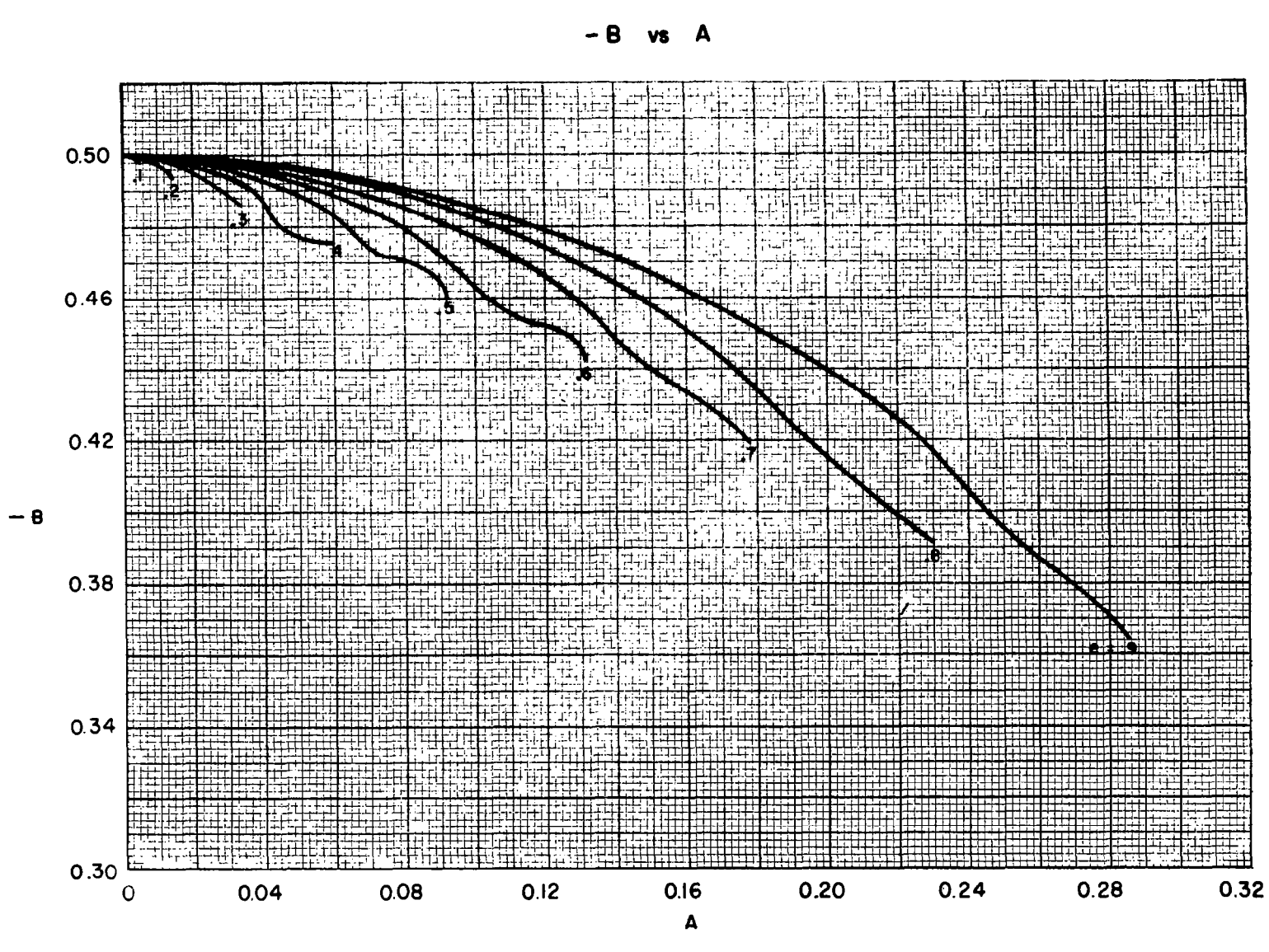
SPIRAL - LIMITED TRANSFERS
- B vs A
0.50
0.46
0.42
0.38
0.34
0.30
- B
0
0.04
0.08
0.12
0.16
0.20
0.24
0.28
0.32
A
1
2
3
4
5
6
7
8
9

FIG. 7

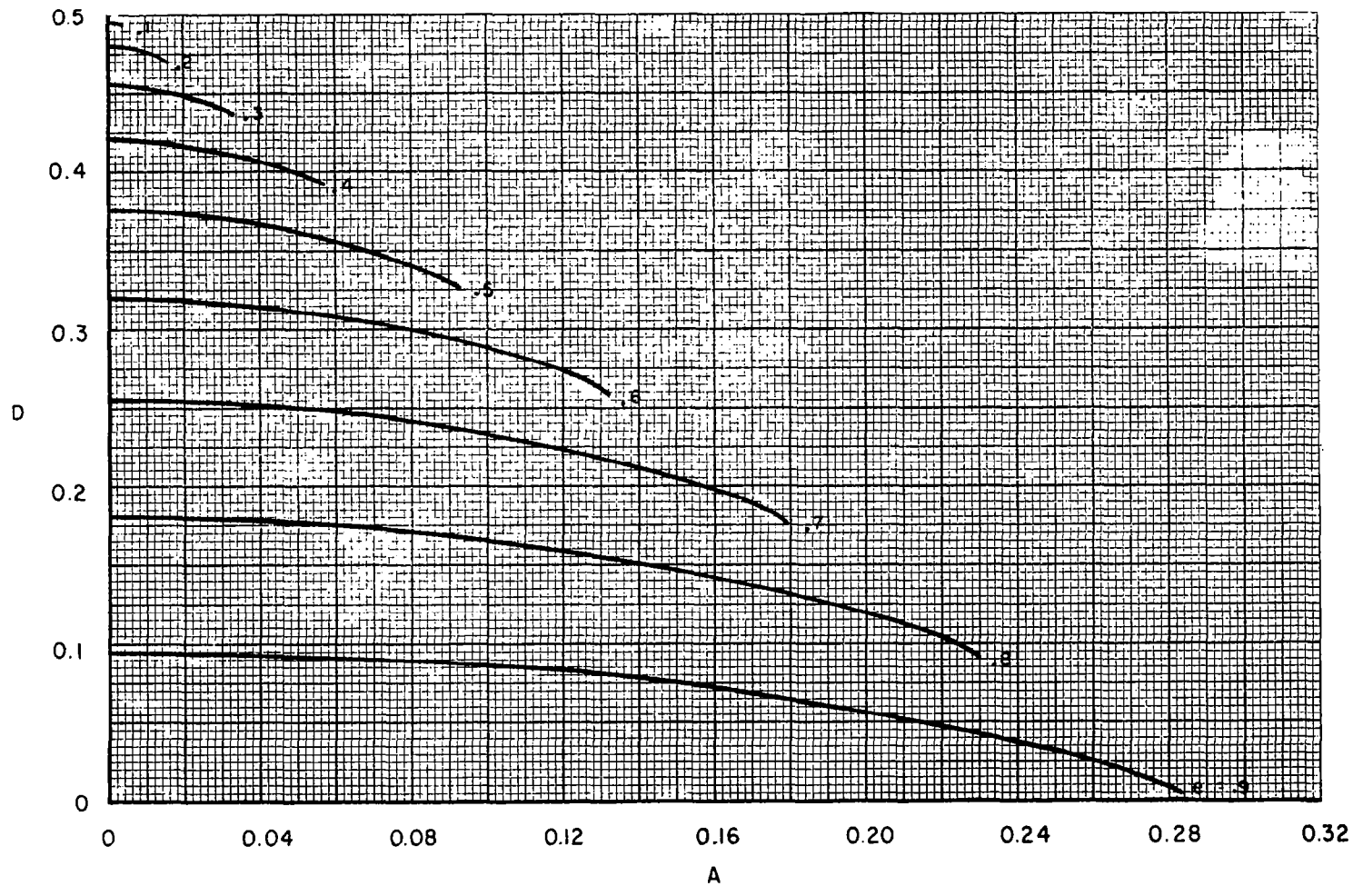
SPIRAL-LIMITED TRANSFERS
-D vs A
0.5
0.4
0.3
0.2
0.1
0
D
0
0.04
0.08
0.12
0.16
0.20
0.24
0.28
0.32
A
.1
.2
.3
.4
.5
.6
.7
.8
.9

FIG. 8

SPIRAL - LIMITED TRANSFERS

f_1 vs A

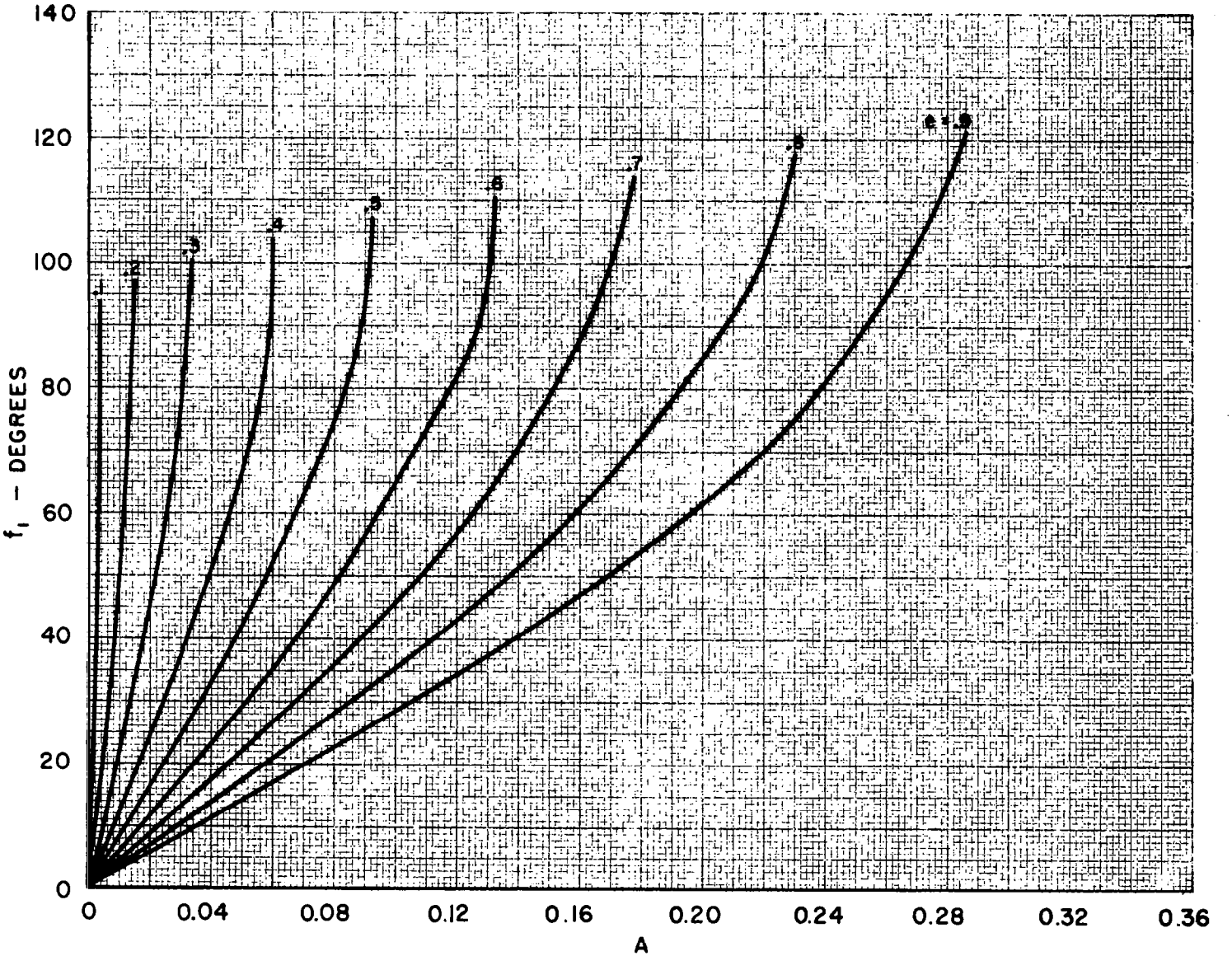

FIG. 9

SPIRAL-LIMITED TRANSFERS

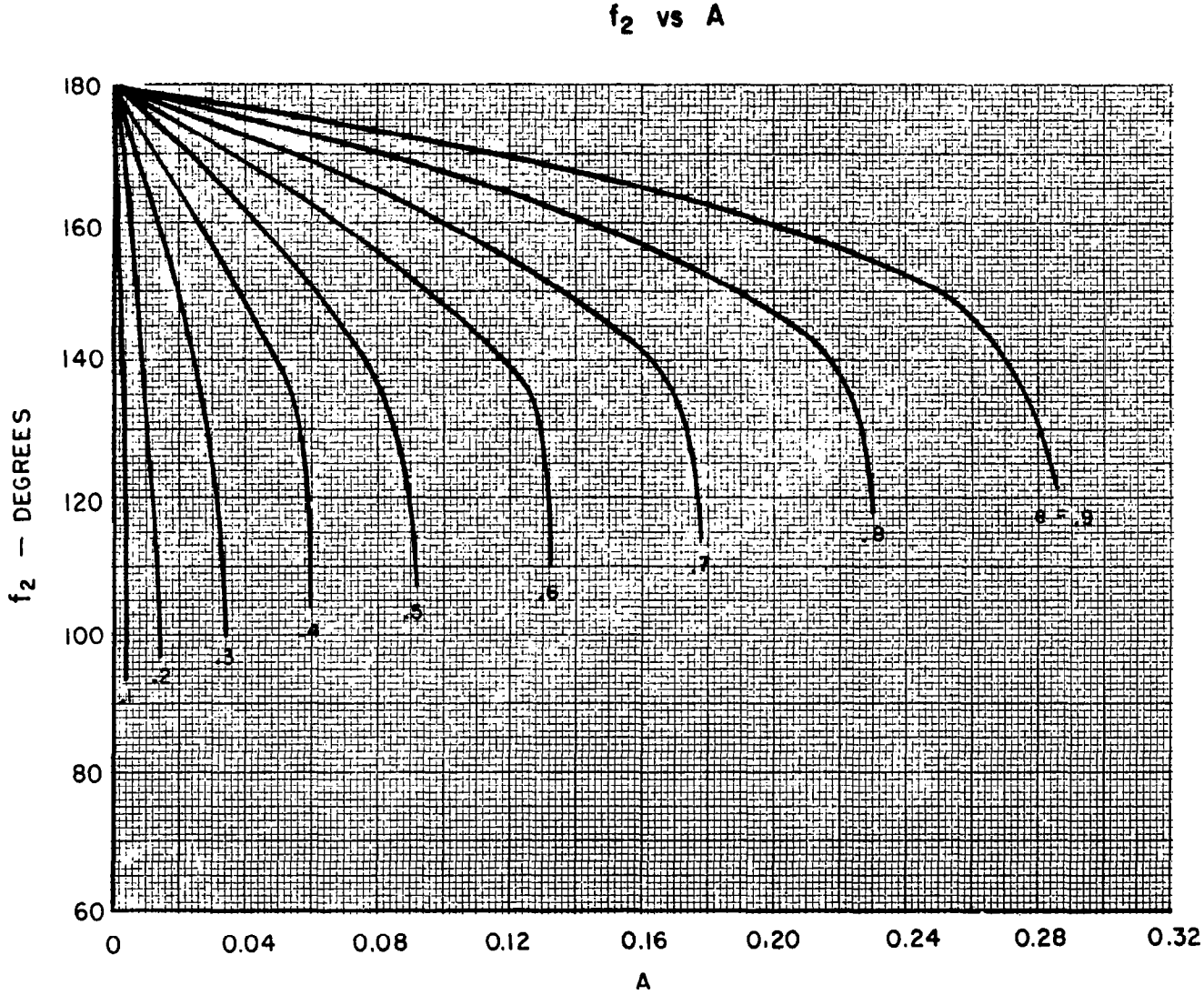

FIG. 10

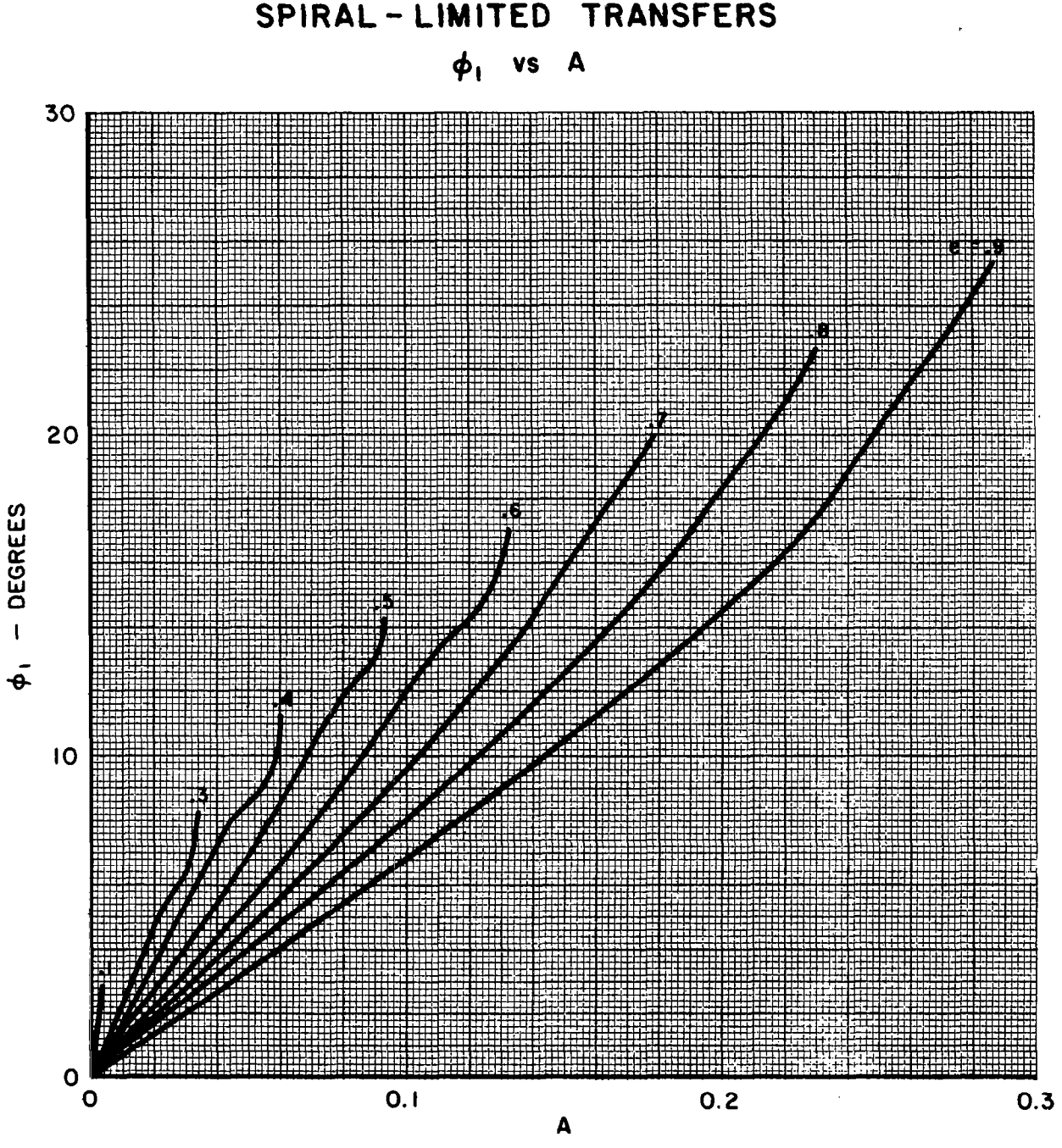
SPIRAL - LIMITED TRANSFERS
ϕ_1 vs A
30
20
10
0
ϕ_1 - DEGREES
0
0.1
0.2
0.3
A
.1
.2
.3
.4
.5
.6
.7
.8
e = .9

FIG. 11

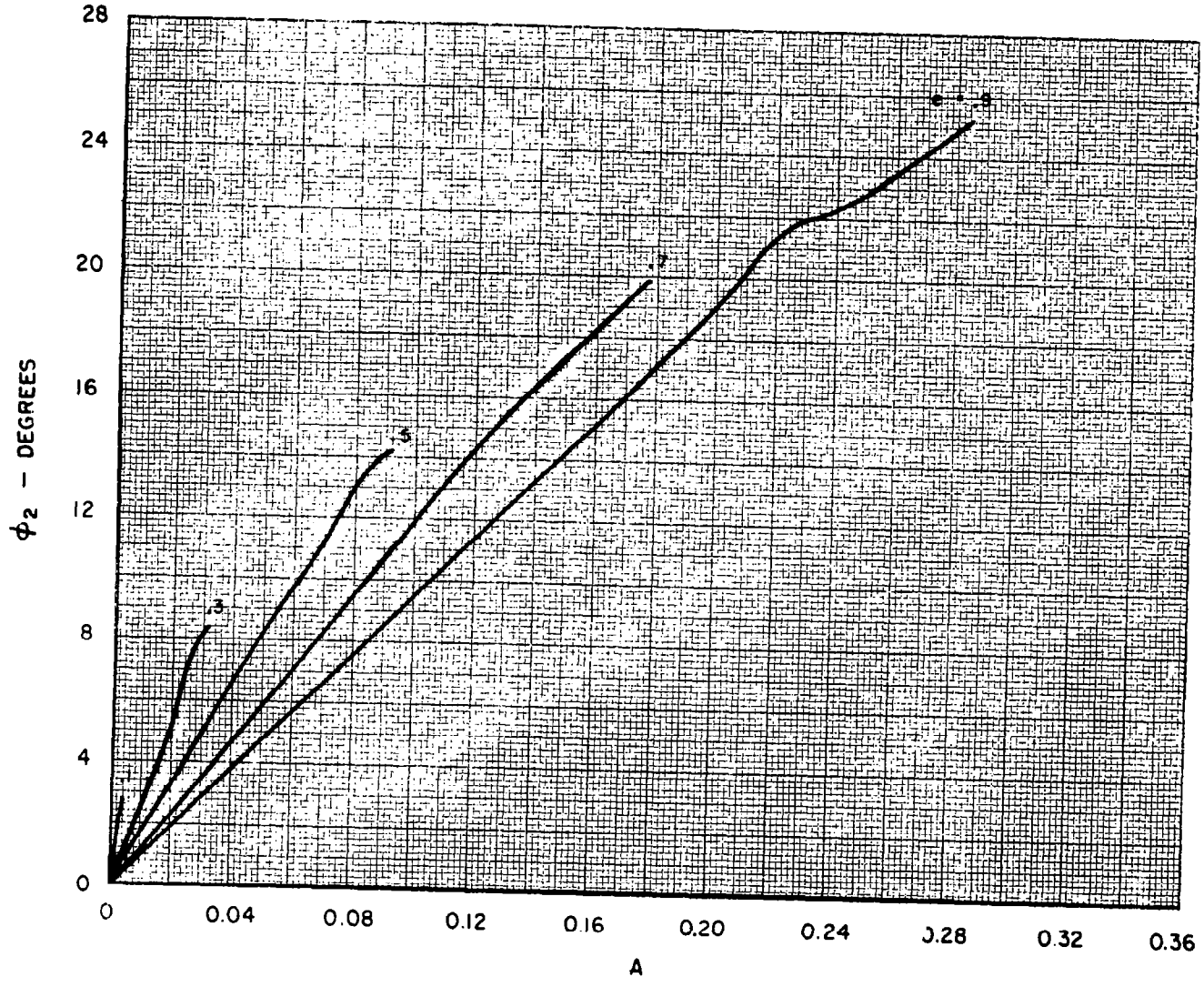
SPIRAL-LIMITED TRANSFERS
ϕ_2 vs A
ϕ_2 - DEGREES
28
24
20
16
12
8
4
0
0
0.04
0.08
0.12
0.16
0.20
0.24
0.28
0.32
0.36
A
3
5
7
9

FIG. 12

FIG. 13.

SYMMETRIC - LIMITED TRANSFERS

- B vs A

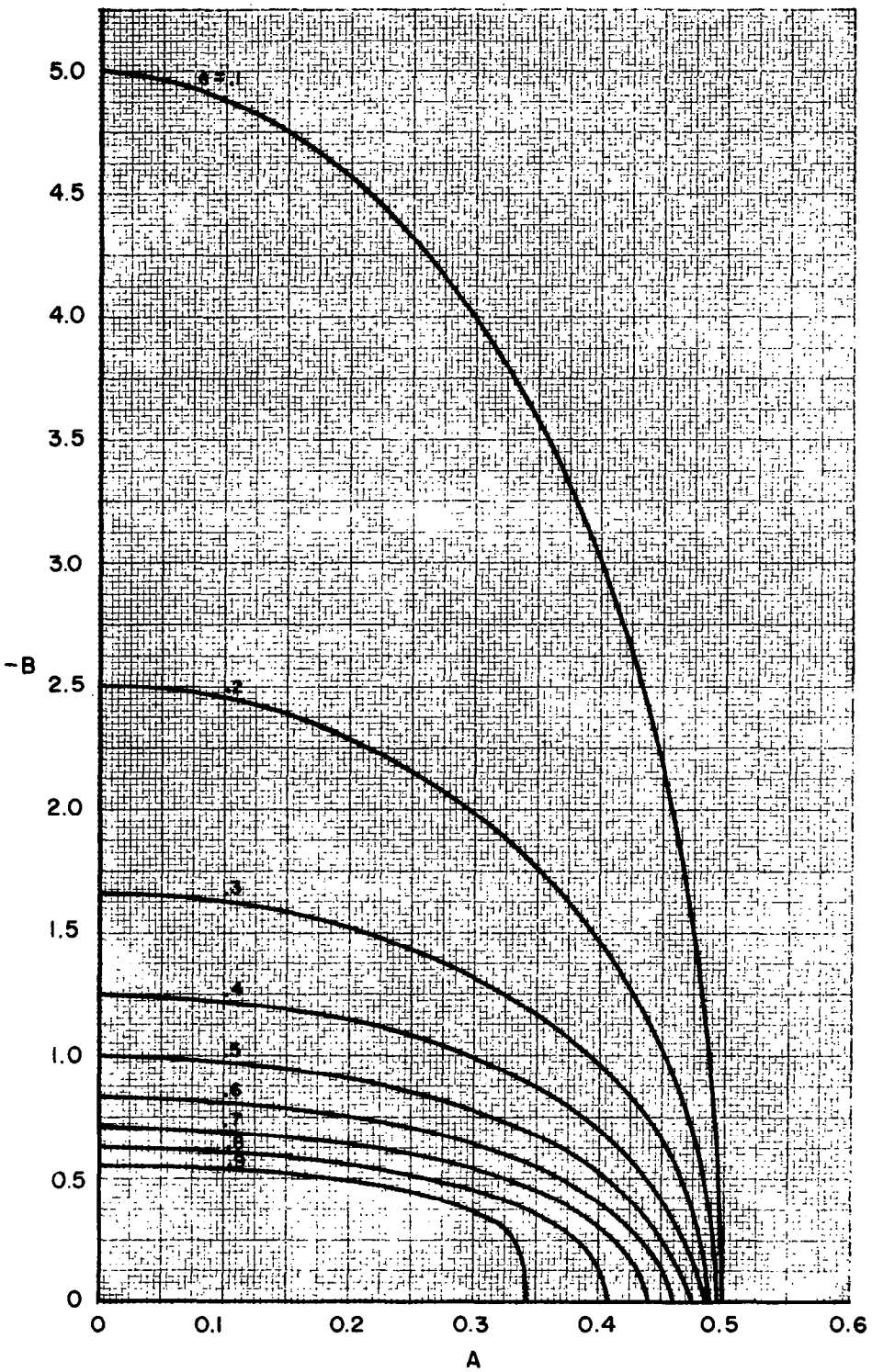

FIG. 14

SYMMETRIC - LIMITED TRANSFERS

D vs A

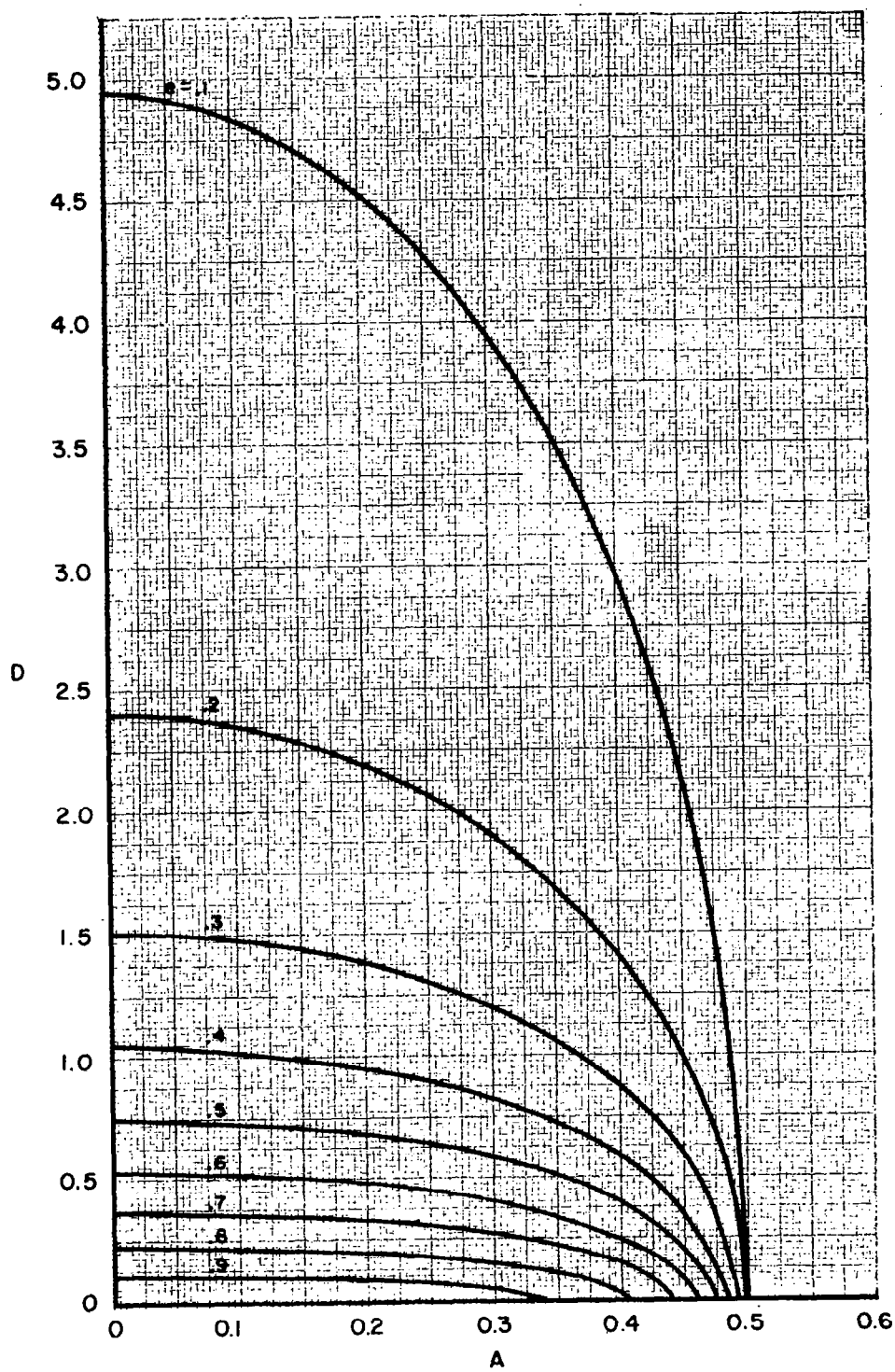

FIG. 15

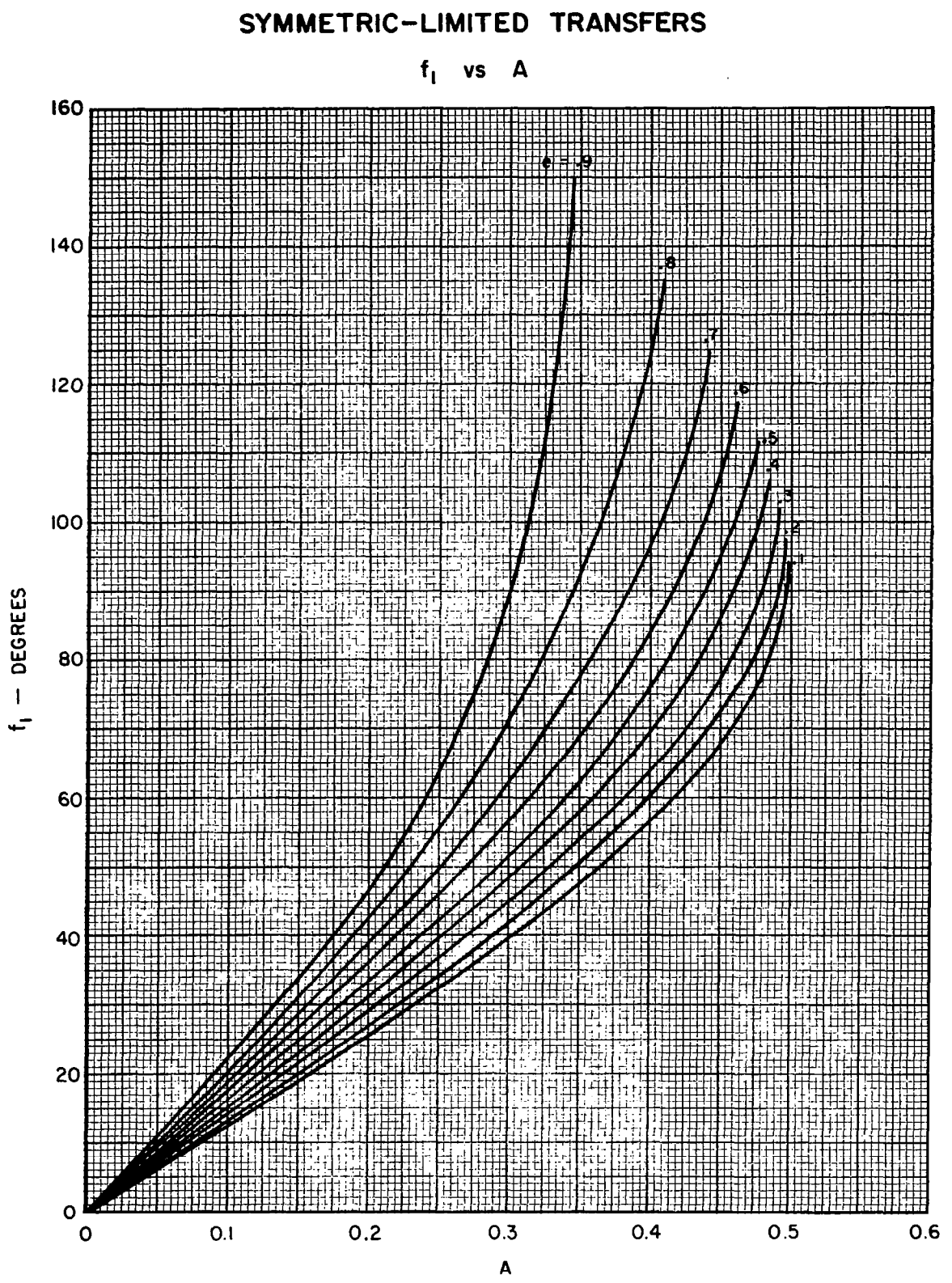
SYMMETRIC-LIMITED TRANSFERS
f_1 vs A
160
140
120
100
80
60
40
20
0
f_1 — DEGREES
0
0.1
0.2
0.3
0.4
0.5
0.6
A
ϕ = 9
8
7
6
5
4
3
2
1

FIG. 16

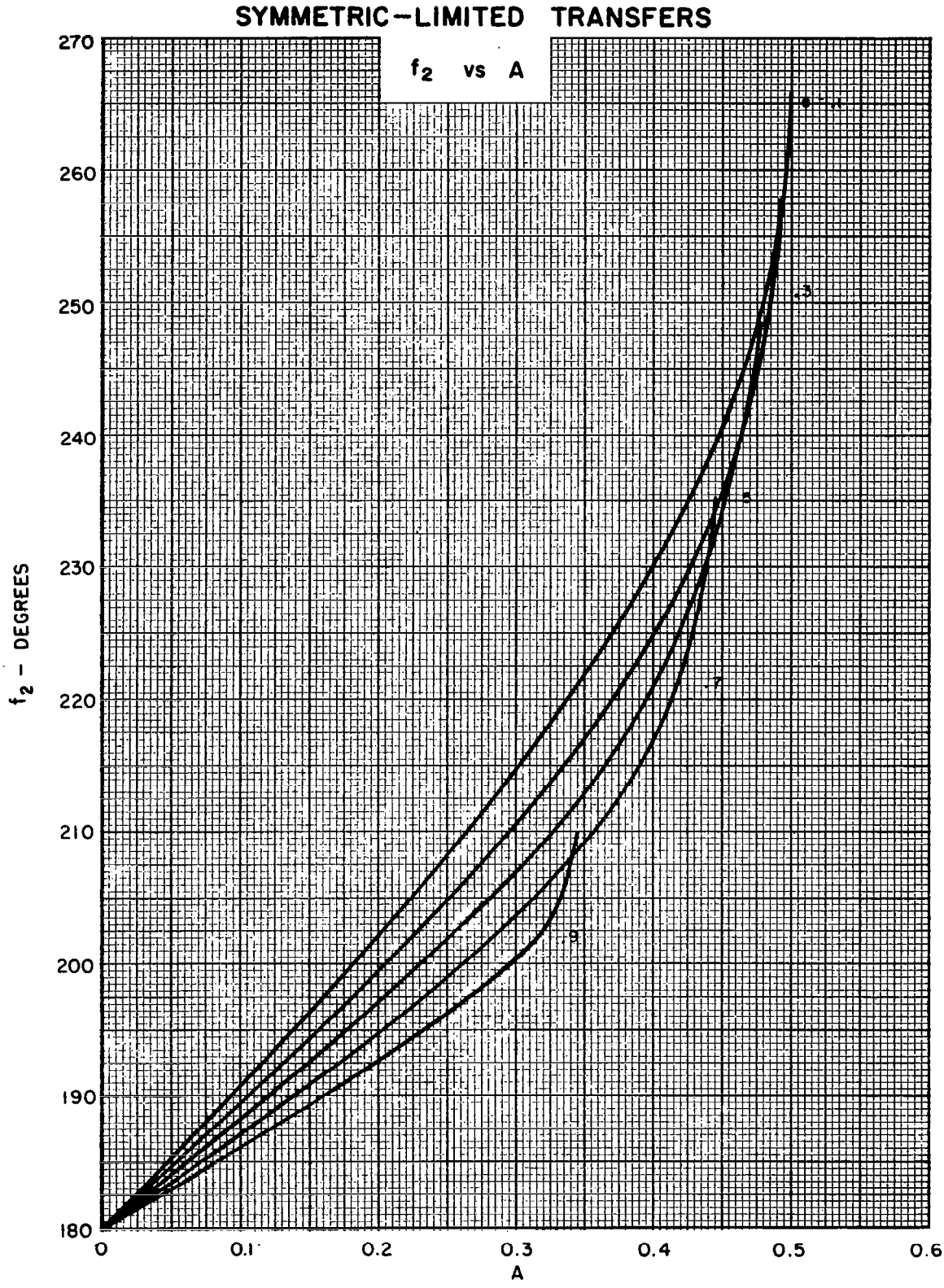
SYMMETRIC—LIMITED TRANSFERS
f_2 vs A
270
260
250
240
230
220
210
200
190
180
f_2 – DEGREES
0
0.1
0.2
0.3
0.4
0.5
0.6
A
9

FIG. 17

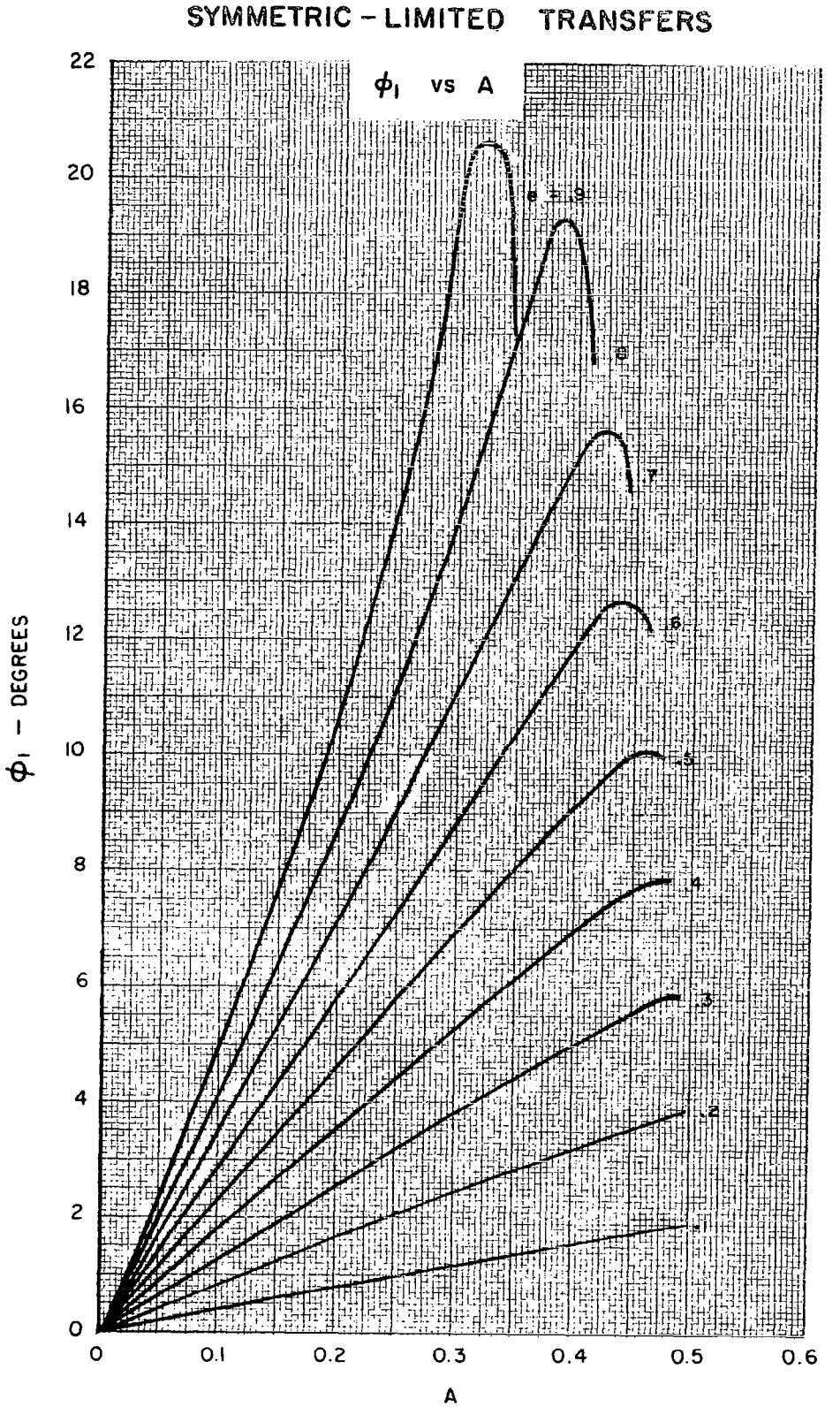
SYMMETRIC – LIMITED TRANSFERS
ϕ_1 vs A
ϕ_1 – DEGREES
A
22
20
18
16
14
12
10
8
6
4
2
0
0
0.1
0.2
0.3
0.4
0.5
0.6
.9
.8
.7
.6
.5
.4
.3
.2
.1

FIG. 18

SYMMETRIC – LIMITED TRANSFERS

ϕ_2 vs A

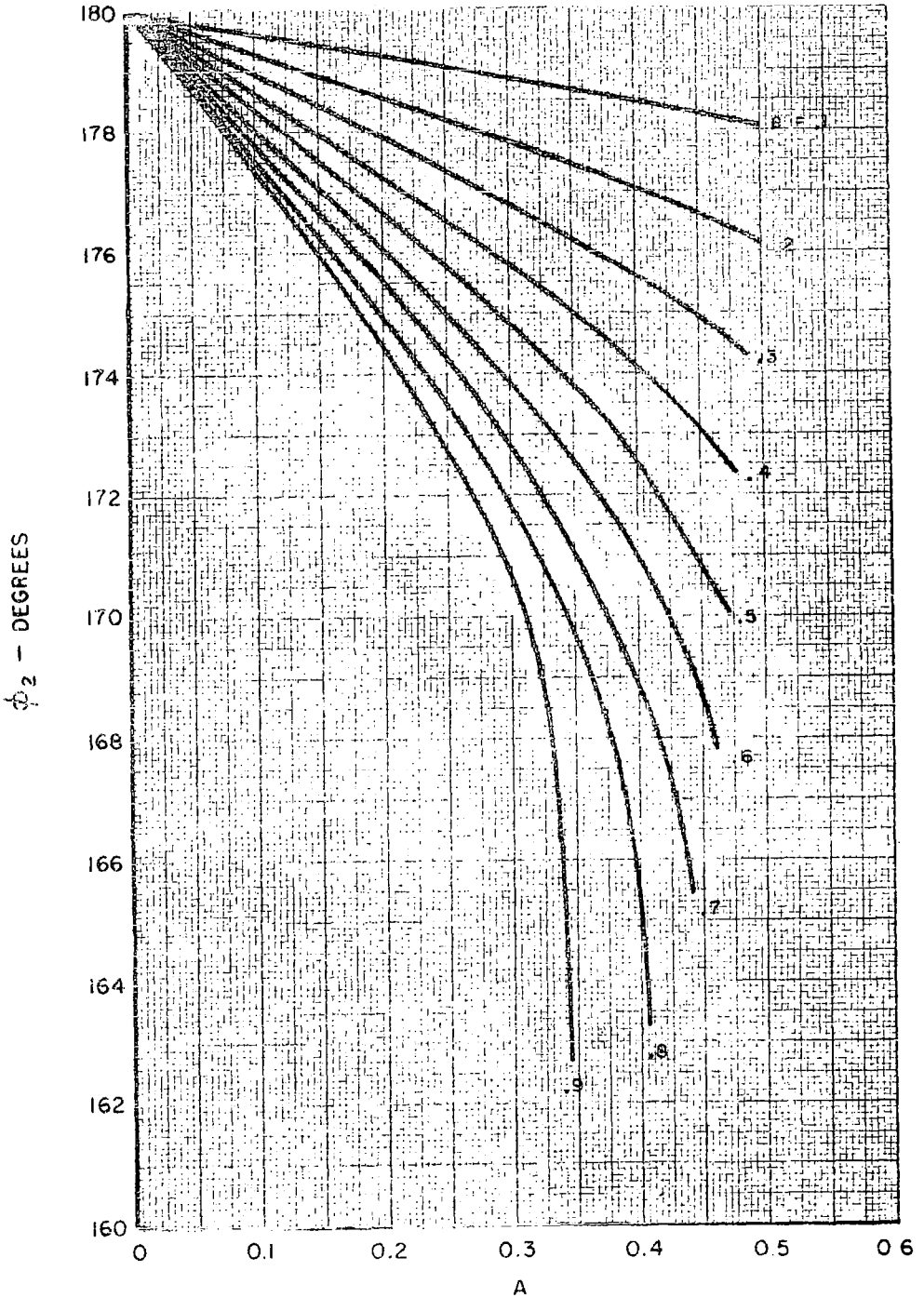

SPIRAL – LIMITED TRANSFERS

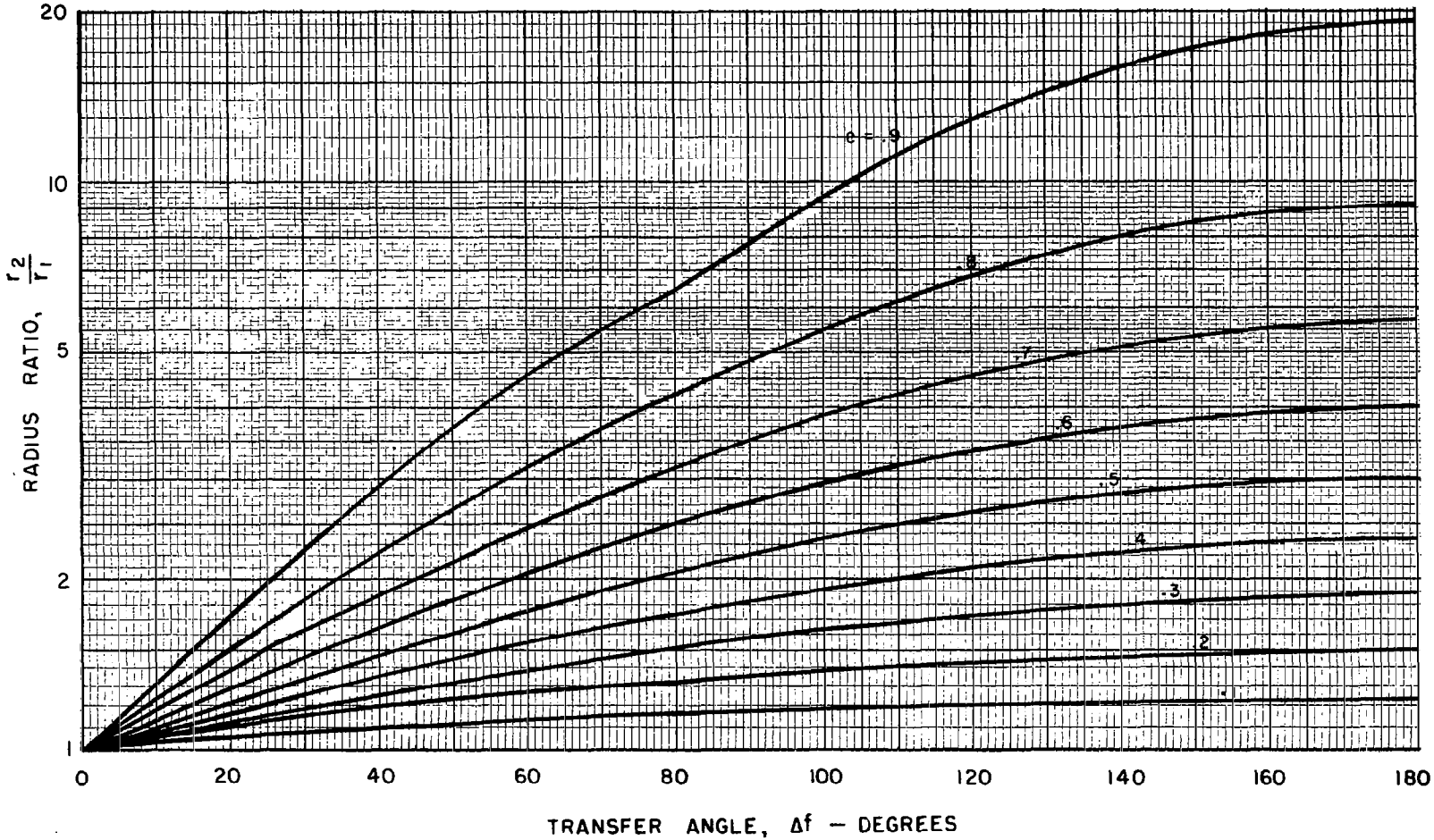

FIG. 19

SPIRAL-LIMITED TRANSFERS

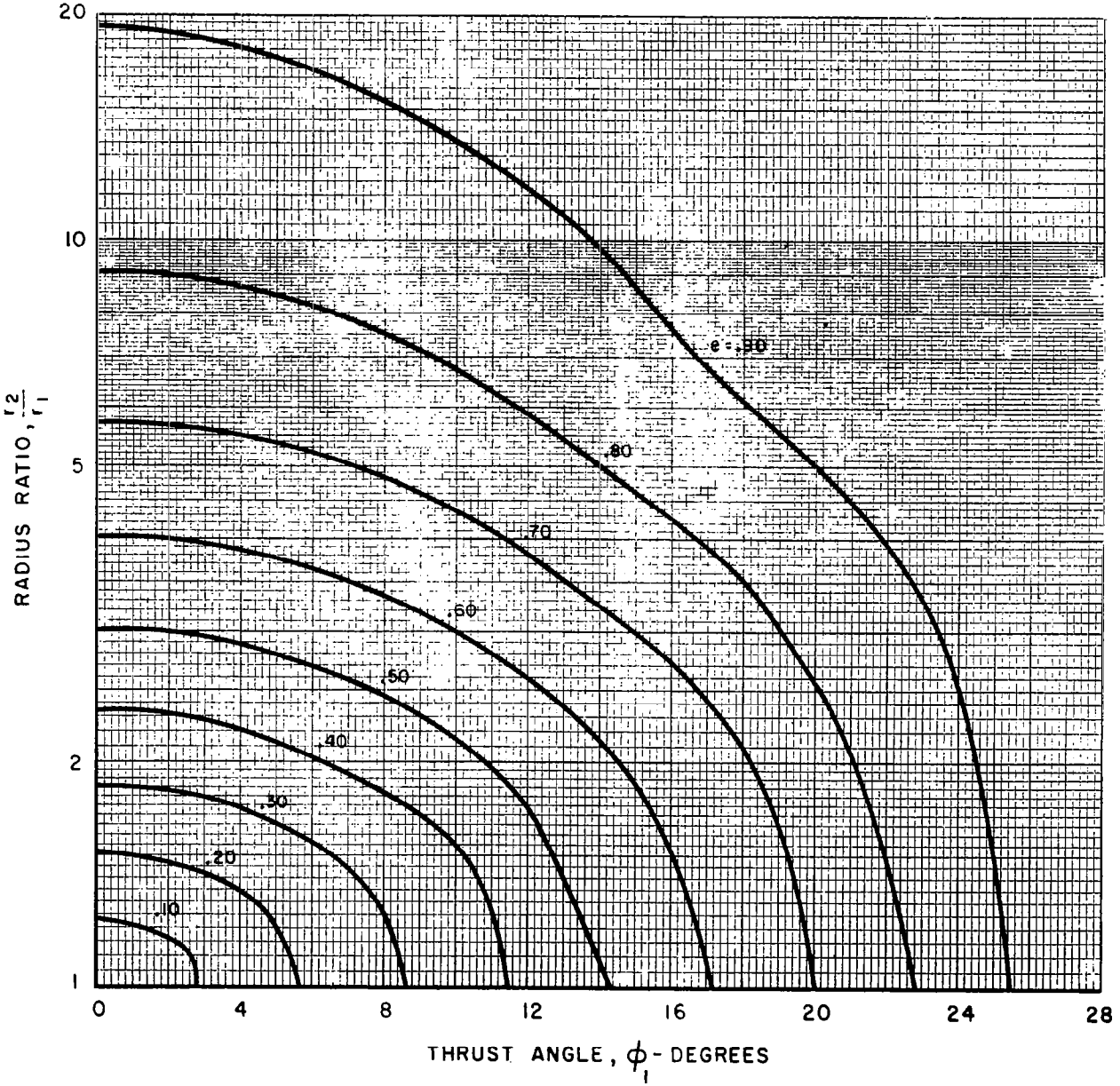

FIG. 20

SPIRAL-LIMITED TRANSFERS

FIG. 21

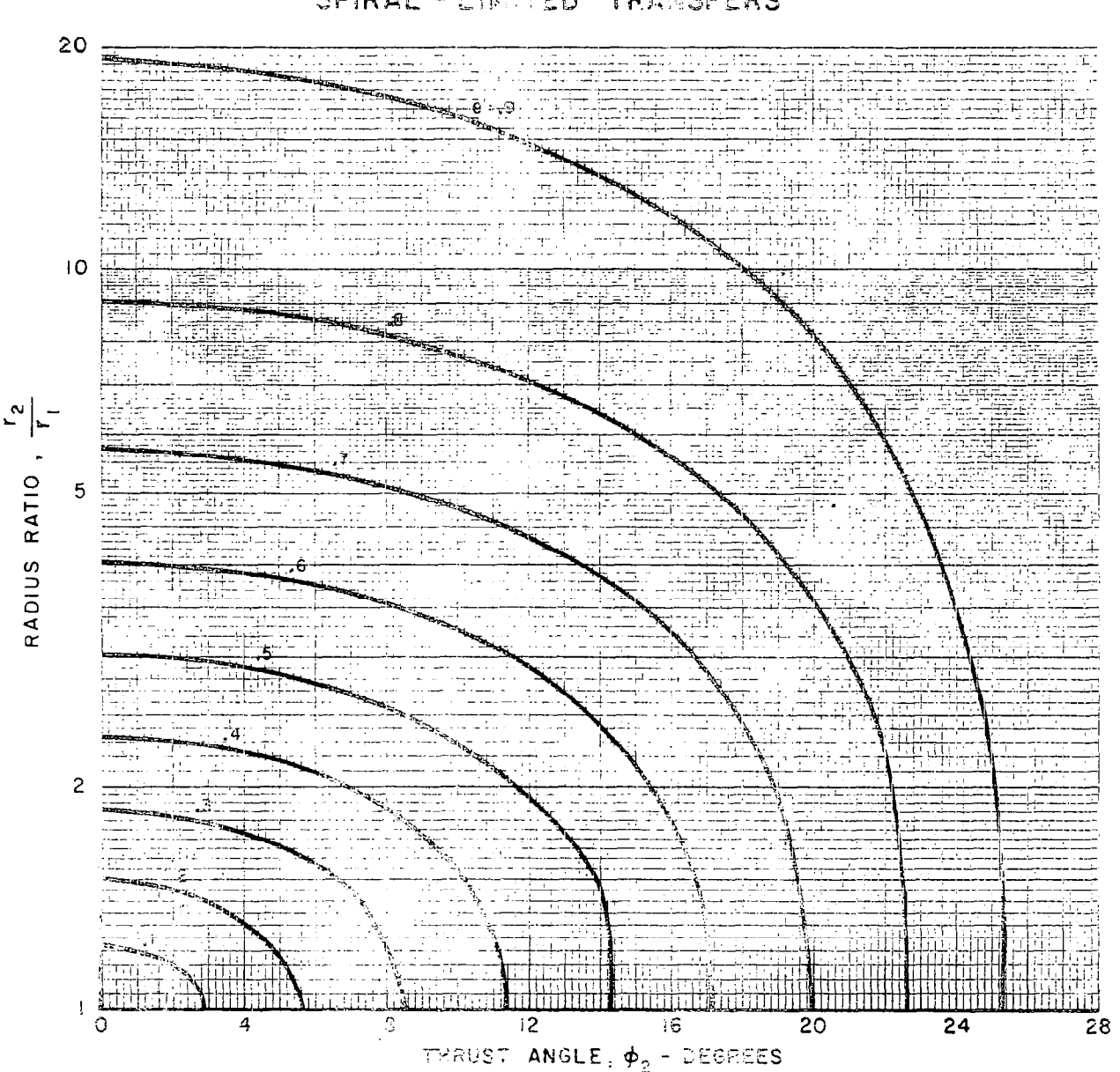
SPIRAL - LIMITED TRANSFERS
RADIUS RATIO, $\frac{r_2}{r_1}$
THRUST ANGLE, ϕ_2 - DEGREES
20
10
5
2
1
0
4
8
12
16
20
24
28
.9
.8
.7
.6
.5
.4

FIG. 22

SPIRAL-LIMITED TRANSFERS

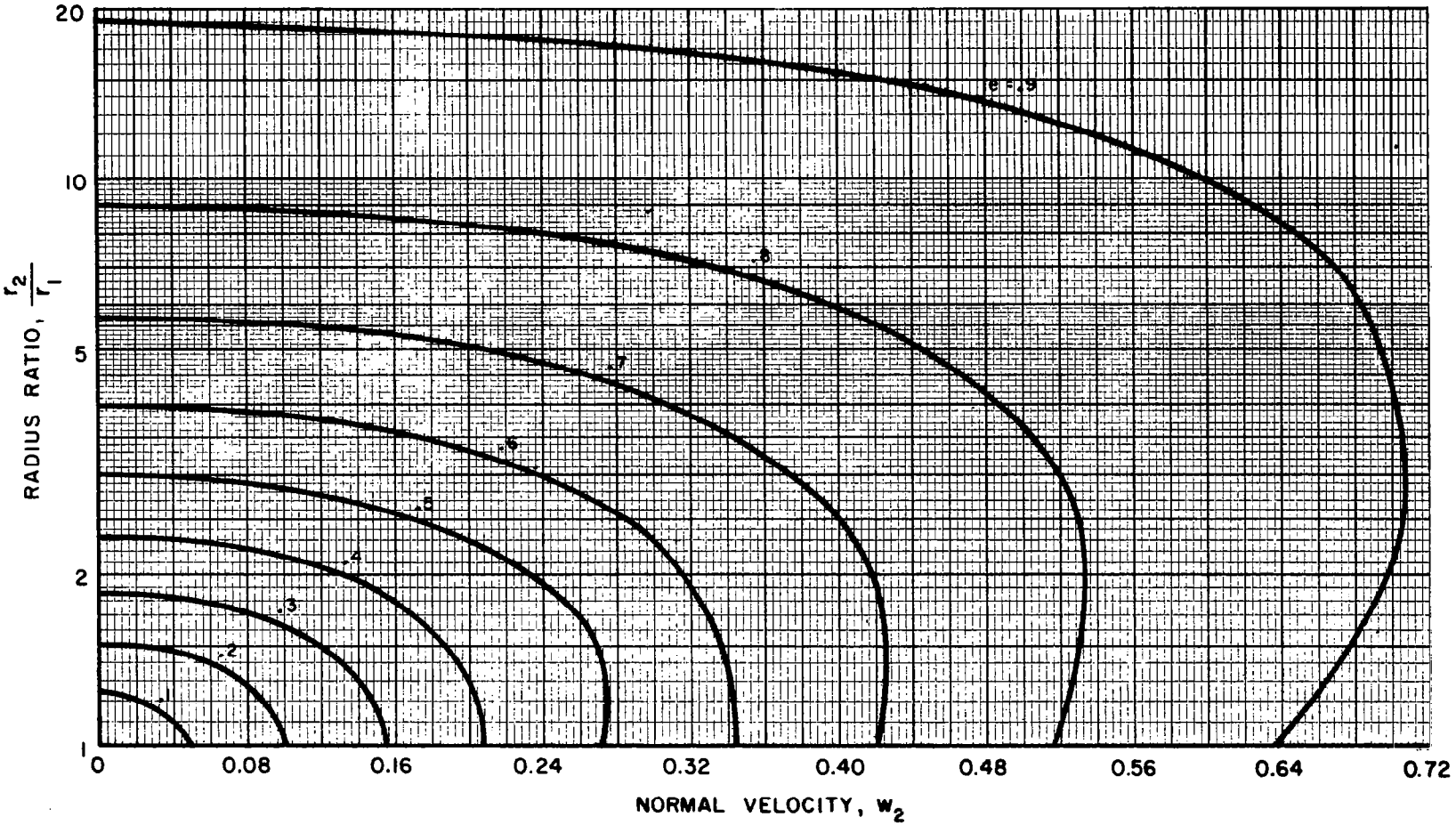

FIG. 23

FIG. 24

SYMMETRIC - LIMITED TRANSFERS

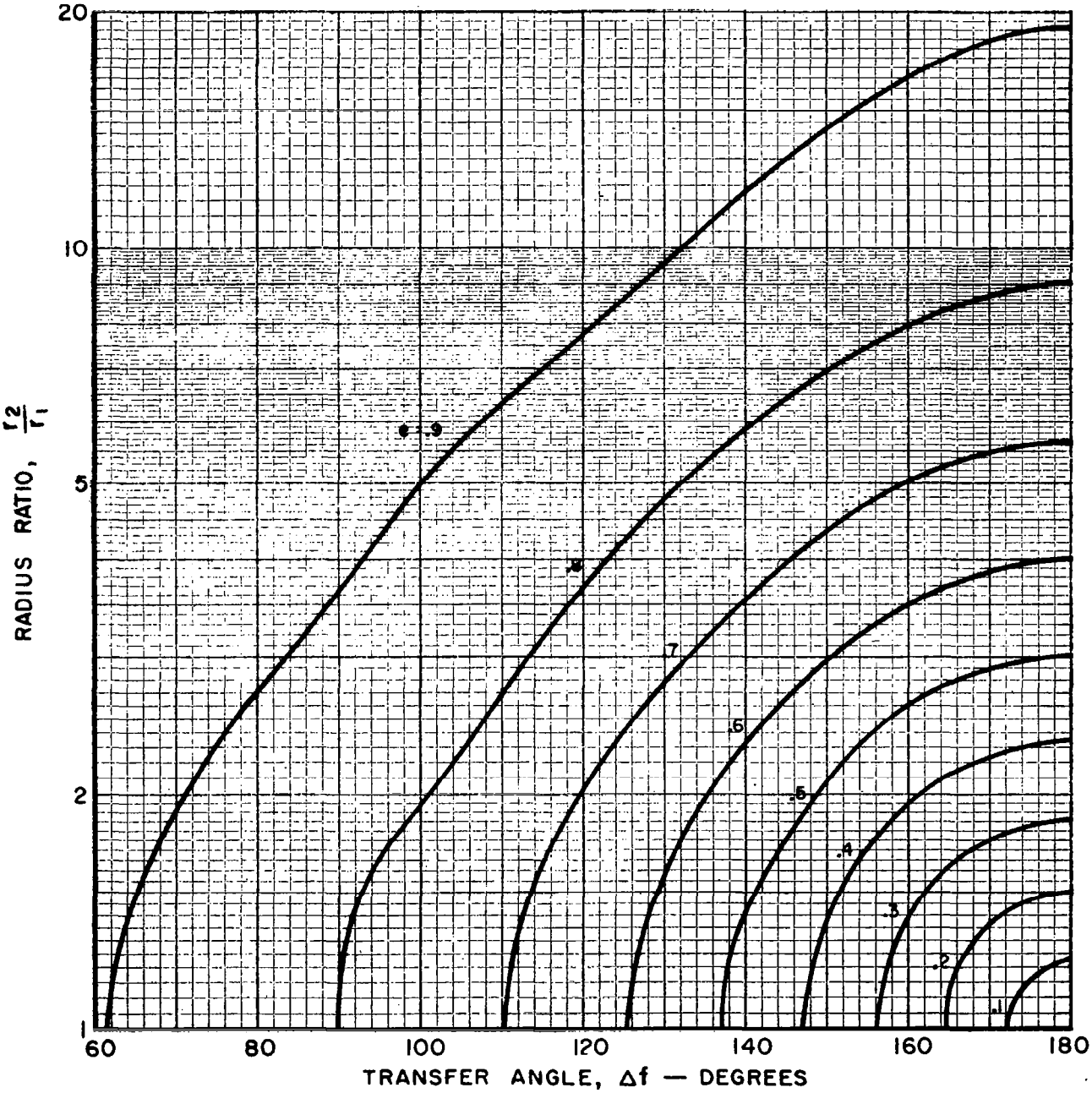

FIG. 25

SYMMETRIC - LIMITED TRANSFERS

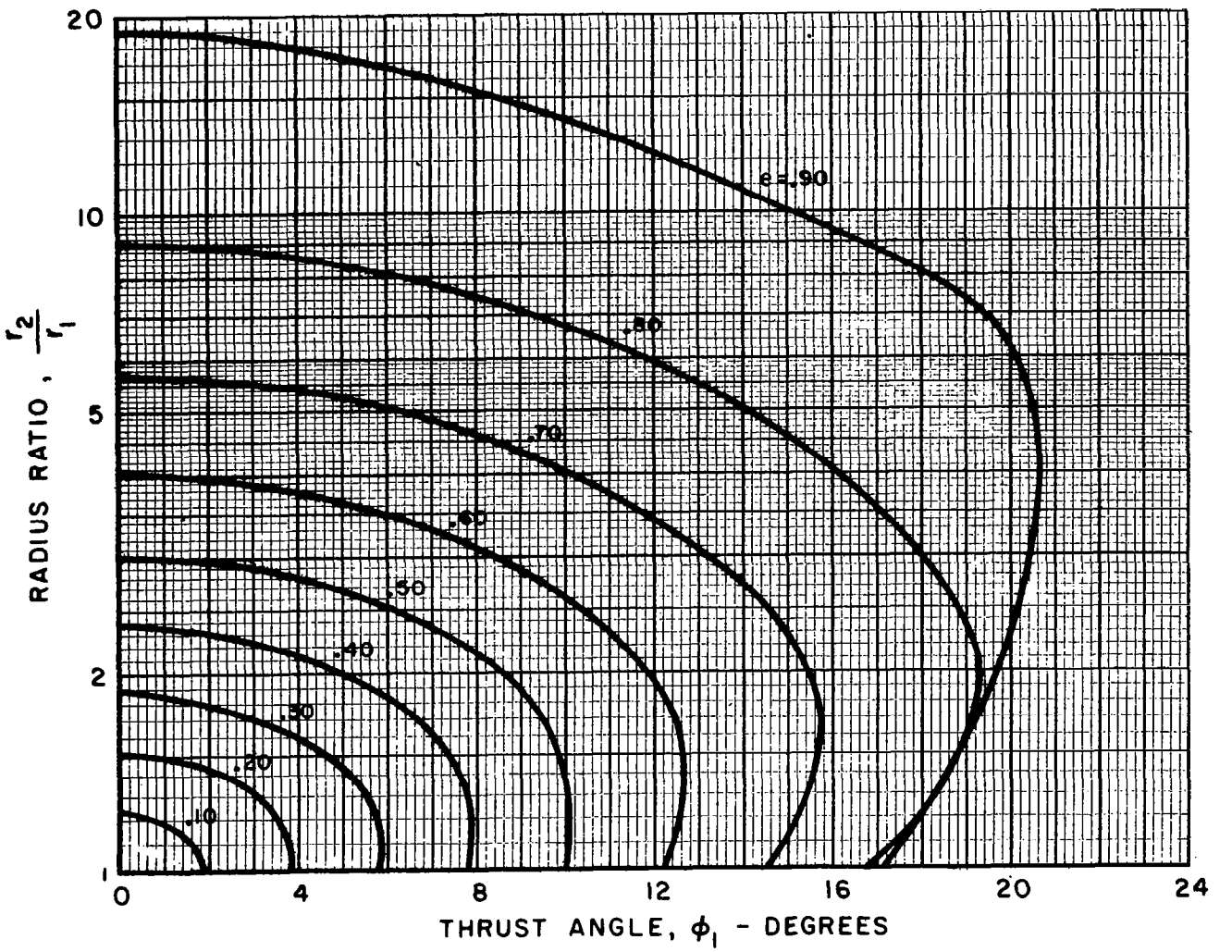

FIG. 26

SYMMETRIC – LIMITED TRANSFERS

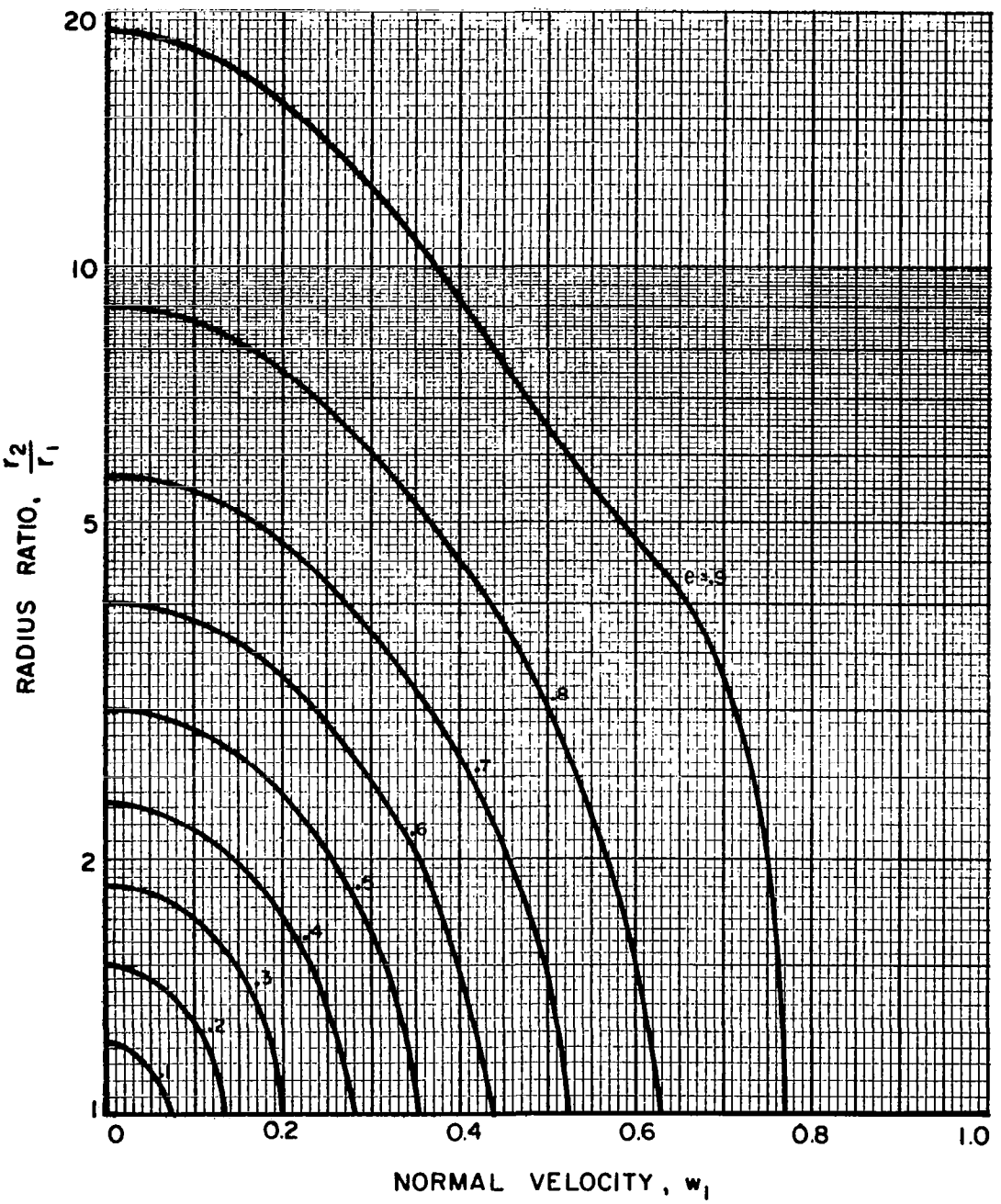

FIG. 27

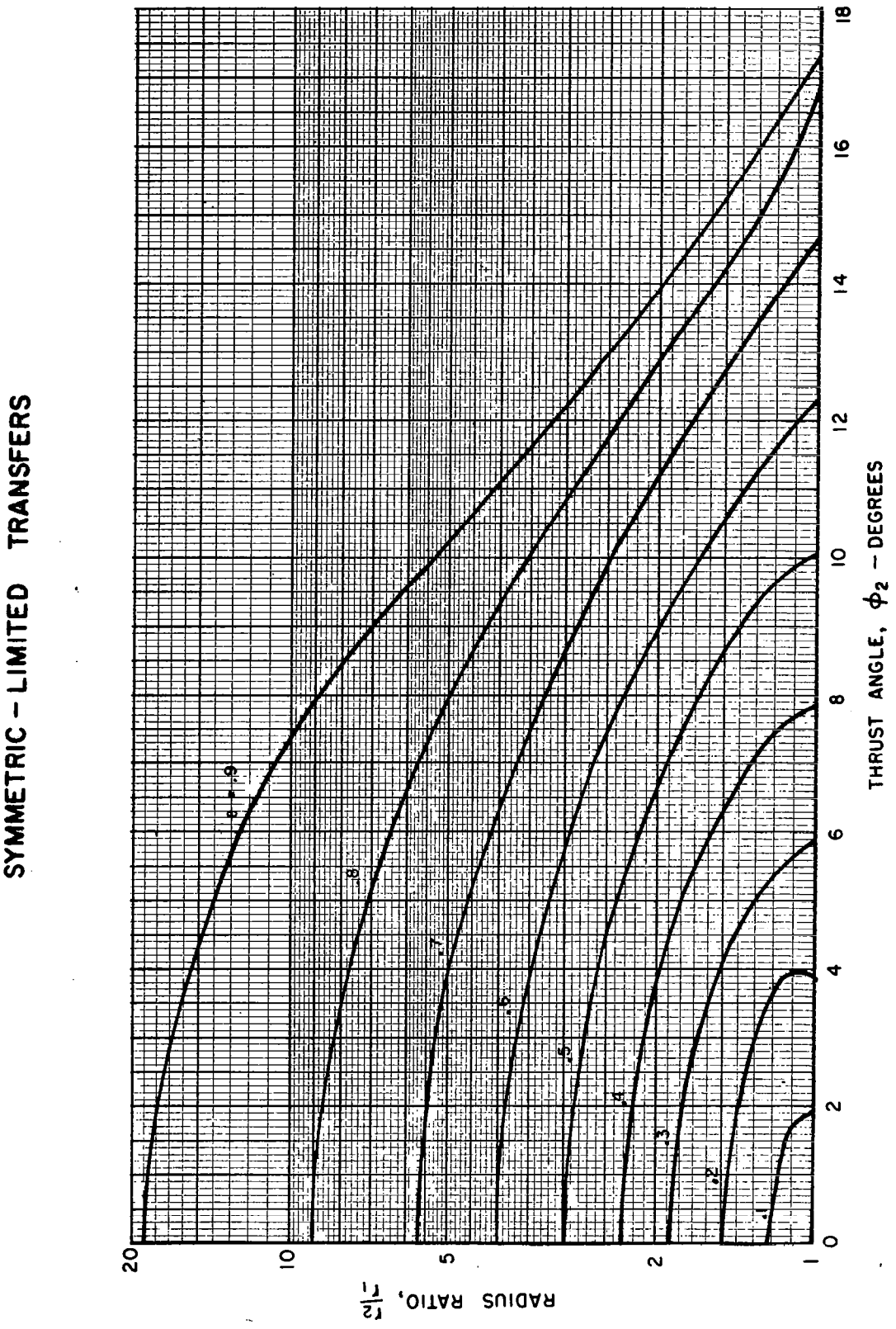
SYMMETRIC – LIMITED TRANSFERS
RADIUS RATIO, $\frac{r_2}{r_1}$
20
10
5
2
1
0
2
4
6
8
10
12
14
16
18
THRUST ANGLE, ϕ_2 – DEGREES
e = 0
.8
.7
.6
.5
.4
.3
.2
.1

FIG. 28

SYMMETRIC - LIMITED TRANSFERS

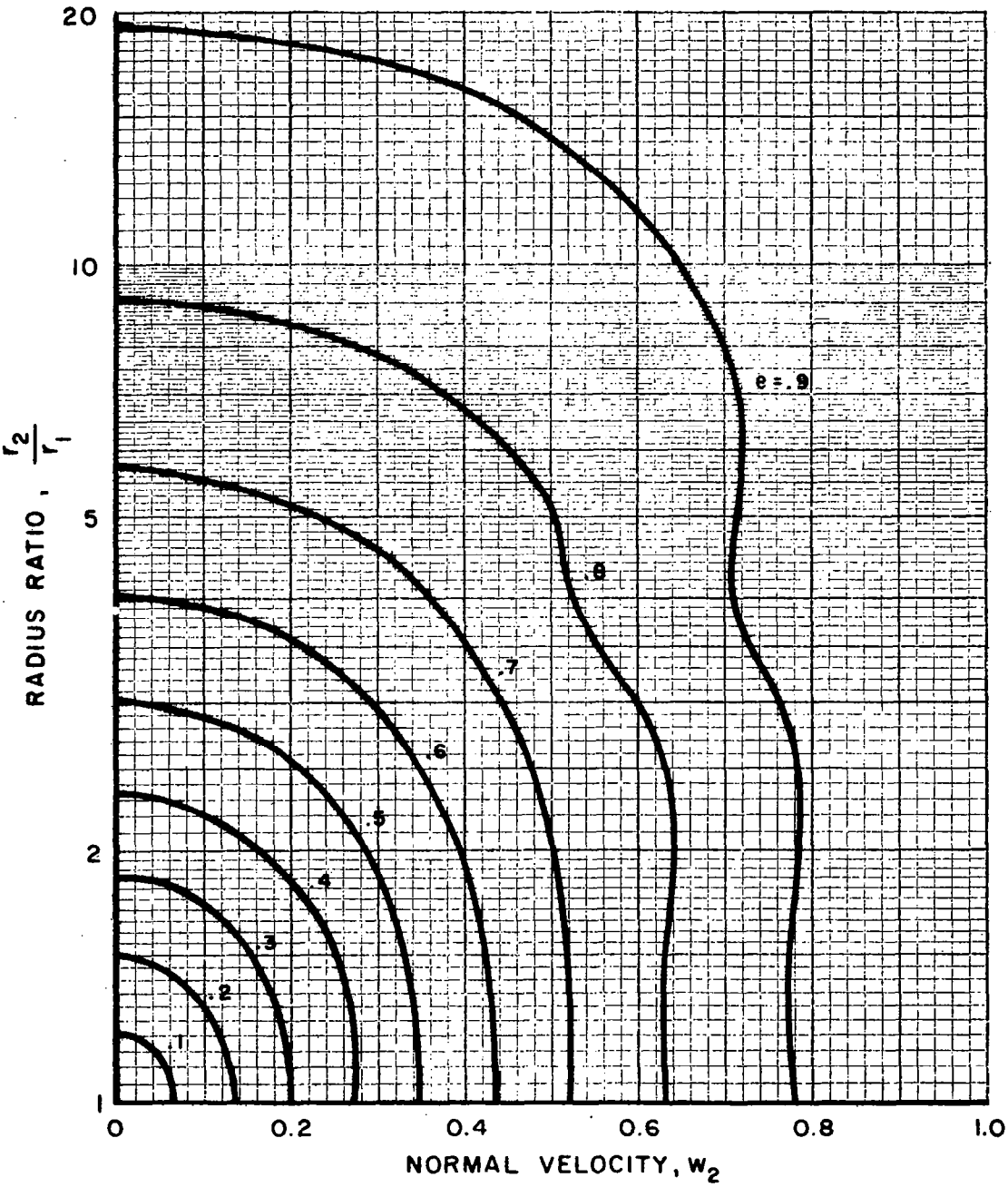

PRIMER VECTOR LOCI

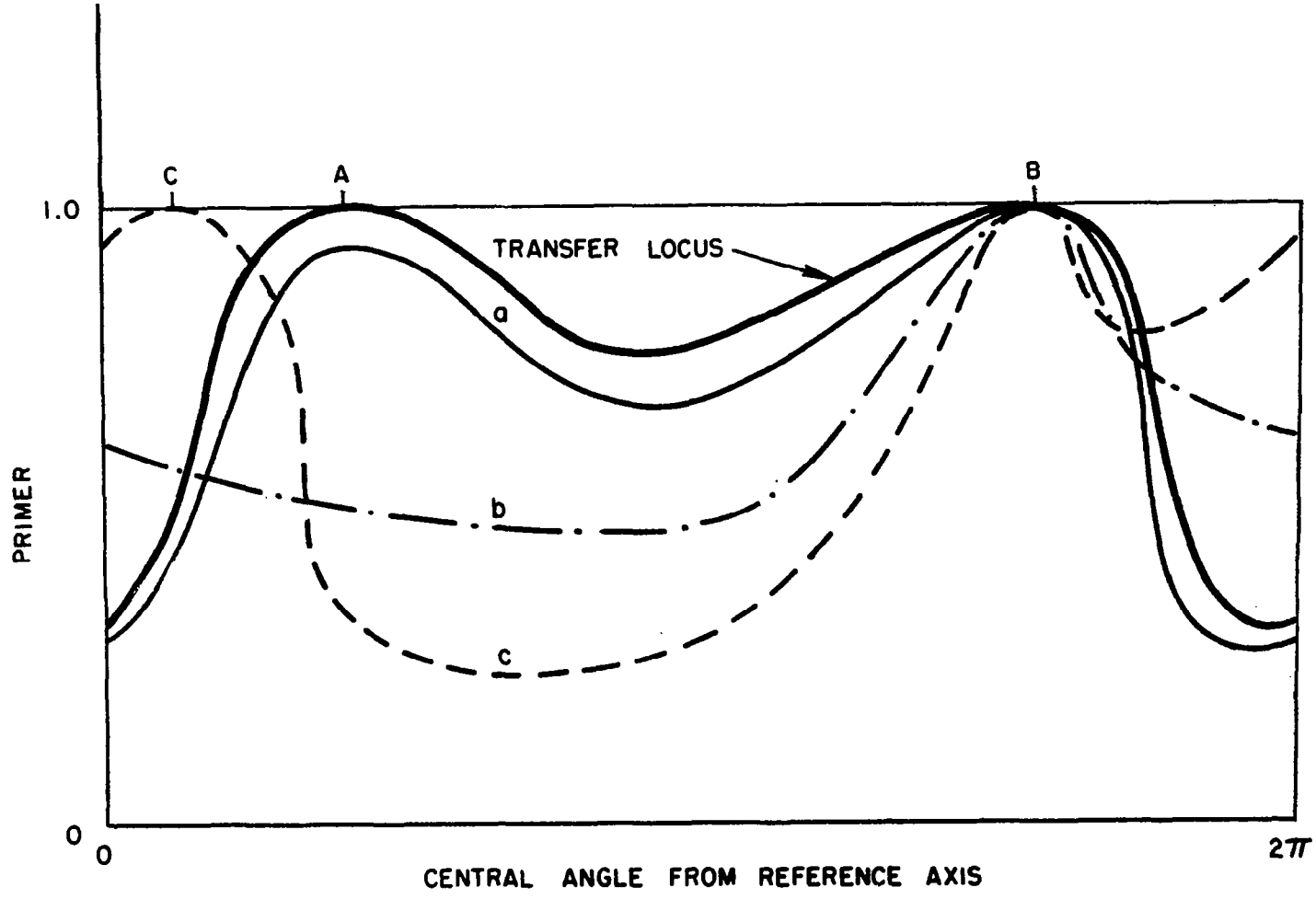

FIG. 29

FIG. 30

ORBIT GEOMETRY

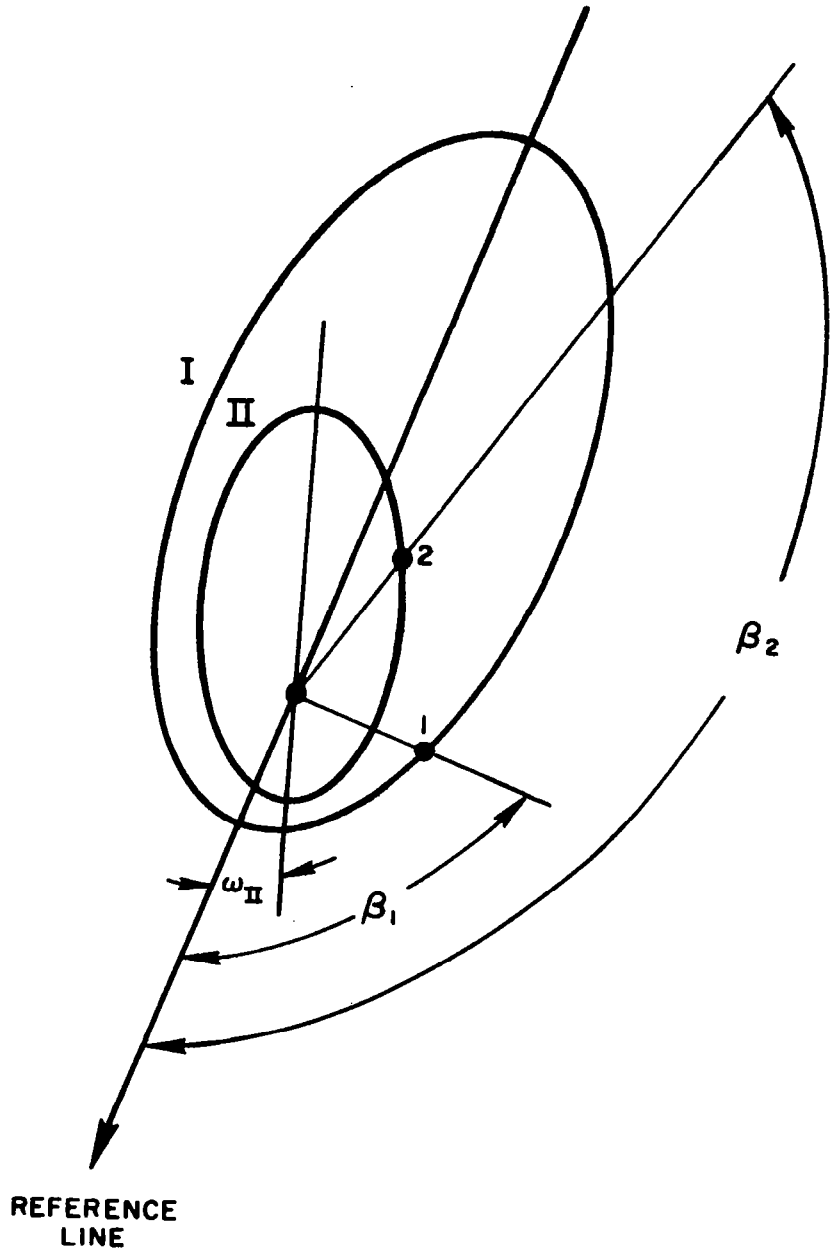

FIG. 31

GEOMETRY AT IMPULSE POINT

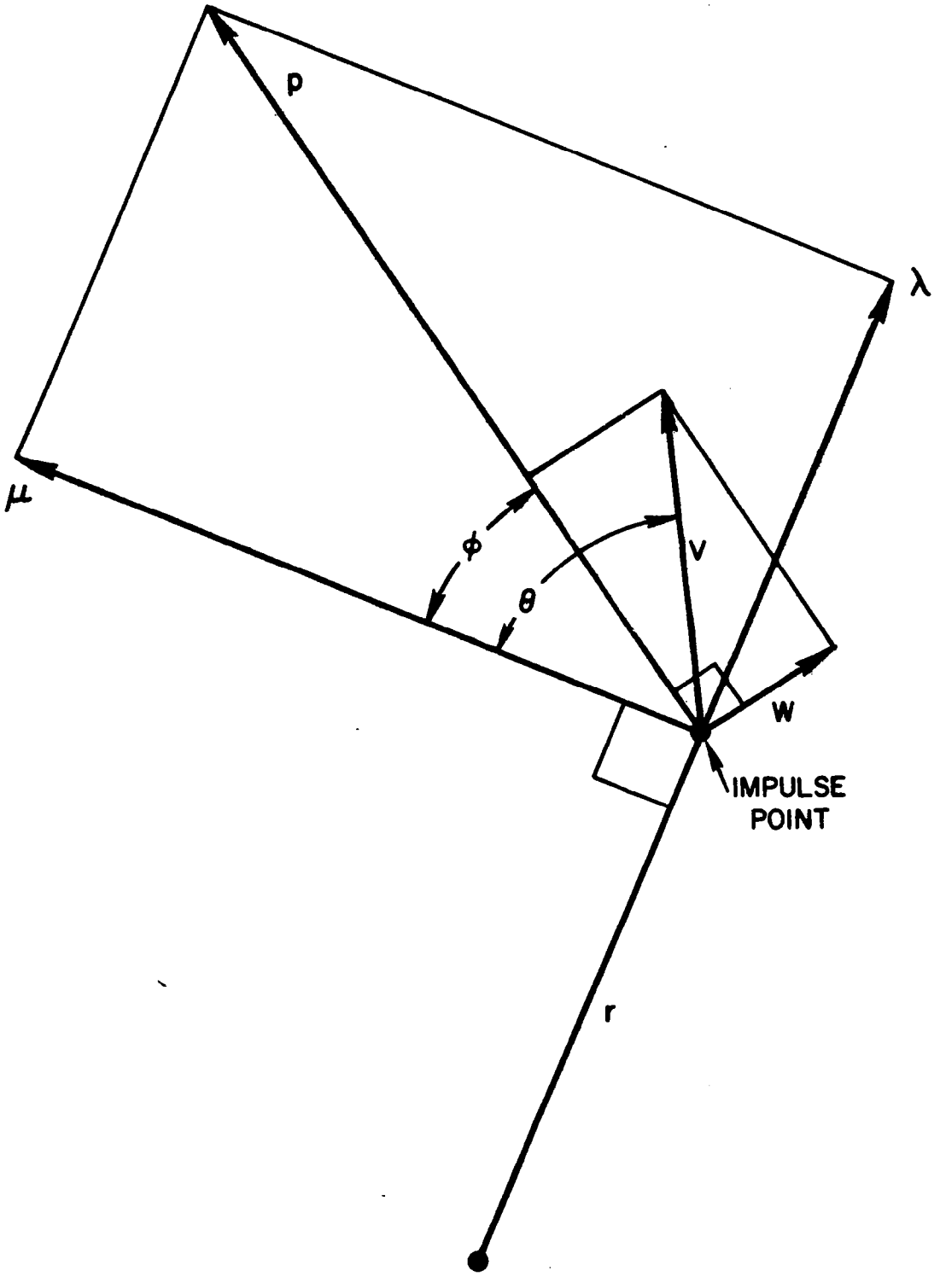

FIG. 32

SPIRAL-LIMITED FAMILY

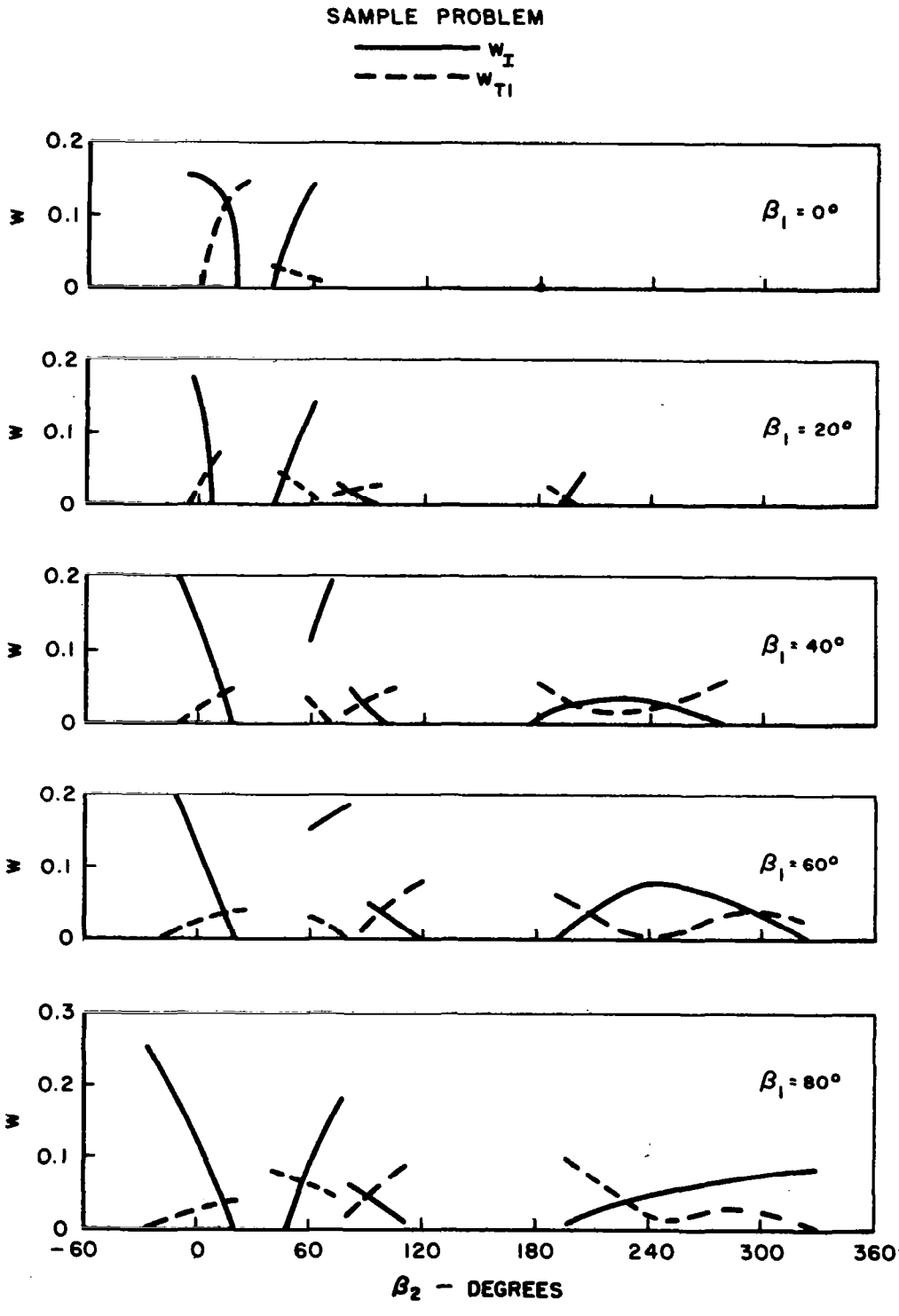

FIG. 33

SPIRAL-LIMITED FAMILY

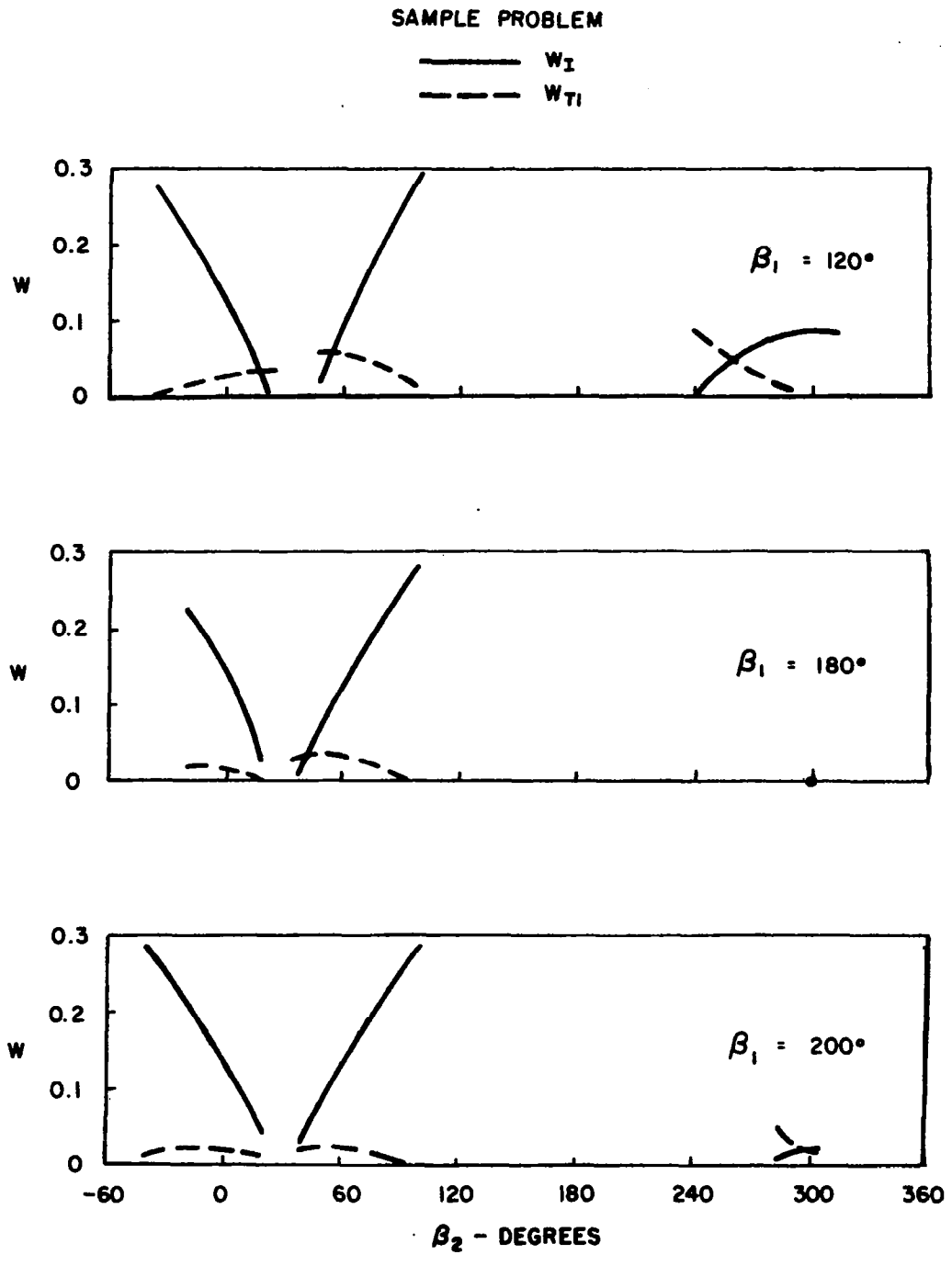

SPIRAL-LIMITED FAMILY

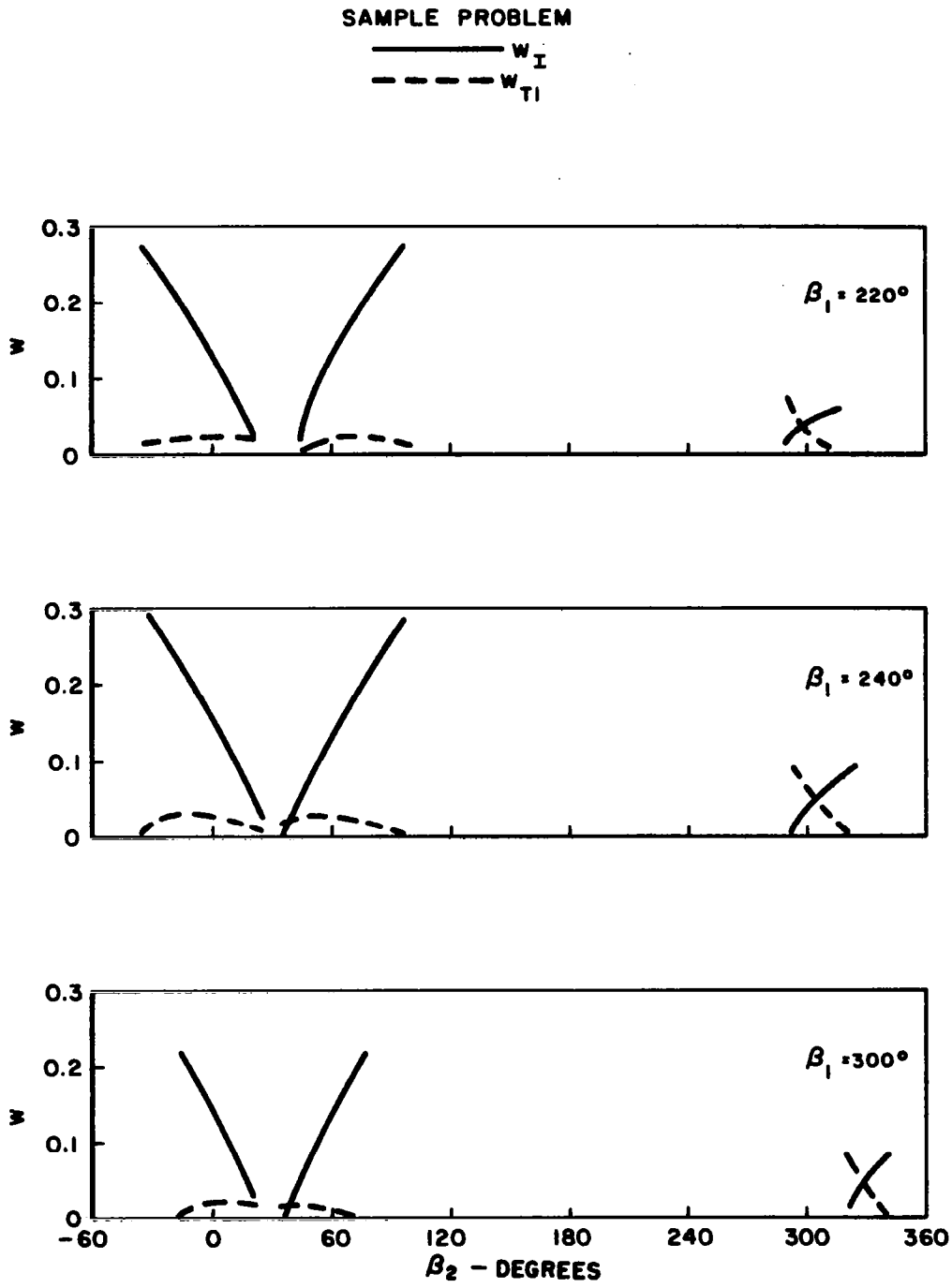

FIG. 35

SPIRAL-LIMITED FAMILY

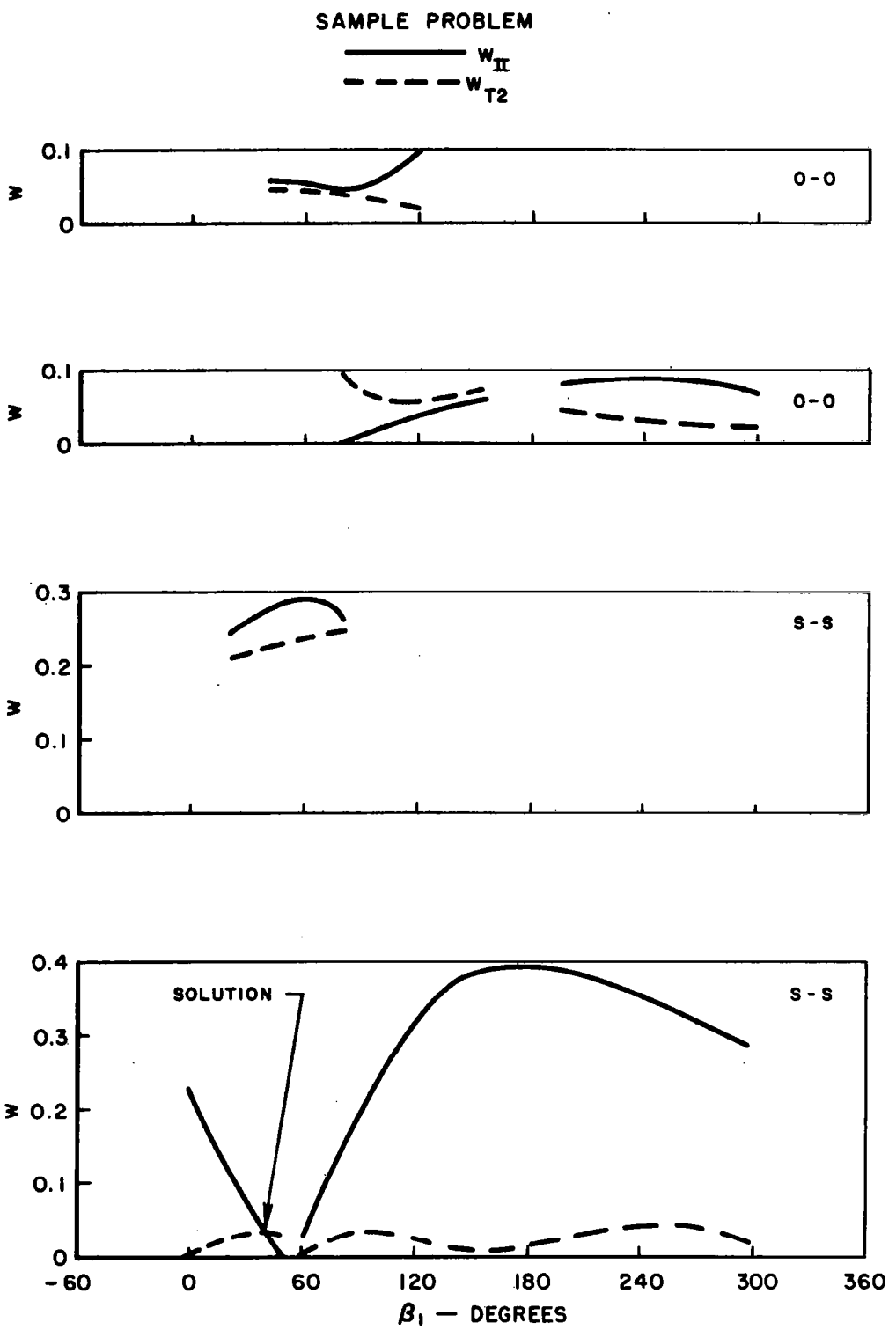

SYMMETRIC – LIMITED FAMILY

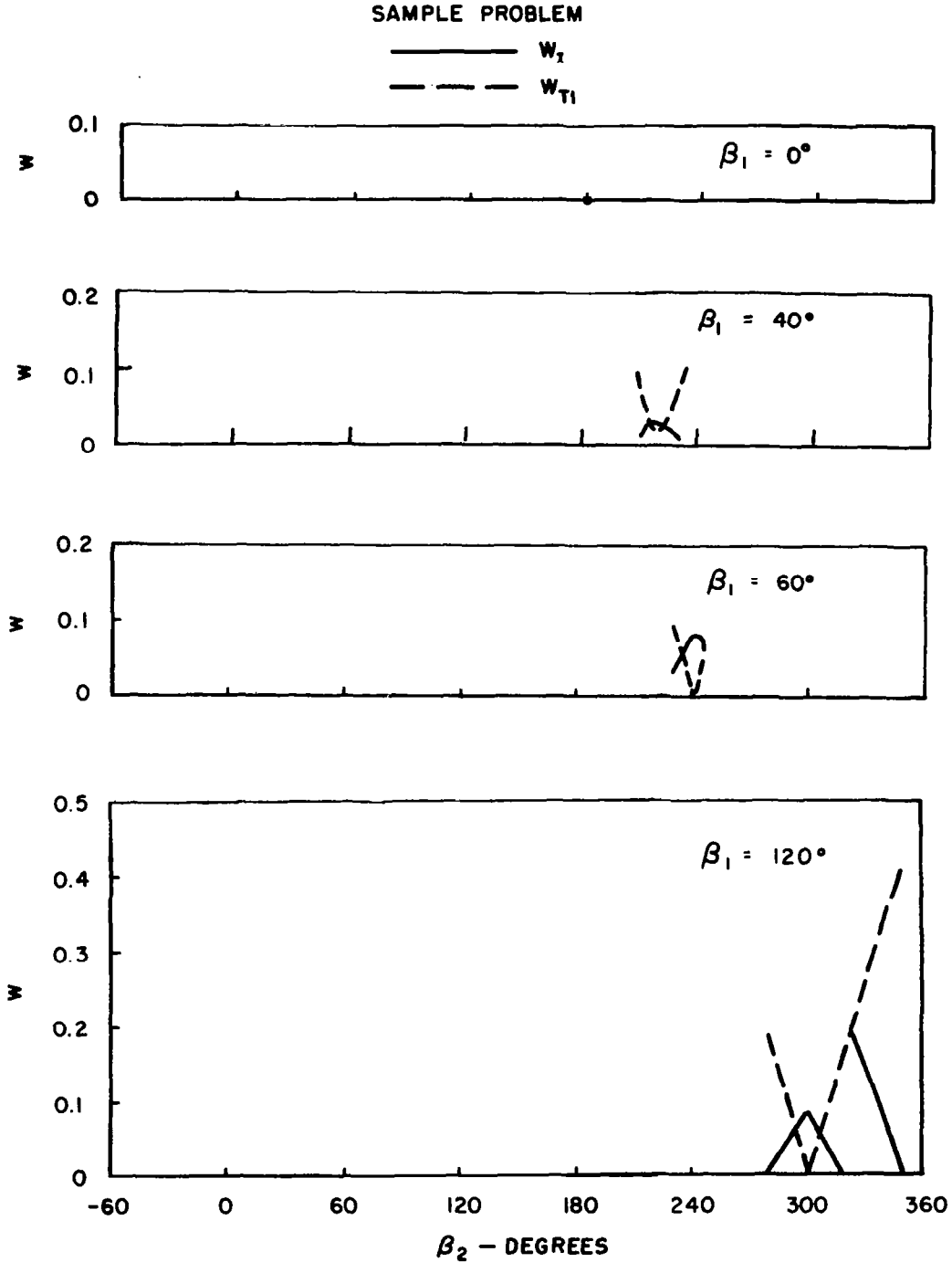

SYMMETRIC - LIMITED FAMILY

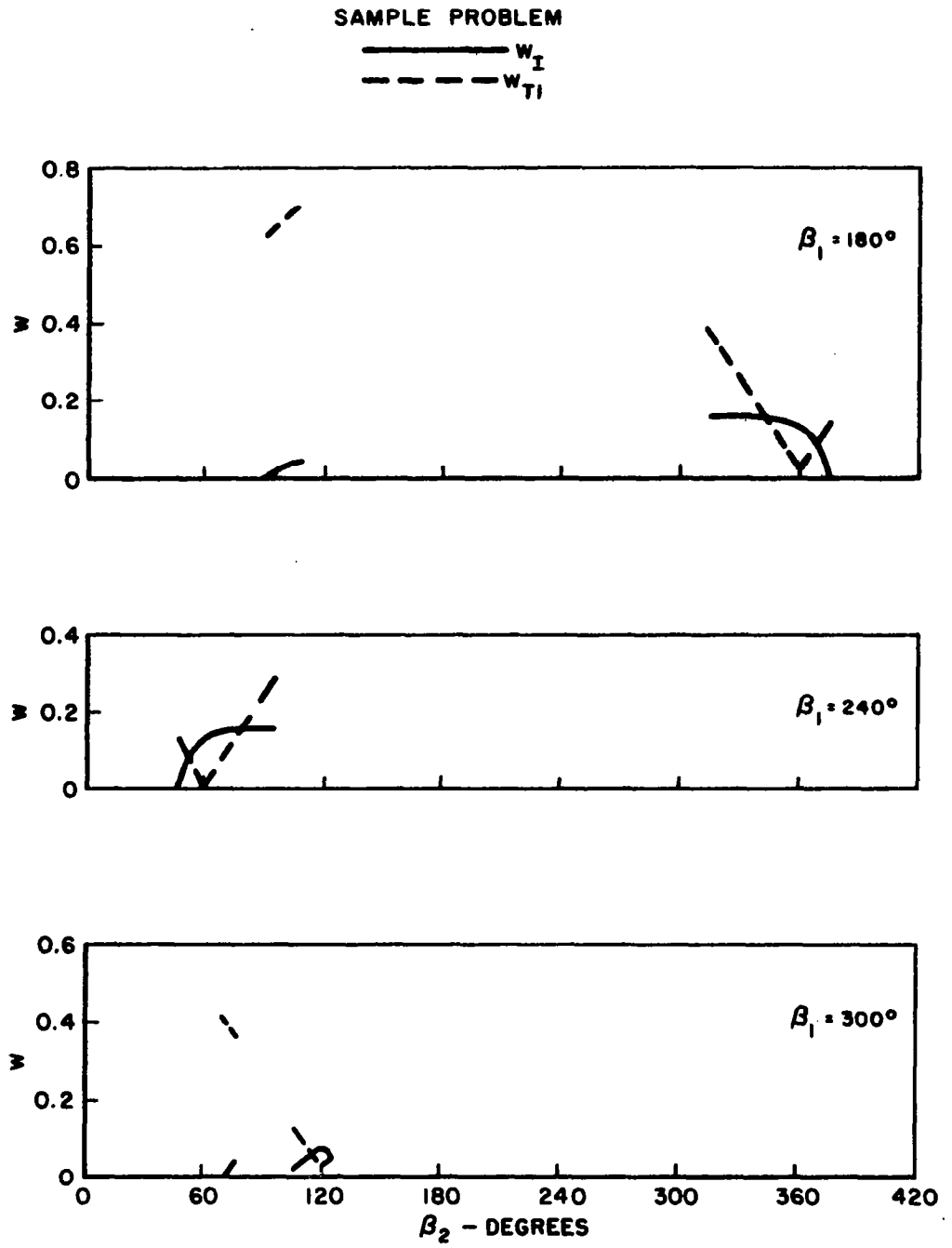

SYMMETRIC - LIMITED FAMILY

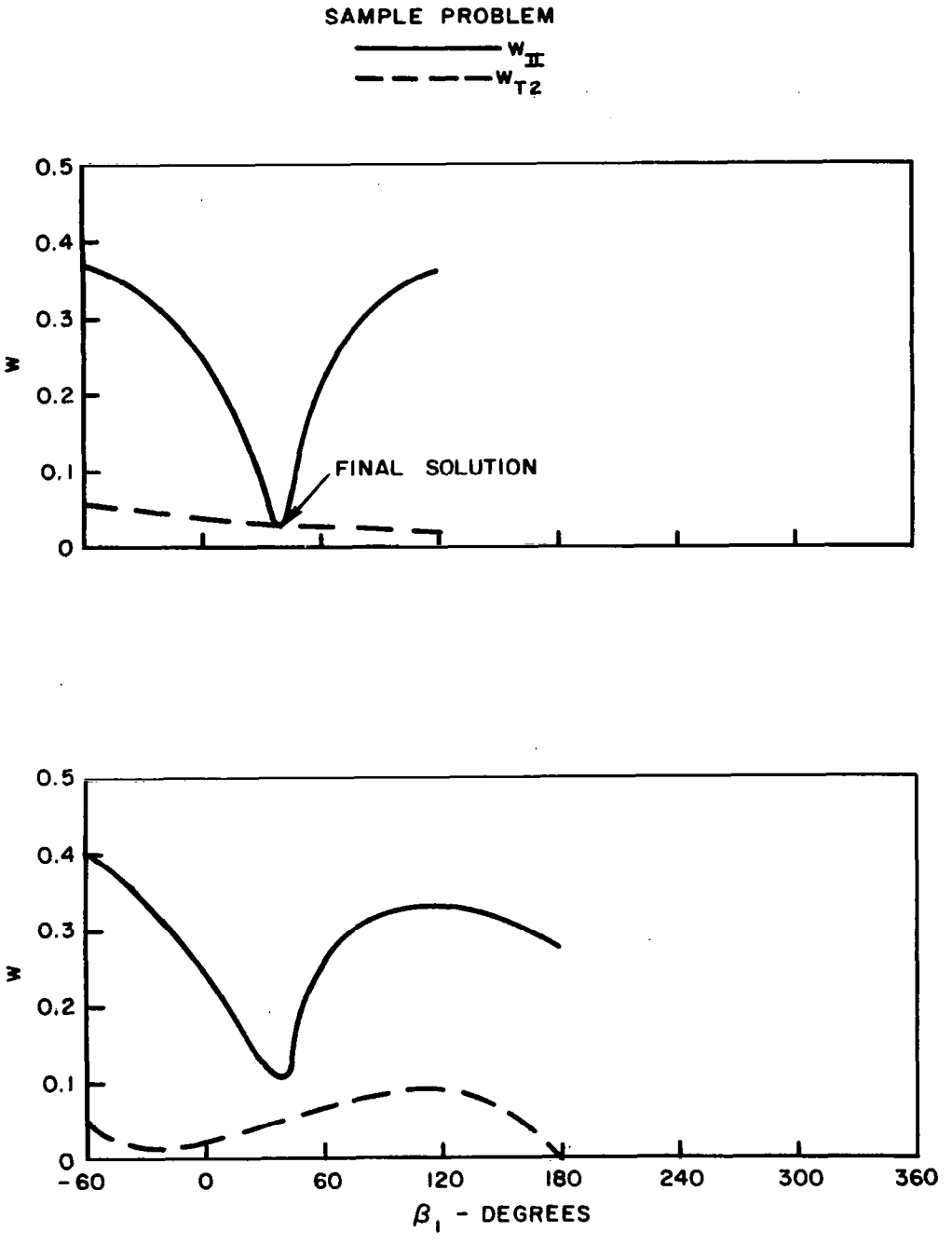

FIG. 39

CONTENSOU'S SPOOLS

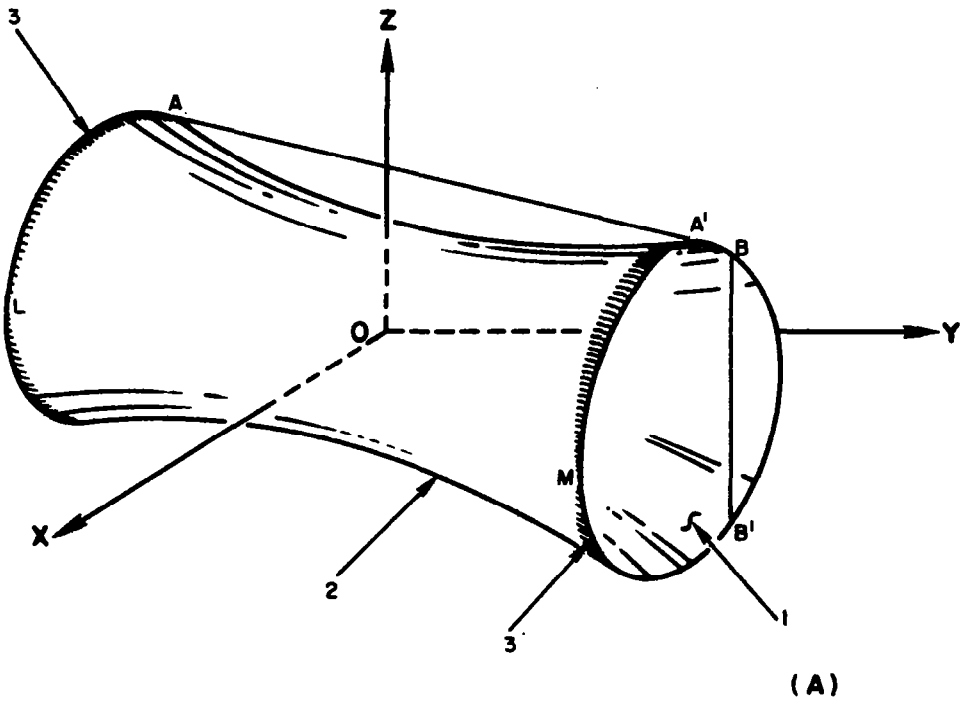

(A)

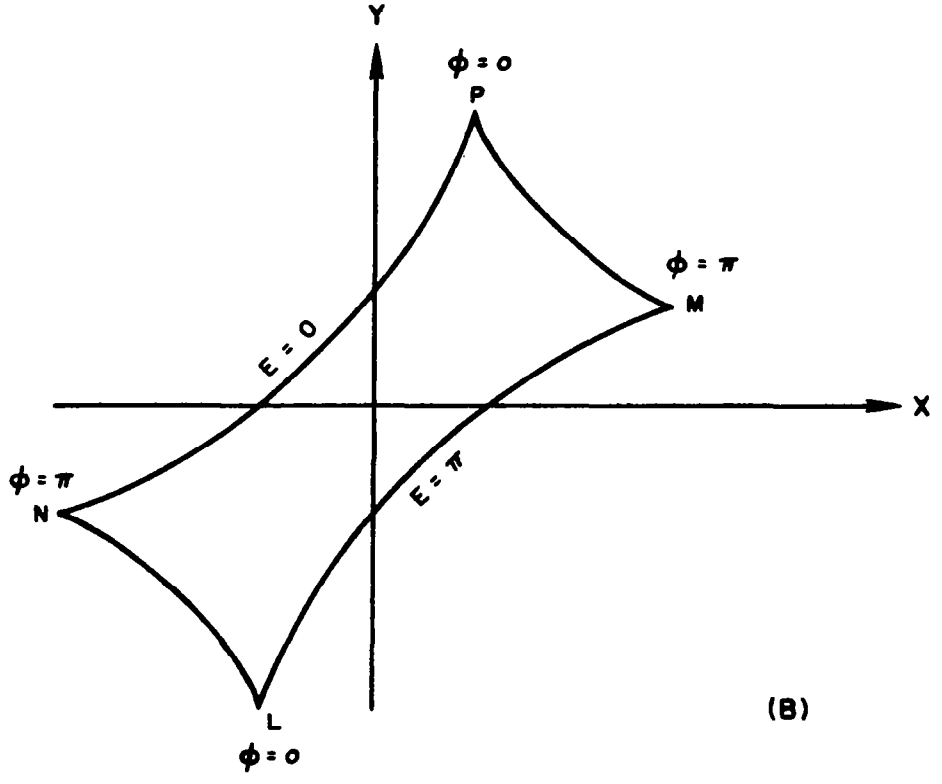

(B)

FIG. 40

# CONTENSOU'S SPOOL
e = 0.5
LINES OF E

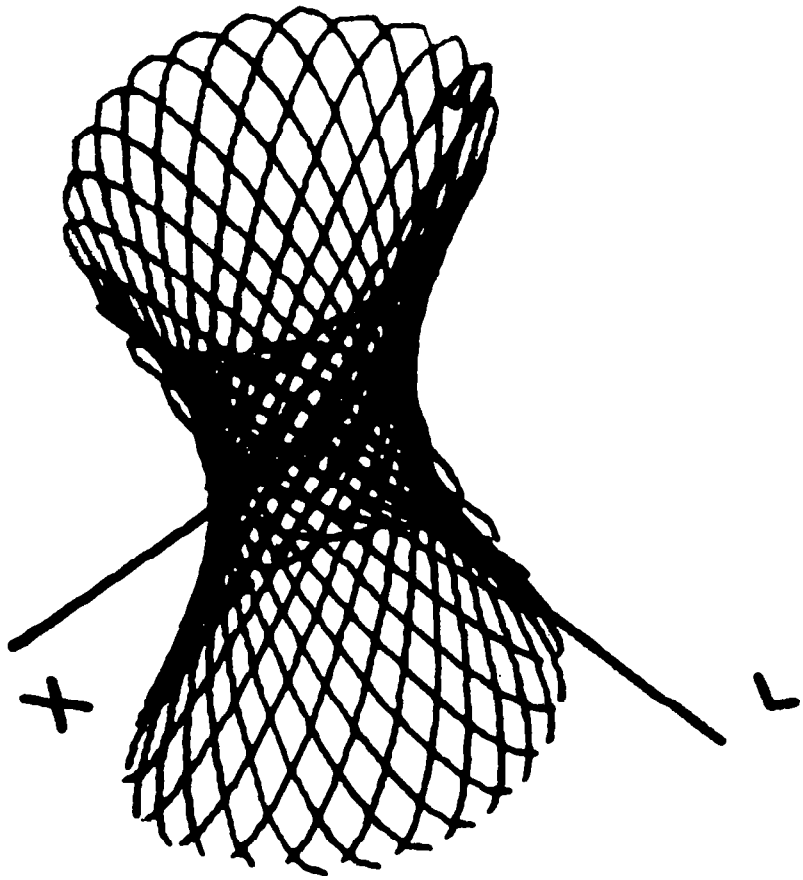

FIG. 41

CONTENSOU'S SPOOL

e = 0.5

LINES OF ϕ

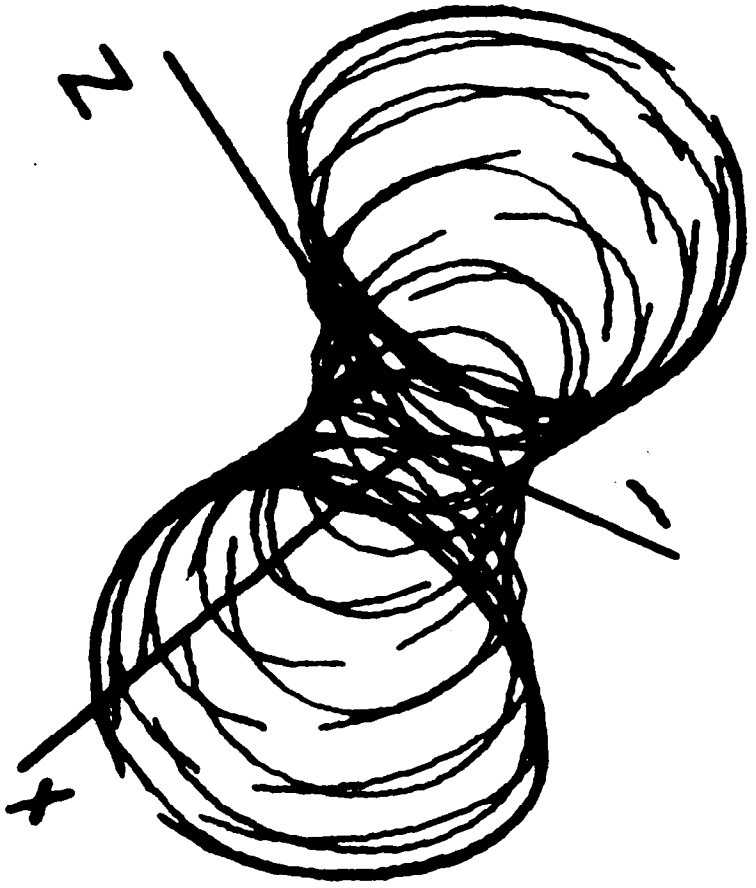

FIG. 42

CONTENSOU'S SPOOL

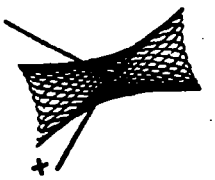

e = 0.5
X-Y PLANE
LINES OF E

e =0.5
Y-Z PLANE
LINES OF E AND ϕ

FIG. 43

CONTENSOU'S SPOOL

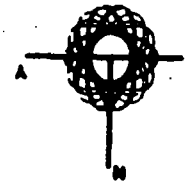

e = 0.5
END OF SPOOL
LINES OF E

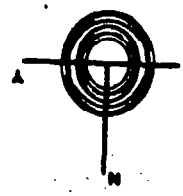

e = 0.5
END OF SPOOL
LINES OF ϕ

FIG. 44

CONTENSOU'S SPOOL

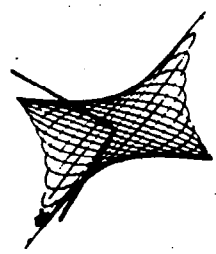

e = 0.75
X-Y PLANE
LINES OF E

e = 0.75
Y-Z PLANE
LINES OF E AND ϕ

e = 0.75
END OF SPOOL
LINES OF E AND ϕ

FIG. 45

CONTENSOU'S SPOOL

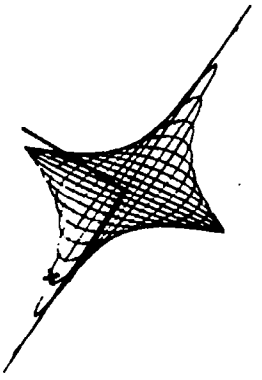

e =0.875
X-Y PLANE
LINES OF E

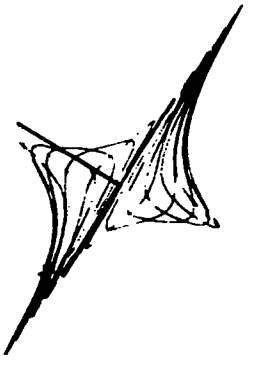

e =0.875
X-Y PLANE
LINES OF ϕ

CONTENSOU'S SPOOL

e = 0.875
Y - Z PLANE
LINES OF ϕ

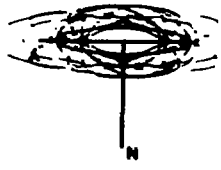

e = 0.875
END OF SPOOL
LINES OF E AND ϕ

SPOOL FOR e = 1.0

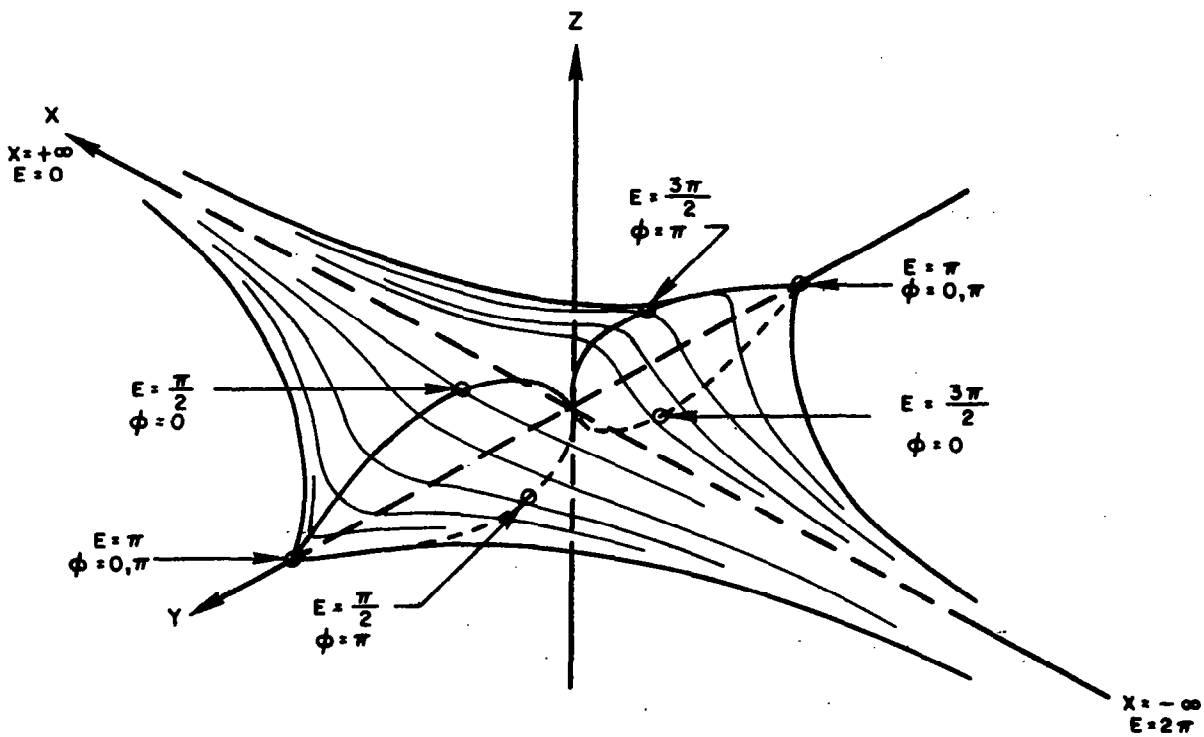

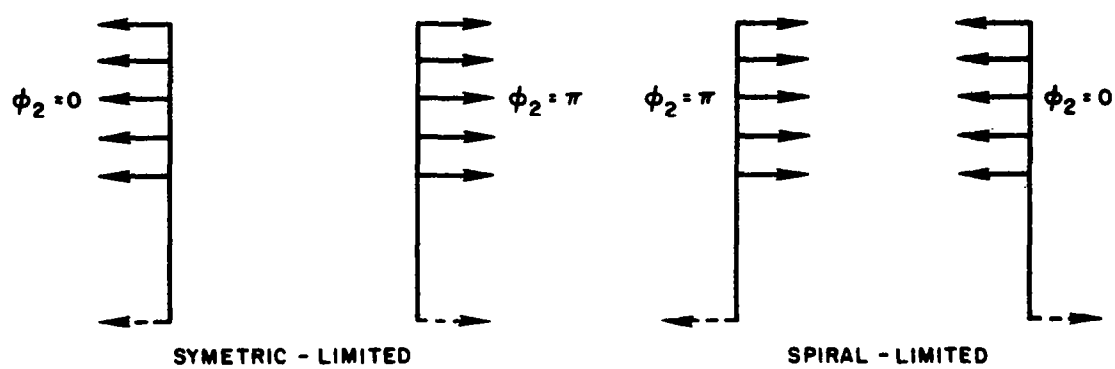

FIG. 48

CONTENSOU'S SPOOL

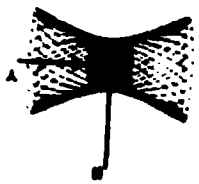

e = 0.25
Y-Z PLANE
LINES OF E

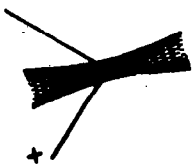

e = 0.25
X-Y PLANE
LINES OF E

FIG. 49

SPOOL FOR $\theta = 0$

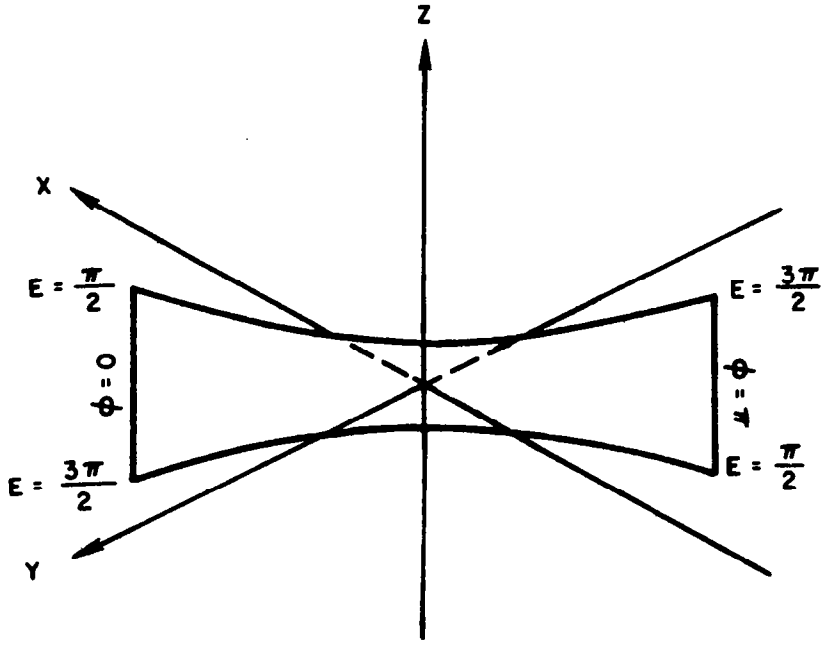

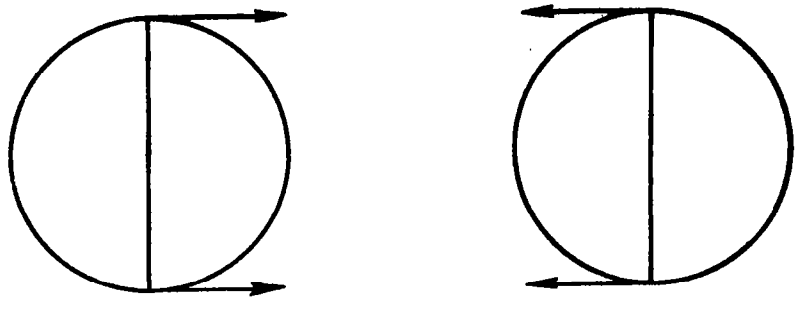

SYMMETRIC - LIMITED

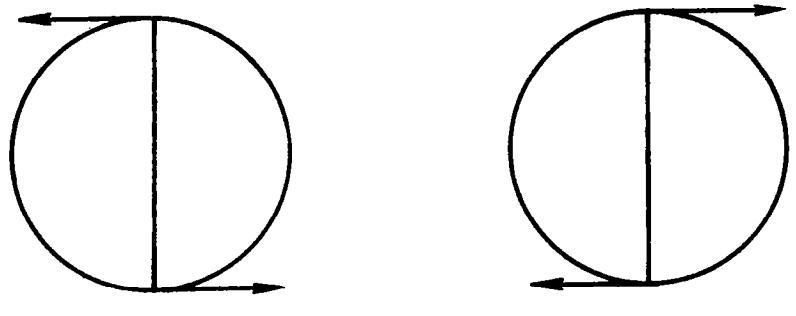

SPIRAL - LIMITED

FIG. 50

DEFINITIONS OF VECTOR PARAMETERS

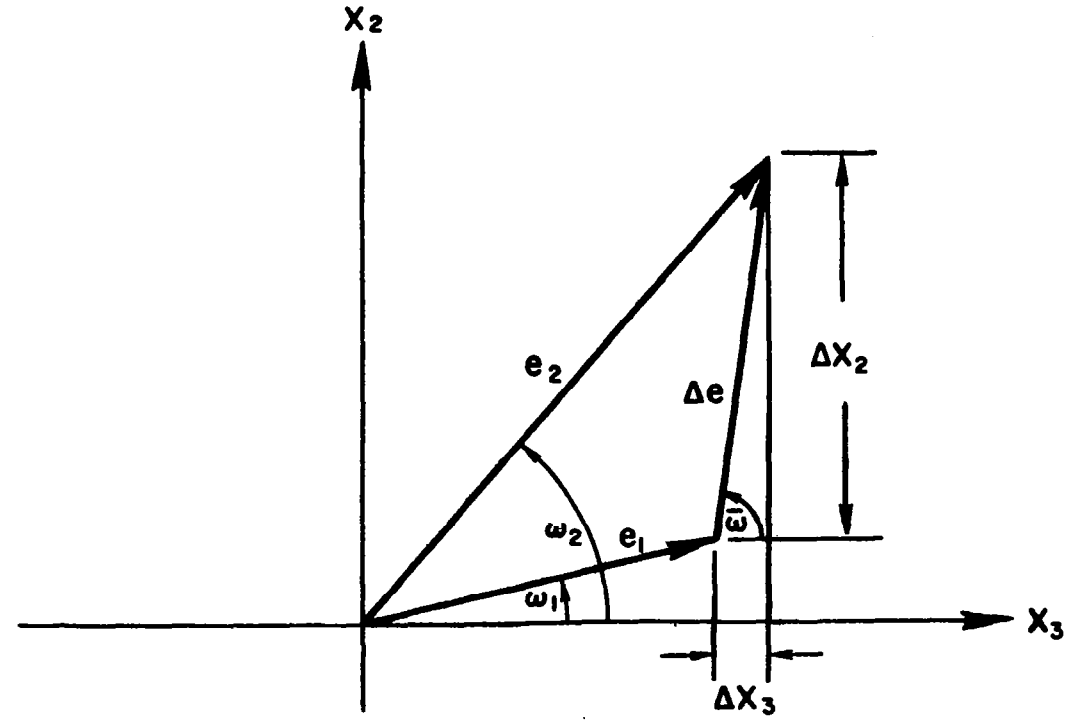

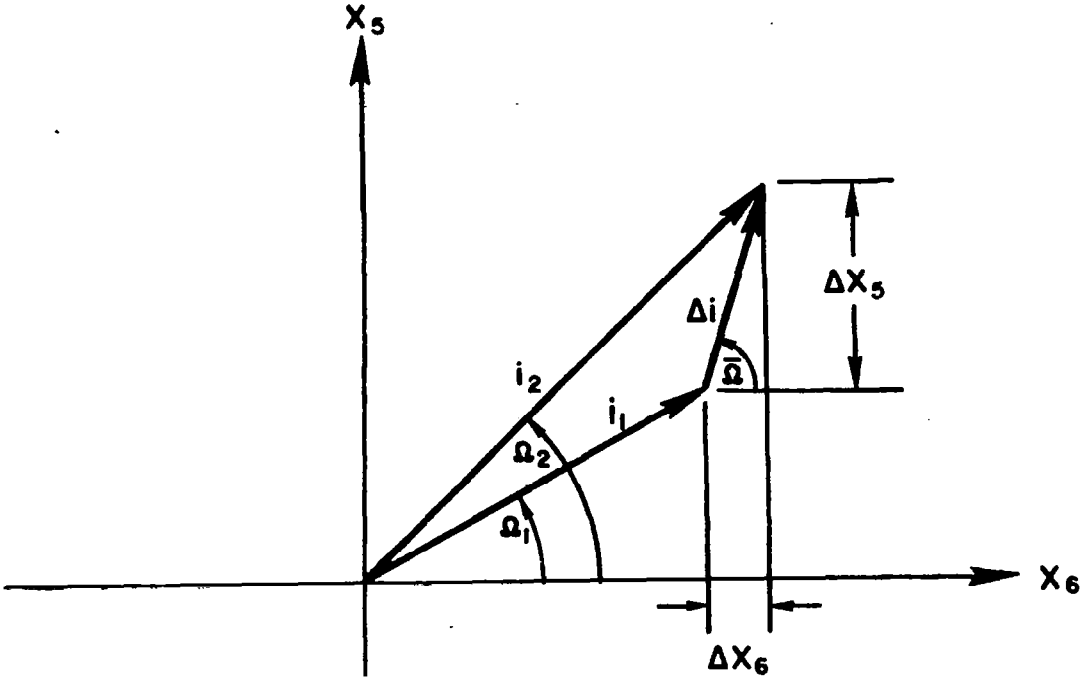

FIG. 51

FAMILIES OF THREE-DIMENSIONAL TRANSFERS

$\bar{\omega} - \bar{\Omega} = 0°$

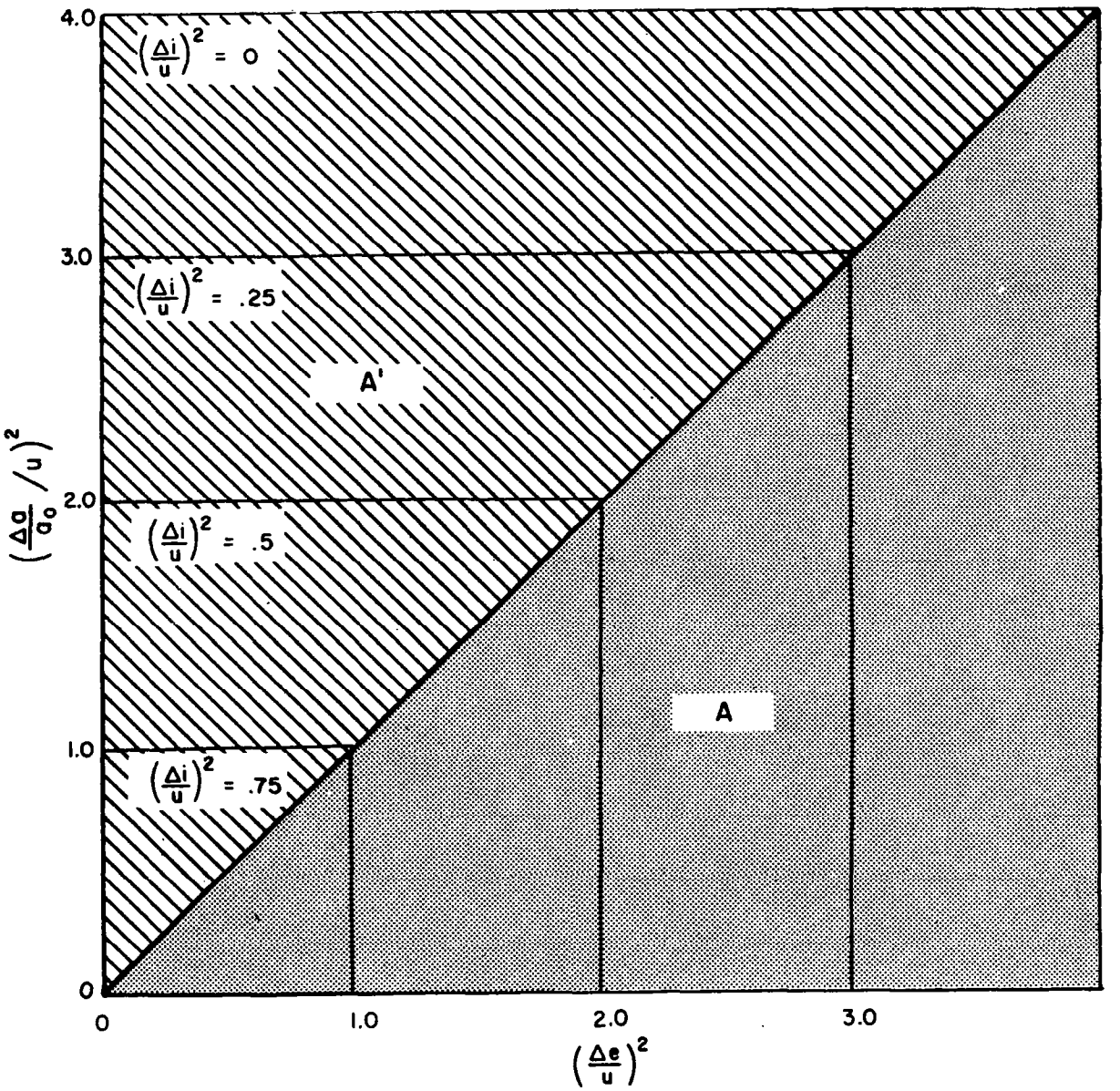

FIG. 52

FAMILIES OF THREE – DIMENSIONAL TRANSFERS

$\bar{\omega} - \bar{\Omega} = 20°$

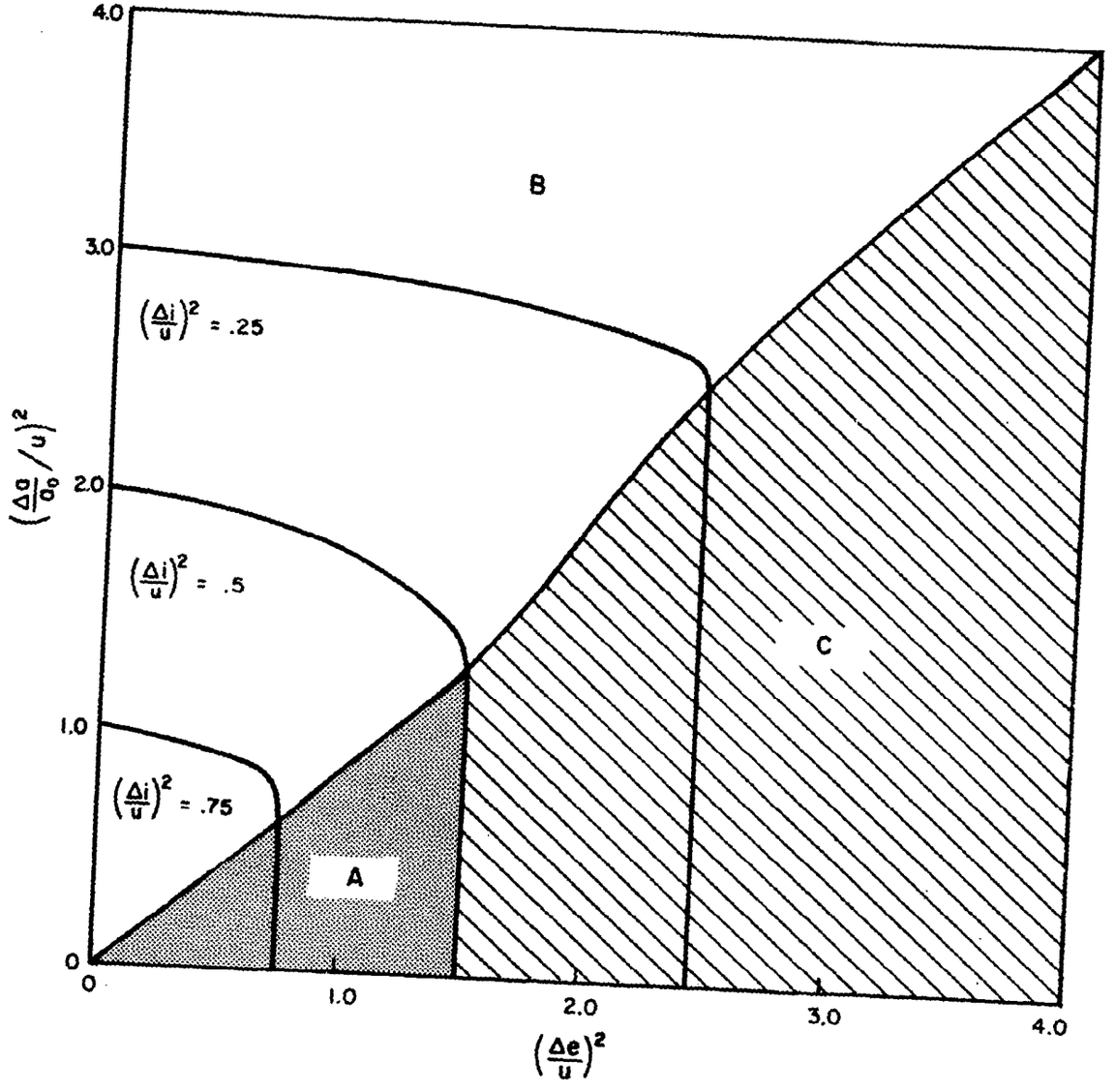

FAMILIES OF THREE-DIMENSIONAL TRANSFERS

$\bar{\omega} - \bar{\Omega} = 30°$

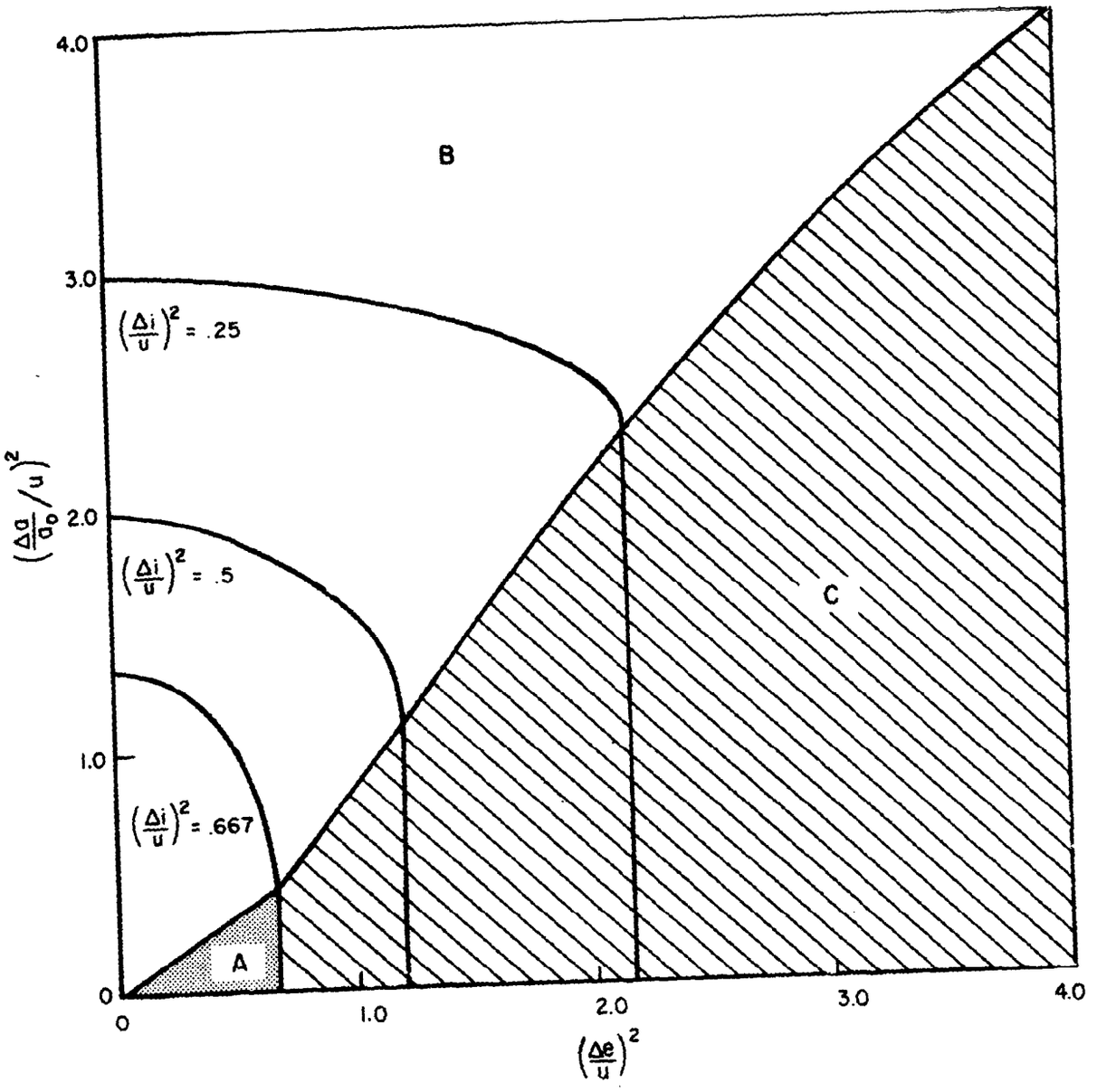

NASA-Langley, 1966 CR-636